

**Order under the guise of chaos: functional neuroanatomy of the
somatosensory “barrel” cortex of the *reeler* mutant mouse**

Dissertation
for the award of the degree
“Doctor rerum naturalium.”

Faculty of Biology
of the Georg-August-Universität Göttingen

submitted by

Julien Guy

Born in Strasbourg, France

Göttingen, 2015

Prof. Dr. med. Jochen F. Staiger (first reviewer)
Institute for Neuroanatomy, University Medical Center, Göttingen

Prof. Dr. Tim Gollisch (second reviewer)
Department of Ophtalmology, University Medical Center, Göttingen

Prof. Dr. Siegrid Löwel
Systems Neuroscience Group, Johann-Friedrich-Blumenbach-Institute of Zoology and
Anthropology, University of Göttingen

Date of the oral examination:

I, Julien Guy, hereby certify that the present thesis has been written independently and with no other sources and aids than quoted. All results presented here were the fruit of my own labour unless stated otherwise.

.....

Göttingen, 07.10.2015

Table of Contents

Introduction	1
Fertile concepts in functional neuroanatomy	1
The rodent somatosensory system	4
A mutant that questions cortical layers	9
Aims and approaches	15
Visualization of the barrel field in LIV^{tdTomato} animals	17
Material and methods	20
Animals	20
<i>Mice line used</i>	20
<i>In vivo functional imaging</i>	21
<i>Labelling of blood vessels</i>	21
<i>In vitro electrophysiology</i>	21
Optic chamber implantation	21
Whisker stimulation	22
Intrinsic signal optical imaging	22
Perfusion and tissue collection	23
Stereotaxic injections	24
Slice preparation	25
<i>In vitro</i> electrophysiology	26
Subcellular channelrhodopsin-assisted circuit mapping (sCRACM)	27
Histochemistry	28
Data analysis	29
<i>Intrinsic signal optical imaging</i>	29
<i>Electrophysiology</i>	31
Statistics	32
Results	34
Intrinsic signal optical imaging	34
Sensory map organization	36
Single whisker stimulus representation in barrel cortex	39
Transcolumnar connectivity revealed by intrinsic imaging	42
Cortical vasculature in reeler and wild type mice	43
Lessons drawn from intrinsic signal imaging	46

Thalamic axon projection domains in reeler and wild type mice	47
Cellular identity of tdTomato positive neurons	49
Intrinsic properties of tdTomato positive neurons	52
Optogenetic control of thalamic relay neurons	54
Channelrhodopsin-2 evoked responses in spiny stellate neurons	56
Properties of thalamic input to reeler spiny stellate neurons	60
Subcellular distribution of thalamocortical input to spiny stellate neurons	63
Discussion	70
Functional organization of the reeler somatosensory cortex	70
Functional connectivity in reeler barrel-related columns	72
Evoked responses: the reeler paradox	76
Possible causes of a weakened thalamocortical input in reeler	79
Compensation mechanisms for a weak thalamocortical input: solving the reeler paradox	80
Altered somatodendritic distribution of thalamocortical input in reeler	82
Functional implications for the reeler cortex	85
Conclusion and perspectives	86
Summary	90
References	91
Publications arising from the present thesis	109
Acknowledgments	111
Curriculum vitae	113
Publications	114

Figures

Figure 1. Anatomy of the whisker to barrel pathway and the organization of the somatosensory cortex.	7
Figure 2. Cortical lamination defect in the <i>reeler</i> somatosensory cortex.	11
Figure 3. Cytoarchitecture of the barrel field in LIV ^{tdTomato} WT and <i>reeler</i> mice.	19
Figure 4. The hemodynamic response to single whisker stimulation.	35
Figure 5. Somatotopic organization of the barrel cortex.	38
Figure 6. Stimulus representation in somatosensory cortex.....	41
Figure 7. Vascular network in the barrel cortex.	44
Figure 8. Distribution of tdTomato and eYFP expression in somatosensory cortex.	48
Figure 9. Morphology of biocytin-filled neurons.....	50
Figure 10. Intrinsic properties of SpS neurons.	53
Figure 11. ChR2 evoked responses in thalamic relay neurons.	55
Figure 12. ChR2 evoked responses in SpS neurons.	58
Figure 13. Properties of TC input to SpS neurons.....	62
Figure 14. ChR2-assisted mapping of TC input to SpS..	66
Figure 15. Distribution of spines on the dendrites of reconstructed SpS neurons..	68
Figure 16. Proposed model of alterations in the circuits of LIV of the reeler somatosensory cortex..	88

Tables

Table 1. Areal quantification of the sensory evoked intrinsic signal.....	43
Table 2. Quantitative analysis of SpS neuron morphology.....	51
Table 3. Values for intrinsic properties of SpS neurons.....	54

List of abbreviations

AAV	Adeno-associated virus
ANOVA	Analysis of variance
AP	Antero-posterior (e.g. page 24) / Action potential (e.g. page 14)
ApoER2	Apolipoprotein E receptor 2
CCD	Charge-coupled device
C-fos	FBJ osteosarcoma oncogene-protein
ChR2	Channelrhodopsin-2
DAB	Diaminobenzidine
Dab1	Disabled-1
DAPI	4',6-Diamidino-2-phenylindole
DC	Direct current
DV	Dorso-ventral
dVM	Membrane voltage variation
EGTA	Ethylene glycol tetraacetic acid
EPSP	Excitatory postsynaptic potential
eYFP	Enhanced yellow fluorescent protein
FFI	Feedforward inhibition
FS	Fast spiking
GABA	Gamma-aminobutyric acid
HCN1	Hyperpolarization activated cyclic nucleotide gated potassium channel 1
Hepes	4-(2-hydroxyethyl)-1-piperazineethanesulfonic acid
I_h	Hyperpolarization-activated current
IPSP	Inhibitory postsynaptic potential
ISOI	Intrinsic signal optical imaging
I-V	Current-voltage relationship
LX	layer X (X is a roman numeral ranging from I to VI)
mAHP	medium afterhyperpolarization
ML	Medio-lateral
NMDA	N-methyl-D-aspartate
PB	Phosphate buffer
PFA	Paraformaldehyde
PMBSF	Posterior medial barrel subfield

PSTH	Peristimulus time histogram
PV	Parvalbumin
R_{in}	Input resistance
ROI	Region of interest
SFKs	Src family nonreceptor tyrosine kinase
SNAP25	Synaptosomal-associated Protein
SNARE	Soluble NSF attachment protein receptor
STA	Spike triggered average
sCRACM	Subcellular channelrhodopsin-2 mediated circuit mapping
SD	Standard deviation
sem	Standard error on the mean
SpS	Spiny stellate
TB	Tris buffer
TBS	Tris buffer saline
TBST	Tris buffer 0.5% Triton-X 100
TC	Thalamocortical
TN	Thalamic relay neuron
TTX	Tetrodotoxin
VLDLR	Very-low-density-lipoprotein receptor
VPm	Ventral posteromedial nucleus
V_{rmp}	Resting membrane potential
WM	White matter
WT	Wild type
τ	Time constant
4-AP	4-aminopyridine

Introduction

Our capacity to experience and interact with the material world depends largely on our senses. Sensory systems, from receptors to sensory cortices, endow mammals with the ability to collect information on the surrounding environment across a range of modalities – visual, tactile, vestibular, auditory, gustatory, and olfactory. These sensations, in turn, form the fabric from which our perceptions are generated, that is, our capacity to recognize a speeding red Ferrari from the various, segregated sensory stimuli it elicits as it roars past in a colourful blur. The cerebral cortex in particular is believed to be critically involved in generating a mental representation of the surrounding world that serves as an interface with it. An overarching aim in systems neuroscience is therefore to deepen our understanding of how sensory cortices process incoming information from the periphery and extract meaning from it. In this endeavour, a great emphasis has been placed on elucidating the structure-function relationship of sensory cortices, and considerable effort has been invested in mapping the connections between the numerous types of neurons populating the cortex as well as in probing their response properties. Because of the sheer size and complexity of the cerebral cortex, and because of the broad diversity of its cellular composition, such a task may at first glance appear hopelessly overwhelming in spite of the many decades of diligent work it has inspired. However, important conceptual advances have offered a glimmer of hope in simplifying it. Two important concepts in functional neuroanatomy are indeed guiding research in understanding the functional organization of the cortex: cortical layers and the cortical column.

Fertile concepts in functional neuroanatomy

A striking and highly conserved feature of the neocortex is its regular, laminated structure composed of 6 layers. The first hint of a layered structure in the cortex is often credited to Francesco Gennari of Parma, who noticed a white line running horizontally in the cerebral cortex of several species and which was later named the line of Gennari ([Gennari, 1784](#)).

This observation was corroborated in 1786 by Vicq d’Azyr, personal physician of Queen Marie Antoinette, who reports rather amusingly that *“an anatomist of Pavia had made the same observation”* (Vicq d’Azyr, 1786). A more detailed and impactful description of cortical lamination would not emerge before 1840, however, when Baillarger reported his own observations on the cerebral cortex (Baillarger, 1840). He described a pattern of 6 alternating transparent and opaque layers visible in thin sections through the cortical mantle examined with transmitted light. Remarkably, these early reports derived from inspection of brain tissue with naked eye, and a determining milestone was reached when Meynert, relying on microscopic methods instead, recognized that the 6 cortical layers also differ in their cellular composition (Meynert, 1867, 1868; von Economo, 1927; Clarke and O’Malley, 1968; Gilbert, 1983). These original observations were refined following the development of the Golgi staining method. The technical leap enabled distinguished investigators such as Cajal to visualize the full morphology of individual neurons, resulting in the first elaborate descriptions of dendritic arbors, dendritic spines, and axonal ramifications (Ramon y Cajal, 1893). It rapidly became apparent that cortical layers differed not only in their cellular composition, but also in the afferent received, and the pattern of efferent connections. As an example, layer IV (LIV) receives the strongest input from the thalamus in sensory systems (Wimmer et al., 2010; Oberlaender et al., 2012), and is therefore considered the main input layer to the cortex. Thalamocortical (TC) synapses converge on spiny stellate (SpS) neurons, a cell type particularly abundant in LIV, and these neurons in turn project vertically oriented axons predominantly to LII/III and to a lesser extent to LVa, while the reciprocal connections from LII/III to LIV are sparse (Lefort et al., 2009; Staiger et al., 2015). In the somatosensory cortex, LI is the main target of projections from the motor cortex, which projects only weakly to other layers and ignores LIV almost entirely (Kinnischtzke et al., 2013). LI only contains very few neurons but is rich in the ramifications of apical dendrites of for example the large LV neurons pyramidal neurons, which project to a variety of subcortical structures (Welker et al., 1988; Mercier et al., 1990; Wright et al., 1999 and 2000). Such apparent laminar specializations in cellular makeup, inputs and outputs are naturally suggestive of a division of labour among cortical layers, such that *“in order to understand the computations being performed by the cortex, we need to understand the nature of the processing undertaken by each layer”* (Miller et al., 2001; Miller, 2003).

The second of these helpful concepts is the cortical column. As early as 1933, Lorente de Nó anticipated the existence of functionally distinct neuronal assemblies in the cerebral cortex. These elementary units are composed of afferent fibers, short axon neurons and pyramidal cells, and were postulated to form “cylinders” spanning the depths of the cortex and imparted with a coherent function (Lorente de Nó, 1949; Larriva-Sahd, 2014). The advent of electrophysiological recordings brought about the possibility to directly observe functionally distinct cortical columns, which was first carried out in a study of the cat somatosensory cortex (Mountcastle et al., 1957; Mountcastle, 1957). This seminal study used extracellular recordings to probe the responses of individual cortical neurons to a variety of mechanical stimuli delivered either to the skin (movement of hair, pressure on the skin) or to deep tissues (pressure on deep fascia or rotation of a joint). A remarkable result was that upon penetrating the cortex perpendicularly, the recording electrode encountered neurons that responded exclusively to one of these modalities – stimulation of cutaneous or deep mechanoreceptors. When the angle of penetration was slanted to 45°, however, the electrode first met neurons responding to one modality, before a transition to the other was observed as the electrode advanced deeper into the cortex. These data led Vernon B. Mountcastle to his formulation of the concept of the cortical column: “...*there is an elementary unit of organization in the somatic cortex made up of a vertical group of cells extending through all the cellular layers. The neurons of such a group are related to the same, or nearly the same, peripheral receptive field upon the body surface.*” (Mountcastle, 1957). The dimensions of the column were estimated to be below 500 µm in diameter and spanning all layers. These results were soon reinforced by similar observations from the visual cortex of cats and monkeys (Hubel and Wiesel, 1962, 1968), and much experimental evidence has since consolidated the concept, which endures as a fundamental principle of cortical organization (Lübke and Feldmeyer, 2007; da Costa and Martin, 2010; Feldmeyer et al., 2013)

The interplay of these concepts has given rise to the widely held view that cortical columns represent elementary modules in cortical processing and are home to what is referred to as a “canonical microcircuit” that can be generalized, with relatively little variation, to any area

of the neocortex (Lübke and Feldmeyer, 2007; Fox, 2008; Feldmeyer, 2012; Feldmeyer et al., 2013). According to this view, processing of input to sensory cortex is segregated between cortical columns according to their stimulus feature selectivity, and processing within a column involves a sequential, interlaminar flow of information (Lübke and Feldmeyer, 2007; Lefort et al., 2009; Feldmeyer et al., 2013). The model proposes that sensory input reaches the cortex in LIV. LIV neurons, in turn, project strongly to LII/III and, to a lesser extent, to LV. LII/III neurons heavily project to LV neurons as well, and LV projects to a variety of subcortical targets (Welker et al., 1988; Mercier et al., 1990; Wright et al., 1999 and 2000). Although a variety of other connections exist that bequeath the model considerable flexibility, these represent the most substantial connections of the canonical microcircuit and account for the sequential, thalamus – LIV – LII/III – LV – thalamus processing loop (Lübke and Feldmeyer, 2007; Lefort et al., 2009; Feldmeyer et al., 2013). What makes this concept so attractive is that it considerably simplifies experimental approaches to the sensory cortex: indeed, elucidating the intra and interlaminar flow of information within a column should shed considerable light into its function, and because the cortex is considered a juxtaposition of largely similarly organized cortical columns, the lessons learned from individual columns in individual sensory systems can easily be generalized. And indeed, contemporary descriptions of cortical circuits make liberal use of the concept of cortical columns, which conveniently accounts for experimental results – and perhaps nowhere as conveniently as in the primary somatosensory cortex of rodents, for reasons we will examine.

The rodent somatosensory system

Like many species of mammals, rodents possess an array of facial vibrissae or whiskers on each side of their snout. The relevance of whiskers to rodent perception, however, is likely to be more important in nocturnal and burrow dwelling species such as mice and rats as it is in cats or seals (Hartmann, 2011). Indeed, a classical study revealed that rats were more impaired in learning a maze when deprived of their whiskers than when deprived of vision, hearing or olfaction (Vincent, 1912), demonstrating the reliance of this species on tactile information. Individual whiskers are inserted into individual follicles, which are attached to striate muscles under voluntary control that provide exquisite control over the whisker pad

(Fox, 2008; Haidarliu et al., 2010). As a result, rodents can be observed sweeping their whiskers back and forth while engaging in exploratory behaviour, a movement referred to as “whisking” (Berg and Kleinfeld, 2003; Hartmann, 2011). A convenient hallmark of this array of whiskers is its stereotypical spatial arrangement on the animal’s snout. Indeed, follicles are aligned in five horizontal rows labelled A to E, and in vertical arcs numbered 1 to 7 (Brecht et al., 1997; Diamond and Arabzadeh, 2012). Individual whiskers can therefore be identified within a naturally occurring coordinate system with a combination of letter and number (for instance, C2 is a whisker of choice for experimenters). This arrangement has largely contributed to the success of the somatosensory pathway as a model system, as it simplifies the delivery of controlled stimulation to identical whiskers across animals.

Ample evidence exists that rodents actively sweep their whiskers along surfaces and objects in search of tactile information. Accordingly, a wide range of behaviour appear to involve the use of whiskers, starting with locomotion. Rats and mice typically display thigmotactic exploratory behaviour when introduced to a maze, indicating that whiskers are used to keep track of solid surfaces during locomotion, an observation that perhaps reflects adaptation to nesting in tunnels or a strategy aimed at minimizing vulnerable angles while exploring (Vincent, 1912; Ahl, 1986; Simons et al., 1994; Luhmann et al., 2005; Lamprea et al., 2008;). In addition, whiskers can be used to evaluate the width of an aperture such as in the gap crossing task (Jenkinson and Glickstein, 2000; Krupa et al., 2001), where rats choose whether or not to jump a gap based on sensing how distant the far edge is, indicative of their role in object localization. Whiskers are involved in sensory discrimination, and help rodent discriminate texture with high sensitivity (Guić-Robles et al., 1989; Brecht, 2007). Shapes can also be recognized using whiskers, such as triangular or round cookies (Brecht et al., 1997). A particularly telling example of shape recognition is provided by the Etruscan shrew, the smallest known living mammal. These shrews prey on insects, and rely on their whiskers to locate, recognize and bite prey, and can even be lured into attacking dummy crickets made of plastic, while they will ignore other objects of similar dimensions but different shape (Anjum et al., 2006). Interestingly, most attacks are targeted to the thorax of victims, revealing what fine a perception these animals have of their prey. A range of social behaviours involve the use of whiskers as well. Upon meeting unknown conspecifics,

rodents will engage in sniffing each other around the snout, a behaviour preceded by whisker-to-whisker contact, which may guide head placement (Wolfe et al., 2011; Lenschow and Brecht, 2015). A similar use of whiskers can be observed in boxing rats, and actively trimming the whiskers off of cagemates signals social dominance in mice (Long, 1972; Sarna et al., 2000; a behaviour also called barbering or Dalila effect and considered abnormal by some, see Garner et al., 2004). This already long yet non-exhaustive list of behaviours shows that whiskers may be as crucial a tactile organ in rodents as hands in primates.

The anatomy of the whisker sensory system has been described in great detail and is summarized in figure 1. The follicles in which whiskers are inserted consists in a large sinus encasing the so called glassy membrane that ensheathes the whisker shaft, the sinus itself being enclosed in a thick, collagenous membrane (Rice et al., 1986; Fox, 2008; Diamond and Arabzadeh, 2012). The sinus is pressurized with blood and provides stiffness to the follicle and the base of the whisker. As the whisker is bent upon contact with an object, pressure is transmitted to the walls of the turgid sinus (Ahl, 1986; Hartmann, 2011). A variety of nerve endings can be found in the follicle, including but not restricted to, Merkel receptors, Pacini corpuscles, and lanceolate endings that either wrap the follicle like a ring or are arranged vertically and run along it (Rice et al., 1986; Ebara et al., 2002). These nerve endings emanate from neurons located in the trigeminal ganglion, which provide up to 200 axons per follicle (Lee and Woolsey, 1975); unfortunately, in spite of efforts in this direction, it has not been possible as of yet to clearly assign specific nerve endings to specific neurons in the trigeminal ganglion, which would otherwise help greatly in understanding the synthesis of receptive fields along the whisker sensory system (Rice et al., 1997). Neurons of the trigeminal ganglion then project to the trigeminal nuclei of the brainstem, where a first synapse on the way to the cortex is formed. A defining feature of the whisker to cortex pathway appears here. Indeed, individual follicles are represented in the trigeminal nuclei by clusters of cells called barrelettes, which are especially visible in sections through the nucleus principalis stained for cytochrome oxidase. Together, barrelettes form a somatotopic representation of the whisker follicles arrayed on the snout (Belford and Killackey, 1979). Neurons in the trigeminal principalis then project to the thalamus, and most importantly to the ventral posteromedial nucleus (VPM). The same somatotopic

representation of the whisker pad is present in the VPM, where each whisker is represented by a so-called barreloid (Van der Loos, 1976; Lübke and Feldmeyer, 2007; Petersen, 2007; Brecht, 2007; Diamond et al., 2008; Fox, 22008; Feldmeyer et al., 2013).

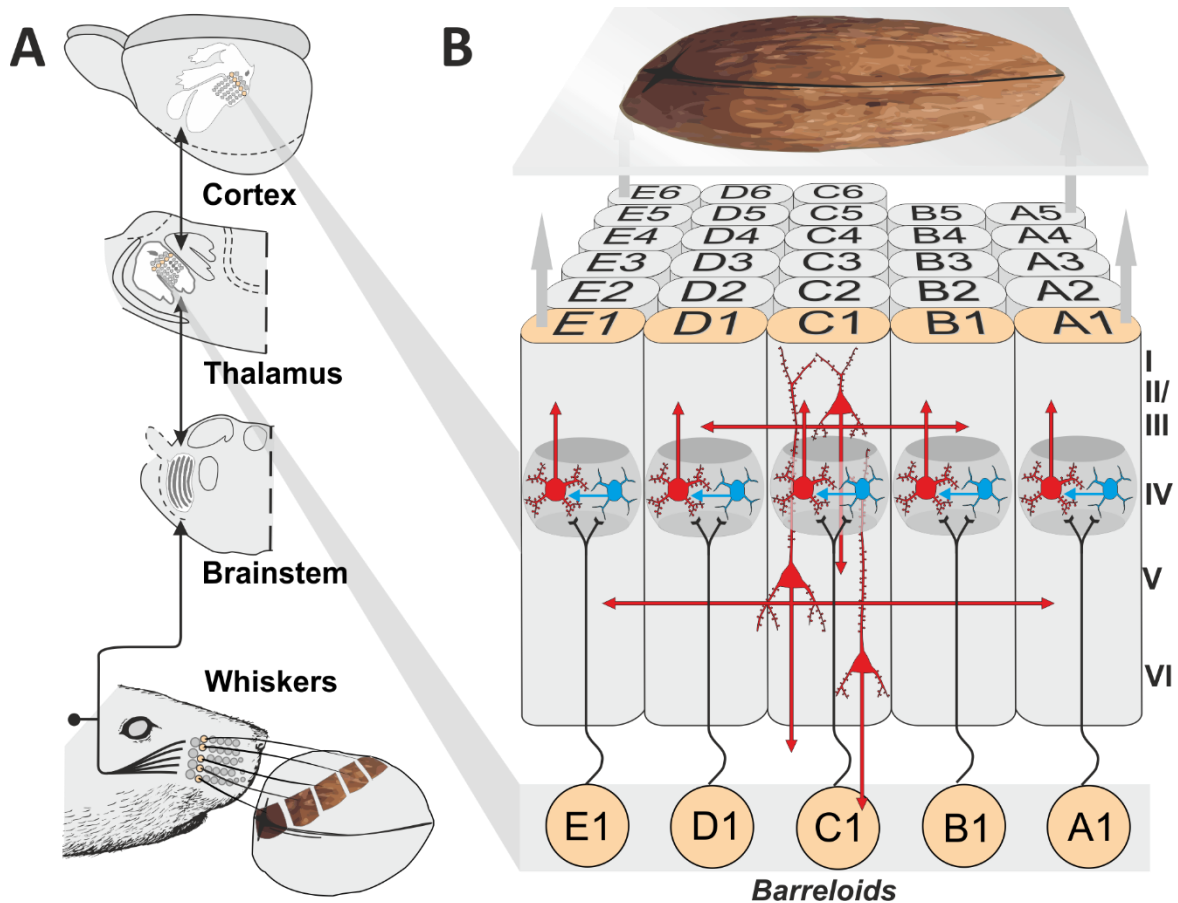


Figure 1. Anatomy of the whisker to barrel pathway and the organization of the somatosensory cortex. **A:** the whisker to barrel pathway. Rats and mice actively use whiskers on their snout to palpate surrounding objects, such as a walnut. Axons innervating the whisker follicles and originating from the trigeminal ganglion carry tactile information to the trigeminal nuclei of the brainstem, which in turn projects to the ventral posteromedial nucleus of the thalamus; thalamocortical axons finally bring this information to the cortex. A somatotopic representation of the whiskers can be found at each stage of the pathway, composed of barrelettes in the brainstem, barreloids in the thalamus and barrels in the cortex. **B:** functional organization of the barrel cortex and canonical microcircuit. Individual whiskers can be identified by a letter and a number corresponding to their position within the arcs and rows formed by the follicles, respectively. Each whisker is represented by a single barrel in the cortex, and each barrel defines the dimensions of a barrel-related column. Stereotyped patterns of connectivity, commonly referred to as the canonical microcircuit, unite the cortical layers that subdivide cortical columns. Briefly, individual barreloids in the thalamus project to the corresponding cortical barrel in a one-to-one fashion. Input reaches the cortex primarily through

LIV, which projects to LII/III and LV and therefore distributes thalamic input to the cortical network. LV projects back to the thalamus, closing the thalamo-cortico-thalamic loop. Individual columns are not separate processing channels, but communicate strongly through horizontal, cortico-cortical connections originating in LV and LII/III. Concerted integration of sensory information reaching the cortex through segregated pathways by cortical columns working in unison is thought to enable the cortex to reconstruct a mental representation of the walnut, that is: a perception. Courtesy of Dr. Dirk Schubert and Prof. Jochen Staiger.

The next step in the whisker sensory system is the primary somatosensory cortex itself, which receives extensive thalamic input. TC fibers from the VPM terminate predominantly in LIV, and to a lesser degree, at the LV/LVI border ([Wimmer et al., 2010](#); [Oberlaender et al., 2012](#)). LIV is remarkable for it contains the so-called barrels, clusters of neurons which correspond to the barreloids and barrelettes occurring at earlier stages of the pathway ([Woolsey and Van der Loos, 1970](#)). Together, barrels form the barrel field, a somatotopic representation of the whiskers on the snout ([Woolsey and Van der Loos, 1970](#); [Masino et al., 1993](#); [Kleinfeld and Delaney, 1996](#)). Indeed, numerous studies have demonstrated that neurons within the barrel strongly respond to a stimulation of the corresponding whisker and with short latencies ([Armstrong-James and Fox, 1987](#); [Brecht and Sakmann, 2002](#)). Responses can also be evoked by stimulation of neighbouring whiskers, albeit weaker and at increased latencies, hence the notion that the receptive fields of barrel related neurons include a principal whisker as well as a number of adjacent whiskers ([Zhu and Connors, 1997](#); [Brecht and Sakmann, 2002](#)). Three types of excitatory neurons populate the barrels, namely, pyramidal, star pyramidal and SpS neurons ([Feldmeyer et al., 1999](#); [Schubert et al., 2003](#); [Staiger et al., 2004](#)). The SpS are of particular interest, as they receive much of the VPM input to the cortex, and possess unique properties ([Benshalom and White, 1986](#)). Morphologically, these cells differ from other excitatory neurons in that they do not possess an apical dendrite. Their dendritic arbor consists in 4-6 dendrites which are largely confined within the border of their home barrel ([Simons and Woolsey, 1984](#); [Staiger et al., 2004](#)). The dendrites are covered with numerous spines, which are the target of thalamic axons. 10 to 25% of all excitatory synapses are TC synapses, a larger proportion than other excitatory neurons, and the overwhelming majority of TC synapses are formed on dendritic spines

(Benshalom and White, 1986). SpS neurons predominantly project to LII/III, and to a lesser extent, LV. Projections to neighbouring barrels are scarce (Staiger et al., 2004; Schubert et al., 2007). Given their strong thalamic input, pattern of output projections, and response properties, these neurons are well suited to initiate the cascade of sequential interlaminar processing proposed in the canonical microcircuit.

A great advantage of the barrel cortex as a model system is derived from its characteristic functional organization: mentally extending the perimeter of a barrel through the depth of the cortex allows one to define a “barrel related column”, or in other words, every barrel specifies the location and approximate borders of an individual cortical column. The barrel cortex is therefore a very suitable system in which to study sensory processing within and across columns (Brecht, 2007; Lübke and Feldmeyer, 2007; Feldmeyer et al., 2013).

Together with the ease with which whisker stimulation can be controlled, and the convenient “built-in” coordinate system of this cortical area, this has led the barrel cortex to become a model of choice in the last few decades.

A mutant that questions cortical layers

A central aspect of the columnar hypothesis is that specific functions can be assigned to the specific layer compartments it is made of, and that these functions are subserved by the specific, non-random connectivity that links layers together. It is therefore interesting to consider what would happen in a cortex devoid of cortical layers.

The *reeler* mouse provides a model in which such a question is amenable to experimental scrutiny. The mutant first appeared spontaneously in 1948 at the Institute of Animal Genetics in Edinburgh (Falconer, 1951; D’Arcangelo, 1998). The gene affected encodes for the extracellular matrix protein reelin, and the mutation consist in an autosomal deletion in excess of 150 kb resulting in the loss of reelin expression. The roles of reelin are diverse and not fully elucidated (Förster et al., 2010), but considerable amount of research highlights its role in cortical development (Caviness, 1982; D’Arcangelo et al., 1995; Frotscher, 1998).

Indeed, reelin is expressed in Cajal-Retzius cells, a transient type of cells that populates the marginal zone (destined to become layer I) during development. Through binding to its receptors, ApoEr2 and VLDLr, reelin guides the migration of newborn neurons along radial glia into their destined position within their home layers (although the exact function of reelin as a stop signal or chemoattractant for migrating neurons remains a complex matter, see [Zhao and Frotscher, 2010](#); [Tissir and Goffinet, 2003](#)). The absence of reelin or its receptors disturbs the process of cortical development and formation of layered structures. In *reeler* mice, the brain displays an abnormally reduced size and the cerebellum in particular displays severe hypoplasia, a cellular dispersion, and a dramatic reduction in the number of Purkinje neurons ([Heckroth et al., 1989](#); [Badea et al., 2007](#)). These cerebellar abnormalities may account for the severe locomotor deficits these animals suffer from ([Falconer 1951](#)). Neurons in the hippocampus, another layered structure, are also dispersed and layers hardly recognizable. ([Caviness and Sidman, 1973](#); [Stanfield and Cowan, 1979](#); [Boyle et al., 2011](#))

The extent of disruption of layered structures is nowhere as striking as in the cerebral cortex, however. The nature of the disorganization was initially described to be an inversion of the cortical layers ([Caviness and Sidman, 1973](#); [Caviness, 1982](#); [D’Arcangelo, 1995](#)). It was proposed that the normal “inside out” pattern of cortical layers resulting from brain development was inverted into an “outside in” pattern, one in which LVI would be just underneath the pia and LI close to the white matter. More recent results indicate a far more chaotic pattern of cellular dispersion ([Wagener et al., 2010](#); [Dekimoto et al., 2010](#); [Boyle et al., 2011](#); [Wagener et al., 2015](#)). To make matters even more complex, the exact nature of the dispersion appears to depend on the cortical area examined. In the motor cortex, for instance, neurons destined to LII/III, IV and V are massively intermingled, although they still arrange themselves in the proper order. LVI neurons, however, are massively present close to the pia and the white matter, essentially flanking other cell types in a sandwich-like pattern ([Mingo Moreno and Wagener](#); unpublished results from our laboratory). This is in contrast with the visual cortex, where cells are also massively intermingled, but with a tendency towards an inverted pattern of layering as the majority of LV and LVI fated cells are found close to the pial surface. The somatosensory cortex presents yet another pattern

of disorganization, with LII/III and LIV fated cells broadly scattered around the middle of the cortical depth and sandwiched by LV and LVI-fated cells, resulting in a so-called “mirror image” in the cortex (see figure 2). A similar pattern is observed in the auditory cortex. The loss of proper cortical layering is therefore a ubiquitous feature in the *reeler* cortex, even though the precise pattern of cellular disorganization can vary from one area to another (Dekimoto et al., 2010; Boyle et al., 2011).

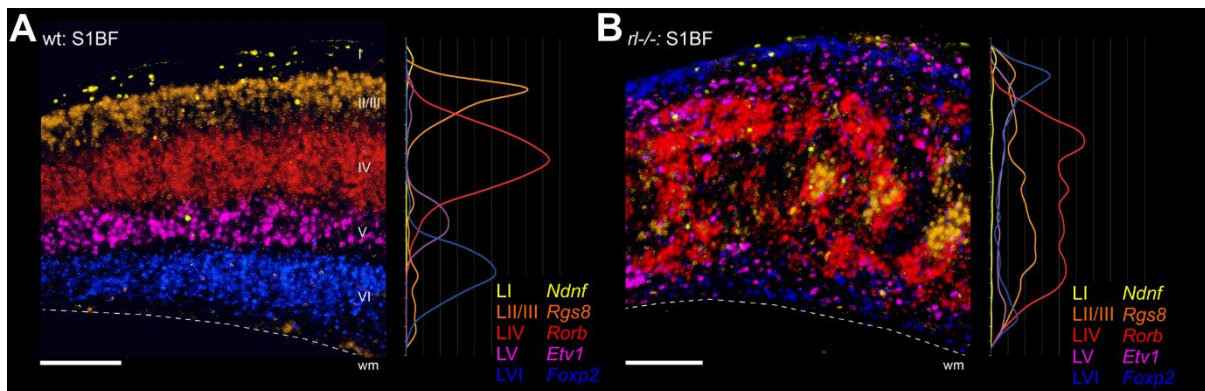


Figure 2. Cortical lamination defect in the *reeler* somatosensory cortex. Coronal sections through the somatosensory cortex of wild type (WT, **A**) and *reeler* (**B**) mice. Cortical layers were visualized with chromogen in situ hybridization for layer specific mRNA in separate sections, and merged into a pseudocolor representation. The pattern of mRNA expression in the WT cortex reveals the well described laminar architecture of the cortex composed of 6 distinct layers (**A**), summarized in a density plot to the right of the photomontage. This ordered pattern is absent from the *reeler* cortex, which shows extensive cellular dispersion instead (**B**). Scalebar: 250 μ m; wm: white matter. Courtesy of Dr. Robin Wagener.

The extensive abnormalities described in *reeler* naturally raises questions about the connectivity and functional organization of its sensory cortex. These questions are especially interesting considering the fact that abnormal connectivity has been described in other systems. In the cerebellum, for instance, aberrant input has been described in the form of synapses from mossy fibers on Purkinje neurons, in addition to ectopic synapses between granule cells and Purkinje neurons (Mariani et al., 1977). In the *reeler* hippocampus, a large

fraction of mossy cells have been found to receive aberrant, direct input from the performant path (Kowalski et al., 2010). Such misconnections may have important functional consequences and warrant further investigation in the functional connectivity of the *reeler* sensory cortex. In this regard, it seems intuitive to first ask whether input from the thalamus can still find its targets in the extensively disorganized cortex of *reeler*.

In the somatosensory cortex, TC input mainly targets LIV barrels. Early studies yielded contradictory results as to whether or not barrels can form at all in *reeler*, but an abundance of research has since demonstrated the existence of dense clusters of cells reminiscent of barrels (Cragg, 1975; Caviness et al., 1976; Welt and Steindler, 1977). However these “barrels equivalent” structures present some abnormalities, in that their radial span is far greater than that of LIV in normal mouse, giving them the appearance of being smeared over the depth of the cortex (Caviness et al., 1976). In addition, their orientation through the cortex often appears slightly oblique rather than purely radial, and their borders are somewhat fuzzy with respect to wild type (WT) barrels. In spite of the altered shape of barrel equivalents and the massive cellular dispersion reported above, tracing studies found that TC fibers seem to find their ectopic, LIV equivalent targets (Steindler et al., 1976; Caviness and Frost, 1983; Wagener et al., 2010). The trajectories of the fibers are not unaffected, however. In a normal brain, TC fibers travel tangentially through the white matter towards their terminal fields; upon reaching them they ascend radially towards layer IV and substantially ramify there. In *reeler*, TC fibers extend towards the pia in an oblique fashion as they exit the internal capsule, run tangentially along the pia to their terminal fields, before diving back into the cortex towards their targets (Caviness and Frost, 1983; Harsan et al., 2013). The specificity of the TC input to the *reeler* cortex with respect to the cell type targeted is evidenced by the fact that the distribution of TC boutons extensively overlap with populations of neurons labelled using a LIV specific marker (Wagener et al., 2015). Thus it appears that TC input does indeed reach LIV equivalent neurons in the somatosensory cortex of the *reeler* mouse, an observation which has been obtained in the visual cortex as well (Pielecka-Fortuna et al., 2014).

Simply observing an apparent colocalization of TC fibers and LIV equivalent neurons is insufficient to demonstrate proper connectivity, however. Indeed, in the context of the somatosensory cortex, it is possible in principle for TC fibers to reach LIV equivalent neurons, but in a way that does not obey the somatotopy observed in WT mice. In other words, the establishment of columnar modules segregated by thalamic input may be compromised in *reeler*. It is therefore of great interest to resort to functional methods to determine whether somatotopy is preserved as all. When the study reported here was initiated, very little effort had been invested in solving this puzzle. To our knowledge, our laboratory had provided the only study addressing this question ([Wagener et al., 2010](#)). The approach was based on the use of the staining of c-fos, an immediate early gene, as a marker for neuronal activity ([Dragunow and Faull, 1989](#); [Staiger et al., 2002](#)). Animals of both genotypes were allowed to freely explore a new, enriched environment for two hours after some of their whiskers had been clipped. At this end of this period, animals were perfused, their brains sectioned, and c-fos staining was performed on sections through the somatosensory cortex, thalamus, and brainstem. C-fos expression in the cortex was present only in those barrel equivalent columns that were activated by sensory stimulation, that is, those barrel equivalents whose corresponding whisker had not been clipped. In tangential sections through the barrel field, the pattern formed by spared columns was in agreement with a somatotopic arrangement of barrel equivalents in *reeler*. Somatotopy was also observed in the VPM as well as in the brainstem. In addition, the number of c-fos positive neurons in apparent *reeler* columns was similar to that in the WT, suggesting that cortical networks were equally active in both genotypes. The study concluded that in spite of absent layering, the *reeler* cortex underwent proper formation and somatotopic activation of columnar modules. It therefore appears that the presence of layers as such is not a prerequisite for the formation and function of cortical columns.

While the study established the existence of somatotopy in the *reeler* barrel field on a functional basis, many questions are left open by the use of c-fos combined with the stimulus paradigm chosen – free exploration. Indeed, c-fos may not reveal differences between the genotypes in term of functional activation, as *reeler* animals may have compensated for potential sensory deficits by adapting their exploratory strategy. For

instance, it is conceivable that *reeler* animals would spend more time investigating an object, completing a higher count of whisker-to-object contacts, in the case where the responsiveness of their cortical networks to sensory input is weaker. This possibility is not only theoretical: single unit extracellular recordings in the visual cortex of *reeler* have already found lower overall firing rates in response to visual stimulation (Dräger, 1981). Ideally, a more accurate estimate of cortical responsiveness would combine a precise control over the stimulation with a global measure of neuronal activity such as local field potential or functional imaging techniques. Even these methods, however, may lack the sensitivity to detect some of the more subtle alterations in the *reeler* brain that have been documented so far.

Indeed, a number of alterations in the properties of individual neurons have been found in *reeler*. In the mutant hippocampus for example, the action potential (AP) timing jitter of mossy cells is substantially more heterogeneous than in WT animals (Kowalski et al., 2010). Temporal imprecision in a neuronal network can blunt its computational capabilities, because feedforward and feedback inhibition impose temporal constraints to the integration of EPSPs in individual neurons, such that excitatory input requires a degree of synchronization to be optimally effective (Wehr and Zador, 2003; Wilent and Contreras, 2005; Bruno and Sakmann, 2006). The morphology of several neuronal types has been found to be altered in *reeler* as well. In the cerebellum, Purkinje neurons have abnormally oriented dendrites (Heckroth et al., 1989), and the dendrites of hippocampal granule cells display similar alterations (Stanfield and Cowan, 1979). Our own lab has also observed that cortical pyramidal neurons have abnormally oriented apical dendrites, with an oblique or even tangential orientation instead of radial. Because the dendritic field of a neuron provides the anatomical substrate on which specific connections are established, abnormally structured dendrites can potentially indicate aberrant input, as has been documented in the cerebellum and hippocampus (Mariani et al., 1977; Kowalski et al., 2010). Intrinsic electrophysiological properties of individual neurons may be altered too, in a way that can affect the response to incoming input. In hippocampal and neocortical LV neurons, reelin is crucial in establishing the gradient of HCN1 channels that underlie the gradient in the hyperpolarization-activated cation current (I_h , Magee, 1998; Kupferman et

al., 2014). Downregulation of Disabled-1 (Dab1) expression, a crucial molecular partner in the signalling cascade initiated by the binding of reelin to its receptors, results in a collapse of I_h in the distal apical dendrites of these large neurons, together with a marked increase in input resistance and a more hyperpolarized resting membrane potential (Kupferman et al., 2014). Beyond the fact that I_h itself regulates temporal summation of EPSPs in distal dendrites, changes in input resistance and resting membrane potential can easily affect the general responsiveness of these neurons to synaptic input. Unfortunately, virtually nothing is known about the properties of identified, LIV equivalent neurons in *reeler* that permits speculation as to their responsiveness to thalamic input.

In summary, the somatosensory cortex of the *reeler* mutant mouse is devoid of cortical layers. Barrel equivalent structures nonetheless seem to form properly, and input from the thalamus find their ectopic targets in a way that preserves somatotopy, suggesting that the establishment of columnar modules does not necessitate the presence of cortical layers. A quantitative description of the strength of responses of the cortical network to controlled stimulation is still lacking, however. In addition, virtually nothing is known of the physiological properties of thalamic input to defined neuronal classes in *reeler*. The present study aims at clarifying these points, in an effort to further document the abnormalities – or lack thereof – in the organization and function of the *reeler* barrel cortex.

Aims and approaches

The purpose of the work presented here is to elucidate some aspects of the functional connectivity of the *reeler* cortex about which knowledge is either incomplete or completely lacking. On the one hand, as mentioned above, an evaluation of cortical responses evoked by controlled stimulation is lacking, and the evidence for somatotopy our laboratory has gathered in the past was obtained from post mortem material (Wagener et al., 2010). We therefore probed the functional activation of *reeler* somatosensory cortex using *in vivo* functional imaging (Masino et al., 1993). On the other hand, investigating the functional connectivity of a network necessitates to obtain information on the connectivity of the variety of neuronal classes that compose the network. In order to further document this

little investigated issue, we resorted to *in vitro* patch clamp in TC slices of *reeler* and WT animals (Porter et al., 2001).

The aims of our functional imaging study were to obtain a confirmation of somatotopy in the *reeler* barrel cortex, as well as a more accurate measure of evoked responses. This work was carried out in animals anesthetised with urethane, which has the advantage of providing long lasting anaesthesia with relatively mild disturbance of cortical networks (Simons et al., 1992; Friedberg et al., 1999). The anesthetised preparation also made it possible to tightly control the parameters of individual whisker stimulation using a computer controlled piezo actuator. Such arrangement enabled us to test the responses to a variety of stimulus frequencies and investigate the dynamic range in which cortex represents stimulation. By stimulated up to nine whiskers sequentially, it was possible to probe the functional organization of the cortex and verify the presence or absence of somatotopy. The imaging technique chosen was intrinsic signal optical imaging (ISOI), a functional imaging method that relies on hemodynamic signals as a surrogate measure for neuronal activity (Vanzetta and Grinvald, 2008). The method can be readily applied to anesthetized animals, provides good spatial and decent temporal resolution and importantly, has a long history of use in probing the functional organization of sensory cortex, including barrel cortex (Grinvald et al., 1986; Frostig et al., 1990; Masino et al., 1993). The results we obtained in this way about the organization of the *reeler* cortex were the first of their kind ever published, and form a substantial part of the present thesis.

The other approach we used, and which forms another part of this thesis, was to investigate the electrophysiological properties and functional connectivity of individual, defined neurons in the *reeler* cortex. Such an approach complements well that based on functional imaging, which does not capture sensory transmission on a cellular level. We decided to restrict our investigation to LIV equivalent neurons in *reeler*. Indeed, LIV neurons receive much of the thalamic input to the cortex in WT animals, and it appeared intuitive to start our investigation of the *reeler* cortical network with what is considered its input stage. More specifically, we decided to investigate the properties of thalamic input to SpS neurons, by

means of *in vitro* patch clamp on TC slices. In order to control thalamic input, we introduced channelrhodopsin 2 into thalamic relay neurons by injection of a viral vector to the VPM. A laser was then used to specifically stimulate thalamic fibers while recording the responses from SpS neurons. These results, together with the electrophysiological and morphological characterizations of the recorded neurons, provide the first detailed description of the properties of SpS neurons in *reeler*, the first neurons in the cortex to process incoming thalamic input.

A major challenge in the study of defined cell types in fresh slices of the *reeler* cortex is that it is nigh impossible to identify neurons a priori based on their location (depth) in the cortex, due to the absence of cortical lamination characteristic of this mutant. Yet, the ability to specifically label and locate LIV equivalent neurons is instrumental in mapping the sensory representation of individual whiskers with respect to underlying anatomical barrels when looking for somatotopy, and it is absolutely essential when attempting to record from SpS neurons during electrophysiological experiments. In order to specifically visualize LIV equivalent neurons, we used the LIV^{tdTomato} mouse line, where LIV neurons and their equivalents in *reeler* are readily recognizable for the fact that they express the tdTomato fluorescent protein (Madisen et al, 2010; Guy et al., 2014). The mouse line was developed in the laboratory of Prof. Jochen F. Staiger by Dr. Robin Wagener, and a brief description of the distribution of tdTomato positive neurons in the brain of such animals, which constitute a further innovation in the study of cortical networks in *reeler*, will follow.

Visualization of the barrel field in LIV^{tdTomato} animals

In LIV^{tdTomato} *reeler* and WT mice lines, Cre recombinase is expressed under the Scnn1a promoter (non-voltage gated sodium channel, subunit alpha) while tdTomato is expressed in a Cre dependent manner (Madisen et al., 2010). The resulting distribution of dTomato positive cells is illustrated in figure 3, where figure 3 A and C are photographs of coronal and tangential sections through the somatosensory cortices of a WT mouse, respectively. In the coronal section, dTomato positive cells are found in LIV of the neocortex and to a lesser degree in thalamic structures, with the strongest expression located in the posterior medial

barrel subfield (PMBSF). More specifically, dTomato positive cells form barrels in LIV of the PMBSF (examples are marked with white asterisks in figure 3). Such structures are also obvious in a tangential section through the PMBSF (figure 3 C), where the characteristic barrel field, organized in arcs and rows, is visible and individual barrels can indeed be recognized (Woolsey and Van der Loos, 1970; Welker and Woolsey, 1974; Welker, 1976). Thus, dTomato expression appears to be enriched in LIV of the LIV^{tdTomato} mouse cortex and can hence provide a mean to reliably identify single barrels in WT animals and their equivalents in *reeler*. Clusters of dTomato expressing cells are also present in the cortex of *reeler* animals (figure 3 B) although they are not restricted to a single layer but span almost the entire cortical thickness, in agreement with the loss of lamination characteristic of this mutant (Boyle et al., 2011; Dekimoto et al., 2010; Wagener et al., 2010). These clusters are also visible in tangential sections (figure 3 D) where they form a recognizable barrel field. A previous study from our laboratory established that barrel equivalents in *reeler* have a significantly less symmetrical shape than their WT counterpart, are smaller, but occupy a proportionally equivalent size when taking the overall hypotrophy of the *reeler* brain into account (Wagener et al., 2010). The cellular composition of the *reeler* cortex has been the subject of scrutiny as well, revealing for instance that the total number of cells within a radial column does not differ from WT (Goffinet et al., 1984; Polleux et al., 1998). Although the composition of the cortical neuronal population has been shown to differ between genotypes, with a relative increase in the proportion of late generated neurons and a corresponding decrease in the share of early generated neurons in *reeler* (Polleux et al., 1998), the number of LIV equivalent cells, which form barrel-like clusters, does not differ from WT (Wagener et al., 2010). The study presented here benefited immensely from the capacity to identify LIV cells based on Cre driven fluorescence that the LIV^{tdTomato} lines provide.

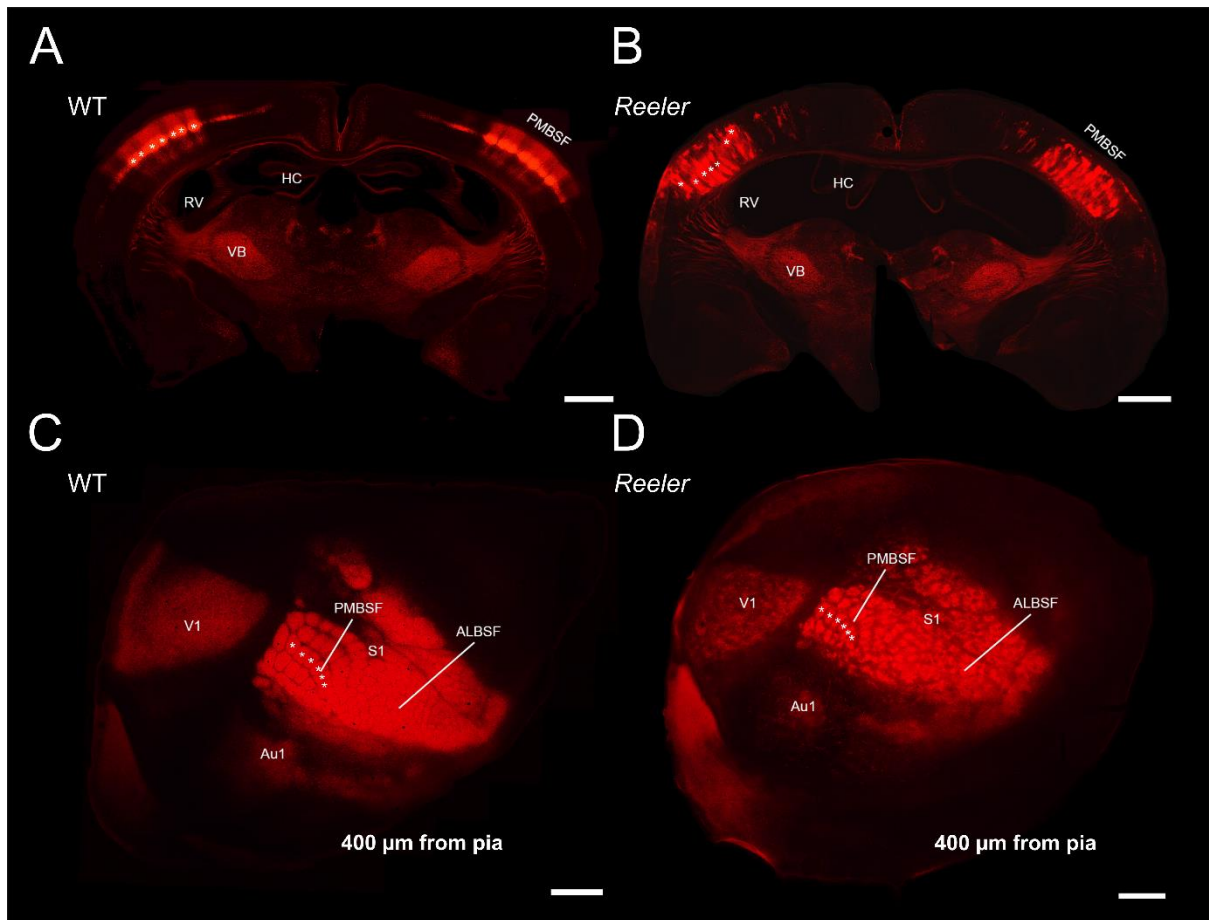


Figure 3. Cytoarchitecture of the barrel field in $LIV^{tdTomato}$ WT and reeler mice. **A, B:** coronal sections through the barrel field of $LIV^{tdTomato}$ WT and reeler respectively. **C, D:** tangential sections through the barrel field of $LIV^{tdTomato}$ WT and reeler respectively. A subset of barrels and barrel equivalents clusters of dTomato positive cells are marked for comparison (white asterisks). Both sections were obtained from comparable depths of about 400 μm below the pia. ALBSF: Anterior Lateral Barrel Subfield; Au1: primary auditory cortex; HC: Hippocampus; PMBSF: Posterior Medial Barrel Subfield; RV: Right Ventricle; V1: primary visual cortex; VB: Ventrobasal nucleus. Scale bar: 1000 μm . Data and figure created by Dr. Robin Wagener. Reproduced from Guy et al., 2014 under the terms of the Creative Commons Attribution Non-commercial License.

Material and methods

Animals

All animal experiments were carried out in accordance with institutional regulations regarding animal use in research. All animals were housed with a 12h light/dark cycle with food and water *ad libitum* prior to the experiments.

Mice line used

Two *reeler* mice lines were used in the study presented here. One is the B6C3Fe line, maintained by the Jackson Laboratory ([D'Arcangelo and Curran, 1998](#)). The other line is henceforth referred to as LIV^{tdTomato}.

Briefly, LIV^{tdTomato} were generated by first crossing heterozygous *reeler* animals (B6C3Fe Reln[±]) with Scnn1a-Tg3-Cre mice (full strain name: B6.Cg-Tg(Scnn1a-cre)3Aibs/J; Stock Number: 009613, Jackson Laboratory). The resulting Scnn1a-Tg3-Cre *reelers* were then crossed again with each other and animals homozygous for Scnn1a and heterozygous for the mutation of *reelin* were chosen for further crossings. ROSA-Tomato-LSL mice (full strain name: B6; 129S6-Gt(ROSA)26Sortm9(CAG-tdTomato)Hze/J; Stock number:007905; Jackson Laboratory) were crossed with heterozygous *reeler* in the same way, the resulting strain was called ROSA-Tomato-LSL *reeler*. Crossing of Scnn1a-Tg3-Cre *reeler* and Tomato-LSL *reeler* resulted in LIV specific expression of tdTomato in LIV fated cells. Thus, the respective mouse line was called LIV^{tdTomato}.

Regardless of the *reeler* mouse line used in specific experiments, WT animals of the same line served as controls and heterozygous *reeler* were excluded. Animals of both sexes were used.

In vivo functional imaging

Two types of functional imaging experiments were conducted on separate subsets of animals.

In a first set of experiments, we mapped the functional representation of 9 whiskers, namely C2 and its eight immediate neighbours, in 6 B6C3Fe WT and 7 B6C3Fe *reeler* mice. A subset of experiments were performed on LIV^{tdTomato} WT and *reeler* (n=2 animals per group).

In a second series of experiments, we determined the mean amplitude and area of the intrinsic signals evoked by stimulation of whisker C2 at discrete frequencies (1, 5, 10 and 25 Hz). 11 B6C3Fe WT and 12 B6C3Fe *reeler* mice were used for that purpose.

Labelling of blood vessels

A further 6 B6C3Fe WT and 6 B6C3Fe *reeler* were used in order to obtain a staining of blood vessels in the barrel cortex.

In vitro electrophysiology

A total of 34 LIV^{tdTomato} mice were included in experiments with *in vitro* electrophysiology and optogenetics, 20 of which WT and 14 *reeler*.

Optic chamber implantation

In order to perform functional imaging on anesthetized animal, a surgery aimed at implanting an optical chamber over the barrel cortex was required, the purpose of which is to enable stable delivery of light to, and recording of reflected light from, the underlying cortical structures. Surgery was performed on all animals used for intrinsic signal optical imaging experiments (n=27). Mice were anesthetized with intraperitoneal injection of urethane (1.8 g/kg, Sigma-Aldrich) dissolved in a 0.9% sodium chloride solution. Atropine (0.5 mg/kg, Sigma-Aldrich) was injected subcutaneously to minimize breathing impairment caused by urethane. Body temperature was maintained at 37°C with a heating pad (ATC 1000, World Precision Instruments) and a life monitoring system was used to monitor breathing rate, heart rate and blood oxygen levels throughout the experiment (Mouse Ox, Starr Life Science Corp.). Data obtained during the functional imaging experiments were

discarded if the oxygen saturation level dropped below 80%. Depth of anaesthesia was monitored by breath rate and by the response to a noxious stimulus delivered to the hind paw. Lidocaine (Xylocaine 2%, AstraZeneca) was injected subcutaneously under the scalp to provide local analgesia. The scalp was dissected out to reveal the skull, and a custom built head post was attached to the right side of the skull with cyanoacrylate adhesive to facilitate head fixation during imaging. The skull over the left somatosensory cortex was carefully thinned to transparency with a dental drill (OS-40, Osada Electric Company) under regular cooling from a 0,9% sodium chloride solution. A ring of dental cement was raised around the resulting cranial window, filled with saline, topped with an 8 mm diameter round cover glass (Electron Microscopy Sciences) and sealed with vaseline, thus forming an optic chamber through which illumination of, and image acquisition from the somatosensory cortex was possible. Functional imaging experiments started immediately following the conclusion of surgery with the same anaesthetic regimen.

Whisker stimulation

Functional activation of the barrel cortex during imaging experiments was brought about by stimulation of the whiskers of anesthetized animals. The whiskers on the contralateral side of the snout were shaved except C2 and its eight immediately adjacent neighbours, which were trimmed to about 1 cm in length instead. Stimulation was achieved by inserting individual whiskers into a glass capillary (1.5 mm outer diameter, World Precision Instruments) glued to a piezo actuator activated by a computer controlled amplifier (E-650 LVPZT, Physik Instrumente). Stimulation consisted in rostro-caudal deflections of about 1 mm, delivered for 2 seconds at controlled frequencies (1, 5, 10 or 25 Hz).

Intrinsic signal optical imaging

In order to acquire images from the cortex, we used a CCD camera (Adimec 1000m, Adimec) mounted on a tandem lens assembly composed of a 50 mm Nikon bottom lens adapted on a 135 mm Nikon top lens for a final magnification of 2.7x. The maximum resolution of the CCD camera was 1000*1000 pixels with a final pixel size of about 2.8*2.8 μm . The CCD camera was coupled to an Imager 3001 data acquisition system (Optical Imaging). We obtained pictures of the superficial blood vessel pattern by focusing the camera on the pial surface while illuminating the cortex with a 100W halogen lamp with stable power supply (Kepco

ATE 15-15M, Kepco), filtered through a 546 nm filter, in order to enhance contrast between blood vessels and surrounding parenchyma. For functional imaging, the focal plane was subsequently moved 300 μm below the pial surface and the illumination wavelength was changed to 630 nm by exchanging filters. The light intensity was adjusted to just below camera saturation in every experiment.

Two data sets were obtained from our experiments. When mapping cortical representation of nine individual whiskers in LIV^{tdTomato} animals, (n=17), full resolution data frames were acquired at a rate of 50 frames per second (fps) and binned to a rate of 5 fps. Data acquisition started 0.2 s after stimulation onset and lasted 2 s, with 30 s between individual trials, and the stimulation was delivered at 5 Hz for 2 s. 30 trials were averaged in order to improve signal to noise ratio. This data set was used to localize the functional representations of individual whisker with respect to one another.

In another set of experiments, a separate data set was obtained on which to quantify the amplitude and area of the intrinsic signal evoked by whisker stimulation (n= 11 B6C3Fe WT and 12 B6C3Fe *reeler*). In these experiments, data frames were acquired as described above with an additional 9x9 spatial binning. Data acquisition started 15 s before stimulation onset and lasted 36 s, with 60 s between individual trials. Whisker stimulation lasted 2 s and was delivered to whisker C2 at varying frequencies (see below). 20 trials were averaged for every stimulus condition. Whisker stimulation and data acquisition were synchronized with custom written LabVIEW routines (National Instruments).

Perfusion and tissue collection

At the end of the imaging experiments, animals were given an overdose of urethane intraperitoneally and were transcardially perfused with 10% sucrose followed by a 4% paraformaldehyde (PFA) solution containing 15% (vol/vol) picric acid in 0.1 M phosphate buffer (PB). The brain was collected; the cortex over the left hemisphere was dissected out, flattened, and postfixed overnight in the same fixative ([Welker and Woolsey, 1974](#)).

Animals used for staining of blood vessels were given an overdose of ketamine hydrochloride intraperitoneally and decapitated before the brain was dissected out and

fixed by immersion in 4% PFA-15% picric acid in 0.1 M PB overnight. Because the quantification of blood vessel density in the cortex relied on the presence of erythrocytes as a surrogate marker for blood vessels, we did not perform transcardial perfusion in order to minimize blood loss from the brain.

Stereotaxic injections

Stereotaxic injections were carried out on animal destined for *in vitro* electrophysiology experiments. The purpose of the injections was to provide a means of stimulating VPM fibers reaching the cortex by having VPM neurons express channelrhodopsin-2 (ChR2). To that effect, adeno-associated virus (AAV5) particles carrying the hSyn.hChR2(H134R)-eYFP vector (Addgene 26973P) were purchased from Penn Vector Core (Perelman School of Medicine, University of Pennsylvania). Stereotaxic injections of AAV5 in the VPM were performed on 21 days old *reeler* and WT mice unless their body weight remained below 5 g, in which case surgery was delayed until the animal reached 5 g. Anesthesia was induced in a sealed transparent container filled with 5% isoflurane delivered in pure oxygen. Once sedated, mice were quickly transferred to a stereotaxic apparatus (Kopf Instruments), where anesthesia was maintained with 1-2% isoflurane in pure oxygen delivered through a mask. Depth of anesthesia was monitored throughout the surgery by visual inspection of the breathing rate and the response to a noxious stimulus delivered to the hind limb, and body temperature was maintained at 37°C with a thermostatic heating pad. The eyes were protected from desiccation by application of ointment (Bepanthen, Bayer). Subcutaneous injections of lidocaine provided local analgesia to incision sites. The scalp was incised along a rostro caudal axis, and a small craniotomy was opened over the VPM of each hemisphere. Long tapered, thin (tip diameter ~20 microns) injection capillaries pulled from borosilicate glass (GB150F-8P, Science Products) using a P-97 puller (Sutter Instruments) were front filled with a solution of AAV5 in phosphate buffer (titer approximately 2.84×10^9 particles/ μ l). The injection capillaries were then lowered into the brain at standard coordinates from Bregma (in mm): -1.7 antero-posterior (AP), +/- 1.75 medio-lateral (ML) and -3.25 dorso-ventral (DV). Because of the generally small and variable size of juvenile mice, a correction factor often needed to be calculated for individual animals and applied to the standard coordinates. Briefly, given an expected Bregma-Lambda distance of 4.2 mm in

adult mice (Paxinos and Franklin, 2001) and a measured Bregma-Lamda distance of D, the corrected injection coordinates were calculated as follows (from Bregma, in mm):

$$AP = -1.7 * \left(\frac{D}{4.2} \right)$$

$$ML = \pm 1.75 * \left(\frac{D}{4.2} \right)$$

$$DV = - \left(\frac{2}{3} * \left(1 - \frac{D}{4.2} \right) + D \right) * 3.25$$

Volumes of 200 to 300 nl of virus containing solution were pressure-injected in each site using a PDES-02DX picospritzer (Npi). The scalp was sutured immediately after retraction of the capillary and the animal was allowed to recover. Carprofen (4 mg/kg, Rimadyl, Pfizer) was administered subcutaneously every 24 hours for a minimal period of three days following surgery, during which the postoperative weight of the mice was carefully monitored. Food and water containing 1.5 mg/ml Metamizol (Novaminsulfon, Ratiopharm) were provided *ad libitum*. No retrogradely labeled neuron was ever observed in the barrel cortex of any animal with confocal and epifluorescence microscopy.

Slice preparation

In vitro electrophysiology experiments took place three to four weeks after stereotaxic injections. Mice were sedated with isoflurane in a sealed container and quickly decapitated. The skull was opened and the brain transferred to ice cold cutting solution (87 mM NaCl, 1.25 mM NaH₂PO₄, 2.5 mM KCl, 10 mM glucose, 75 mM sucrose, 0.5 mM CaCl₂, 7 mM MgCl₂, 26 mM NaHCO₃, bubbled with 95% O₂/5% CO₂ (vol/vol)). The hemispheres were separated and cut into serial, 300 microns thick TC slices through the somatosensory cortex using a VT1200S vibratome (Leica) following standard methods (Porter et al., 2001). Slices were incubated in recording solution (125 mM NaCl, 1.25 mM NaH₂PO₄, 2.5 mM KCl, 25 mM glucose, 2 mM CaCl₂, 1 mM MgCl₂, 26 mM NaHCO₃, bubbled with 95% O₂/5% CO₂ (vol/vol)) at 32°C for 30-60 min and at room temperature thereafter.

***In vitro* electrophysiology**

TC slices were transferred to a recording chamber constantly perfused with recording solution (1-2 ml/min) and visualized using the 2.5x and 40x objectives of a Zeiss Axio Examiner.A1 fixed-stage microscope (Zeiss). Whole cell patch clamp recordings were targeted at visually identified, tdTomato positive SpS neurons located on the edge of a barrel or barrel equivalent. Patch pipettes (resistance 6-10 MΩ) were pulled from borosilicate glass (GB150F-8P, Science Products) using a P-97 or P-1000 puller (Sutter Instruments) and filled with potassium based intracellular solution (135 mM K-gluconate, 5 mM KCl, 0.5 mM EGTA, 10 mM HEPES, 4 mM MgATP, 0.3 mM Na GTP, 10 mM Na-P-creatin, pH 7.4, 300 mOsm) containing 0.5% biocytin (Sigma-Aldrich). Patch pipettes were steered into position with a micromanipulator (Luigs & Neumann). Recordings were carried out at 32°C in discontinuous current clamp mode using a SEC-05XS amplifier (Npi). Access resistance was monitored and compensated for. If access resistance compensation became impossible, the recording was terminated. Membrane potential was held around -70 mV by DC current application throughout the recording after measuring the resting membrane potential (V_{RMP}) on break-in. We did not correct for the liquid junction potential (16 mV).

In order to obtain a thorough characterization of the intrinsic properties of the recorded neurons, we routinely performed standard characterization recordings immediately after establishing the whole cell patch clamp configuration. Passive properties were calculated from the membrane potential responses recorded in response to standard current pulses. Pulses were delivered for 1 s, and were of an amplitude of -10 and -50 pA. Ten responses for each current amplitude were recorded in order to calculate representative averages. In addition, we sequentially recorded the responses to current pulses of incrementing amplitude in order to build I-V curves for individual neurons. The current amplitude used ranged from -100 pA to whichever positive value caused the firing of at least one AP, with increments of 10 pA between individual sweeps. Rheobase recordings were performed by gradually adjusting the amplitude of the injected current to a value that would consistently elicit the firing of only one AP. The firing pattern was recorded by increasing the current amplitude above rheobase in 10 pA steps until enough APs were fired to reliably classify the resulting firing pattern.

Expression of ChR2 in VPM neurons enabled us to specifically activate thalamic fibers in the cortex and compare the properties of their input to cortical neurons. Stimulation of ChR2 expressing thalamic fibers was achieved using a computer controlled 473 nm diode laser (Rapp optoelectronics) guided through the 40x objective of the microscope, resulting in a circular illuminated field of about 100 μm in diameter on the slice. Data acquisition and photostimulation were synchronized using custom-written programs in Signal (CED). Tetrodotoxin (TTX) and 4-aminopyridine (4-AP) containing recording solution (0.5 μM and 0.1 mM, Tocris and Sigma-Aldrich respectively) were prepared for each experiment and perfused into the recording chamber at will.

Upon completion of the recordings, TC slices were incubated in 4% paraformaldehyde (PFA) and 15% picric acid in PB (0.1 M, pH 7.4) at 4°C overnight prior to staining.

Subcellular channelrhodopsin-assisted circuit mapping (sCRACM)

sCRACM was performed to map the distribution of thalamic input on recorded neurons following published methods ([Petreanu et al., 2009](#)). 0.5 μM tetrodotoxin (TTX) and 0.1mM 4-aminopyridine (4-AP) were introduced into the recording chamber. TTX blocks network activity caused by ChR2 stimulation, ensuring that only the thalamic synapses directly in contact with the recorded neuron contribute to its response. 4-AP blocks voltage gated potassium channels of the Kv1 family and thereby enable the depolarization of the presynaptic terminal induced by ChR2 stimulation to reach the threshold for activation of high threshold calcium channels, which in turn cause inflow of calcium and vesicle release. Stimulation of ChR2 was achieved as described above with a notable difference in the size of the illuminated area. Indeed, a shutter placed in the path of the laser restricted the size of the illuminated area to a field of 25 by 25 μm . After setting the focal plane on the center of the soma, the position of the light beam was gradually changed using the Morgentau software (Morgentau solutions) so as to scan an area of n-by-m fields over the cell being recorded. Stimulation, data acquisition and steering of the laser beam were synchronized using custom-written Signal routines. Recordings were performed in

discontinuous current clamp and membrane potential was held at -70 mV with constant direct current injections. Three stimulations were recorded from every field with an inter-stimulus interval of 6 seconds. Laser pulses were 10 ms in duration. The laser power was set individually for every SpS neuron to the highest value which did not elicit a measurable response when flashing just outside of the home barrel but relatively close to the recorded soma.

Histochemistry

The tissue obtained from animals at the conclusion of functional imaging experiments was used to examine the spatial relationships between the functional representations of up to 9 individual whiskers imaged during the experiment with the anatomical barrel field. The flattened cortex of the imaged hemisphere was cut in 100 μ m thick tangential sections with a vibratome (VT1200S, Leica), collected and rinsed in PB (pH 7.4). DAPI staining was carried out on tissue collected from LIV^{tdTomato} animals according to the manufacturer's specifications (Molecular Probes), before the sections were mounted and coverslipped with Aqua-Polymount (Polysciences). Because LIV fated cells constitutively express dTomato in LIV^{tdTomato} animals, no further staining was necessary to reveal the barrel field.

A further pool of tissue obtained from B6C3Fe animals was used for the purpose of measuring blood vessel density in the barrel cortex of WT and *reeler* mice (6 animals per group). This tissue was stained with DAB (diaminobenzidine tetrahydrochloride dihydrate, Roth), which stains erythrocytes when quenching of intrinsic peroxidase is omitted. Serial, 100 μ m-thick coronal sections containing the barrel field were cut on a vibratome, collected and rinsed several times in PB (pH 7.4). They were subsequently incubated for at least 90 minutes in 0.01 M phosphate-buffered saline containing 25% saccharose and 10% glycerol, followed by three freeze/thaw cycles on dry ice. After rinsing with PB (3*15 minutes), 0.05M TRIS buffer (TB, pH 7.4, 15 minutes) and TRIS-buffered saline (TBS, pH 7.4, 2*15 minutes), the sections were incubated overnight at 8°C in TBS containing avidin and biotinylated horseradish peroxidase diluted to 1:400 each (ABC Vectastain). Sections were recovered the next day, rinsed in TBS for 20 minutes and thrice in TB for 20 minutes, before incubation with 0.5 mg/ml DAB in TB. The reaction was started by adding 1 μ l TB containing 1%

hydrogen peroxide, allowed to develop under regular visual control, and stopped by rinsing thrice in TB. We proceeded with a cytochrome oxidase staining as described by Wong-Riley and Welt (1980) to reveal LIV barrels and barrel equivalents. Finally, the sections were mounted and coverslipped with Aqua-Polymount.

TC slices obtained from *in vitro* electrophysiology experiments were stained for biocytin with Alexa633 conjugate streptavidin so as to recover the morphology of the neurons recorded. The fixed slices were removed from PFA and successively rinsed 10 times with PB for 15 min each at room temperature. Slices were then rinsed in TB and TBS (pH 7.6) for 15 min at room temperature, followed by two rinses in Tris Buffer Saline containing 0.5% Triton-X 100 (TBST) for 15 min each. Alexa633 conjugated Streptavidin (Molecular Probes) 1:400 in TBST buffer containing Triton was then incubated with the slices overnight at 4°C on a rocking plate, before a DAPI staining was performed according to the manufacturer's specifications (Molecular Probes). Slices were rinsed in TBS and TB buffer before being mounted and coverslipped with Aqua-Polymount. Histochemistry was performed chiefly by Patricia Sprysch.

Data analysis

Intrinsic signal optical imaging

Analysis of intrinsic signals was performed with custom written MATLAB routines (The MathWorks). Series of camera frames were normalized using the following formula:

$$\frac{\Delta R}{R_0} = \frac{R - R_0}{R_0}$$

where $\Delta R/R_0$ is the fractional change in reflectance from reference, R is the light reflected during any given frame and R_0 the light reflected during the reference frame immediately preceding whisker stimulation onset.

The data obtained from experiments on $LIV^{tdTomato}$ mice, where the functional representations of 9 individual whiskers were mapped, was processed in the following way. The 5 data frames spanning 1.2 to 2.2 seconds after stimulation onset, when the intrinsic signal is clearly visible (figure 4), were averaged. A Gaussian filter ($\sigma = 86 \mu\text{m}$) was applied to the resulting frame to improve threshold detection, and the median of the data frame was subtracted to minimize the effect of noise, especially the slow spontaneous oscillations in reflectance (Mayhew et al., 1996; Drew and Feldman, 2009). In order to localize the intrinsic signals evoked by stimulation of different whiskers with minimal overlap, we extracted the contour lines encompassing the area where the signals were at 90% of their maximum (figure 5 and Chen-Bee et al., 2000).

In order to map intrinsic signals on the barrel field, we reconstructed the barrel field and pial vascular network from serial tangential sections of $LIV^{tdTomato}$ mice cortex under the 5x objective of an Axio Imager M2 microscope (Zeiss) using the NeuroLucida software (MBF Bioscience). Before mapping the location of sensory evoked signals on the reconstructed barrel field, we used a warping algorithm written in MATLAB and designed to align the reconstructed pial vascular network to the one photographed during the experiment, using a set of fiducial points in order to partly compensate for the curvature of the brain and distortion of the tissue (see figure 5).

The data obtained from B6C3Fe animals and used for quantifying the amplitude and area of the response evoked by stimulation at varying frequencies was treated as described above, with a few notable differences. The 15 frames spanning the 1-4 seconds after stimulation onset were averaged, and a Gaussian filter with $\sigma=130 \mu\text{m}$ was applied to the resulting frame. The median of the resulting frame was subtracted. We measured the response amplitude as the peak $\Delta R/R_0$ value in the resulting data frame, which was always located within the region activated by whisker stimulation, and fixed thresholds (1, 2, 3, 4, and $5 \cdot 10^{-4}$) were applied to all experiments for area measurements (see figure 6 and Chen-Bee et al., 2000).

Electrophysiology

Electrophysiological data were analyzed offline using custom written Signal and MATLAB scripts. Signal scripts were written by Dr. Martin Möck. ChR2 evoked responses were accepted if their amplitude crossed the threshold of 3 times the standard deviation of the baseline membrane potential measured in a 100 ms window prior to stimulus onset. In order to compare responses between the two groups on a population basis, we built Peri Stimulus Time Histograms (PSTH) by averaging the membrane potential values obtained from individual traces in 4 ms bins. The bin size was chosen so as to be large enough to fully exclude APs from traces where they appeared (for instance figure 12 F and G) while minimizing the subsequent loss of data. The same bin size was applied to traces that did not contain APs (for instance Fig 12 A, B and C) for the sake of comparability. Intrinsic properties were measured from the membrane potential responses to -10 pA current pulses delivered for 1 second. Input resistance (R_{in}) was measured from the maximal deflection from baseline. Membrane time constant (τ) was measured from an exponential fit applied from stimulus onset to maximal deflection. Sag index was calculated according to the following formula:

$$V_{sag} = 100 * \frac{\left(\frac{1}{R_{inss}} - \frac{1}{R_{inhd}}\right)}{\frac{1}{R_{inss}}}$$

where R_{inss} is the input resistance measured at steady state and R_{inhd} the input resistance measured at maximal deflection (Halabisky et al., 2006; Karagiannis et al., 2009). Rheobase was measured as the minimal stimulus current intensity required to reliably elicit a single AP. Reconstruction of filled neurons and delineation of the barrel and barrel equivalents was carried out by Alexandra Sachkova on confocal stacks using Neurolucida. Scholl analysis was performed on reconstructed neurons using Neurolucida; parameters measured were number of dendritic spines and dendritic length, and the bin size was set to 25 μm .

Histological quantifications

Images of coronal sections stained with DAB and used for blood vessel density analysis were acquired with the 5x objective of an AXIO Imager M2 microscope (Zeiss) controlled by Neurolucida and digitized with an AXIO cam MRm CCD camera. Minimum intensity projections were obtained from stacks of pictures acquired in 5 μm steps through the thickness of each individual 100 μm thick sections (n=6 animals per group). We examined 6 successive coronal sections through the barrel field in each animal. A threshold detection algorithm written in MATLAB was applied to calculate the relative section surface occupied by stained erythrocytes and thus blood vessels within selected regions of interest (ROIs). Briefly, the surface of the pia over the barrel field was manually outlined in pictures of coronal sections. The algorithm automatically generated successive, 100 μm -thick ROIs starting at the outline of the pia and covering the entire cortical thickness. The number of pixels detected above threshold in each successive bin was divided by the total number of pixels in that bin, resulting in an estimate of blood vessels density in dimensionless numbers reported as arbitrary units (see figure 7).

Images of the distribution of eYFP and tdTomato fluorescence in stained TC slices were acquired through the 10x objective of an Axio Imager M2 epifluorescence microscope controlled by Neurolucida. Image stacks (11 planes, 5 μm z steps) restricted to the cortex were acquired with the same objective and quantification of eYFP and tdTomato expression was performed on the corresponding maximum intensity projections. A custom written MATLAB script was used to measure the fluorescence intensity in 50 bins covering the distance from pia to white matter. The script calculated the sum of pixel values contained within each bin, and the resulting fluorescence intensity profile was normalized to its peak.

Statistics

Statistical analyses were performed with SigmaPlot (Systat Software Inc) with a significance threshold fixed at 0.05. Spatial autocorrelation (Moran's I) was calculated using the GeoDa software (GeoDa Center) according to standard methods (Moran, 1950). Briefly, spatial autocorrelation was estimated by calculating an index I according to the following formula:

$$I = \frac{N}{\sum_1^i \sum_1^j w_{ij}} \frac{\sum_1^i \sum_1^j w_{ij} (X_i - \bar{X})(X_j - \bar{X})}{\sum_1^i (X_i - \bar{X})^2}$$

Where ij refers to an indexed n-by-m array of EPSP amplitudes containing N fields, X to the EPSP amplitude in a selected field i , and w_{ij} is an element of an N by N weight matrix. The array of EPSP amplitudes were obtained from sCRACM experiments. Because the input maps frequently contained domains composed of adjacent fields receiving no input (that is, the amplitude equals zero) which can cause an overestimation of I , they were trimmed into the smallest possible n-by-m array that did not exclude fields containing input. The N by N weight matrix was designed following a king's rule, that is only the fields immediately adjacent to the i^{th} in either direction were taken into account in the calculation of I . Theoretical values of I range from -1 to 1. A value close to 1 indicates a spatial pattern where similar amplitudes tend to cluster around each other, a value close to 0 indicates a random pattern of amplitude distribution, and a negative value indicates a pattern where similar amplitudes avoid each other.

Results

Intrinsic signal optical imaging

A major goal of the present study is to elucidate the functional organization of the *reeler* barrel field with respect to somatotopy. We chose to investigate this issue by *in vivo* intrinsic signal optical imaging in urethane anesthetized mouse combined with controlled whisker stimulation. Urethane was chosen because of the very long lasting anaesthesia it provides, and because of its comparatively mild impact on cortical function (Simons et al., 1992; Friedberg et al., 1999). Whisker stimulation was achieved with a computer controlled piezo actuator, which enables precise control over stimulation parameters such as direction, amplitude, frequency, and identity of the whisker selected. Before the intrinsic imaging experiment began, we performed cranial surgery in order to implant optical chambers over the barrel cortex (see Materials and methods). The ring of dental cement was filled with saline and topped with a glass coverslip, enabling unhindered diffusion of light and imaging. This procedure allowed acquisition of detailed images from the cortex where individual vessels were clearly recognizable (figure 4 B and C, left).

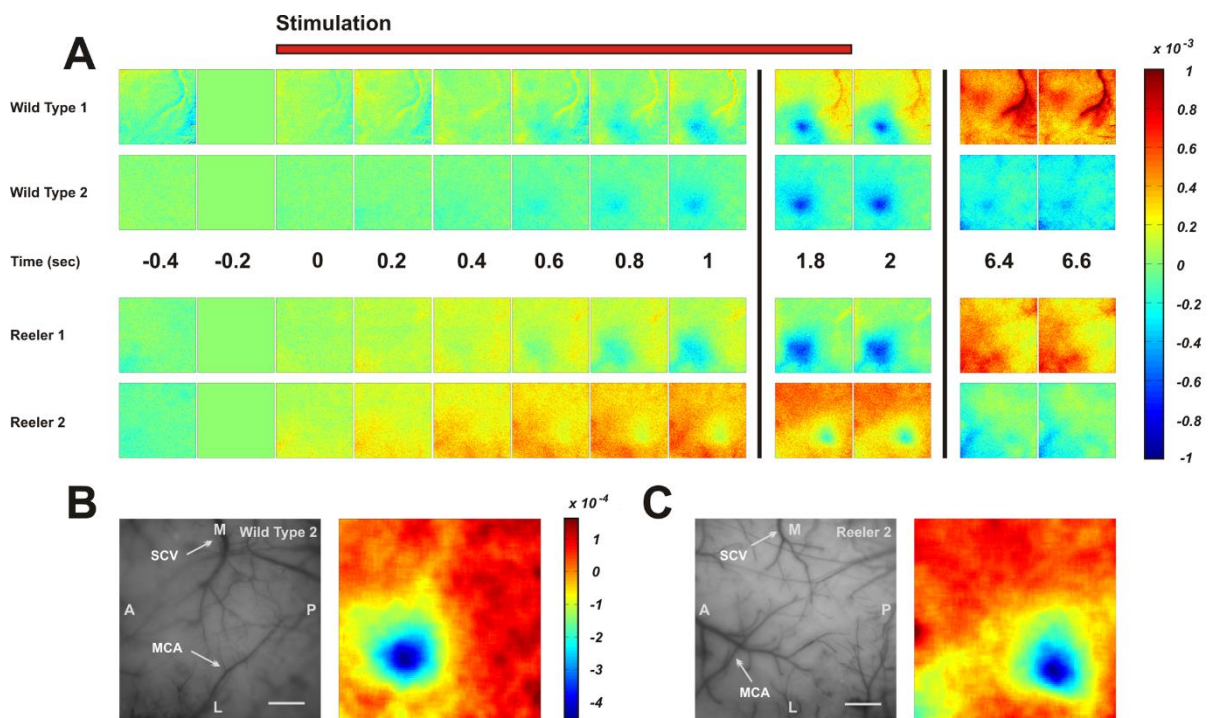


Figure 4. The hemodynamic response to single whisker stimulation. **A:** time series of camera frames illustrating the response to stimulation of whisker C2 at 5 Hz for 2 seconds in two representative examples of WT and *reeler* animals. Stimulation starts at time 0, each frame represents 200ms. The camera frame immediately before stimulation onset was used as reference for normalization; the scale bar represents fractional change in reflectance with respect to that frame. Stimulation evoked a localized hemodynamic response corresponding to the sensory representation of whisker C2 in WT but also in *reeler* mice. Neither the mean latency nor mean duration of the evoked intrinsic signal differed significantly between genotypes (one way ANOVA, $p=0.7$ and $p=0.46$, respectively). **B, C:** left, photograph of the surface vasculature in two representative examples corresponding to the data in A. SCV: Superior Cerebral Vein, MCA: Middle Cerebral Artery, M: Medial, L: Lateral, A: Anterior, P: Posterior. Scale bar: 500 μm . Right, sensory maps obtained by binning 15 frames spanning the period from 1 to 4 seconds after stimulation, applying Gaussian blur with $\sigma = 86 \mu\text{m}$ and subtracting the median of the filtered image. Reproduced from Guy et al., 2014 under the terms of the Creative Commons Attribution Non-commercial License.

A first step towards our goal was to establish the feasibility of *in vivo* imaging in *reeler* mice. Representative results of intrinsic signals evoked by stimulation of whisker C2 in two WT and two *reeler* mice under urethane anaesthesia are shown in figure 4. Variations in blood volume and haemoglobin oxygen saturation levels are expressed as changes in reflectance with respect to a reference frame corresponding to the 200 ms preceding stimulation onset (Time: -0,2 in figure 4), such that increases in blood supply and oxygenation following enhanced neuronal activity, which locally cause an increase in light absorption, are represented in blue shades. The intrinsic signal recorded across entire camera frames over time comprised several components, including spontaneous variations in blood supply to the cortex and vascular artefacts (visible in the later frames of WT 1, for instance). In addition to these spontaneous components, we were able to reliably record hemodynamic signals evoked by sensory stimulation and appearing as spatially restricted increases in blood supply and oxygenation (see frames 1.8 and 2). We investigated the temporal dynamics of the intrinsic signal by measuring its latency and duration for comparison between genotypes. The intrinsic signal typically became visible within 1 s of stimulation onset and returned to baseline within approximately 10 s of stimulation onset in both groups. Neither response latency nor response duration were significantly different when comparing genotypes (mean onset latency and standard deviation: 0.76 ± 0.15 s in WT, 0.73 ± 0.1 s in *reeler*, one way ANOVA: $p=0.7$; mean duration and standard deviation: 8.9 ± 1.7 s

in WT, 8 ± 2 s in *reeler*, one way ANOVA: $p=0.46$; $n=10$ and 9 for WT and *reeler*, respectively). Intrinsic signals can therefore be evoked and captured in *reeler* mice, with a time course that is very similar to that in WT.

Sensory map organization

Having established that barrel equivalent clusters of LIV fated neurons can be recognized in tangential sections through the somatosensory cortex of LIV^{tdTomato} *reeler*, and that intrinsic signals can be recorded from the *reeler* cortex, we combined the two elements and used ISOI to determine whether somatotopy exists in functional maps in the *reeler* barrel cortex. By binning 15 frames spanning 1 to 4 s from whisker stimulation onset, it was possible to reliably extract spatially restricted intrinsic signals corresponding to the sensory representation of the stimulated whiskers in the imaged cortex (figure 4 B and C, right). Therefore, we stimulated an array of 3*3 whiskers (centered on C2 because of its central position in the whisker pad) in LIV^{tdTomato} animals, which enabled us to determine whether their functional representations were aligned along rows and arcs in the same manner barrels are aligned in the barrel field. In addition, we reconstructed the barrel field and superficial blood vessel pattern from tangential sections (representative examples are shown in figure 5 A, C). By aligning the reconstructed superficial vasculature with that photographed during the experiment, it was possible to map the localization of any given whisker representation on the barrel field. Hence, we could examine the spatial relationships of functional whisker representations with one another in functional maps and compare the resulting pattern with that formed by barrels in the anatomical barrel field. In WT animals, sequential stimulation of whiskers along a row, for instance whiskers B1 to B3, yielded intrinsic signals which were aligned along a “row axis”. This alignment matched that observed between the corresponding barrels in the anatomical barrel field (figure 5 B). In addition, sequential stimulation of whiskers along an arc, such as whiskers D1, C1 and B1, evoked intrinsic signals that were also aligned along an “arc axis” similar to that defined by their corresponding barrels. In both the functional and anatomical maps of the whisker pad, the row and arc axis intersected at a roughly perpendicular angle. These similarities between the functional and anatomical maps constitute evidence for the existence of somatotopy in functional sensory maps, as previous authors have demonstrated ([Masino et al., 1993](#); [Kleinfeld and Delaney, 1996](#)).

How is the sensory map of the whisker pad spatially organized in the otherwise highly disorganized *reeler* barrel cortex? We applied the same sequential stimulation of 9 whiskers to *reeler* animals (figure 5 D) to probe the spatial relationships of their functional representations. Stimulation of whiskers along a row evoked intrinsic signals which were aligned, as they were in WT. Upon stimulating whiskers along an arc, the same alignment of their functional representations was observed than in WT. Similarly, the row and arc axis in *reeler* also intersected at a roughly perpendicular angle. It can be concluded from these observations that the spatial organization of functional sensory maps in *reeler* is essentially the same as in WT. The most parsimonious explanation for this finding is that like its WT counterpart, the *reeler* barrel cortex remains organized as a somatotopic representation of the whisker pad in spite of the otherwise extensive disruption of its laminar organization.

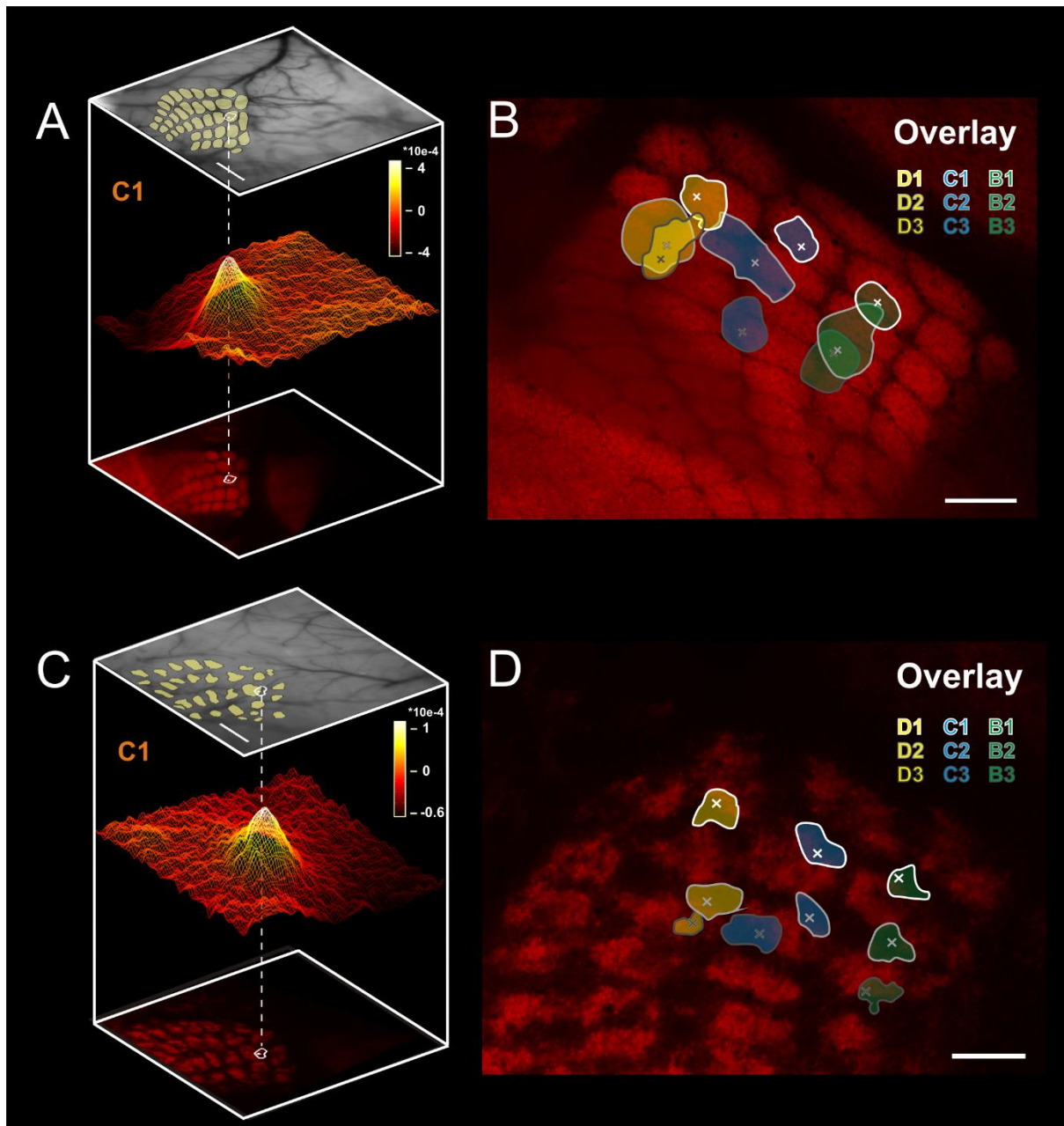


Figure 5. Somatotopic organization of the barrel cortex. **A, C:** pseudo 3D-reconstruction of the location of the hemodynamic response evoked by single whisker stimulation with respect to the barrel field in WT and *reeler*, respectively. Top: photograph of the superficial blood vessels acquired during the experiment under a 546 nm wavelength illumination (Scale bar: 500 μm). Bottom: the barrel field was imaged and reconstructed post mortem from tangential sections through the barrel cortex of *LIV^{tdTomato}* mice. Middle: surface plot of the averaged intrinsic signal evoked by stimulating the C1 whisker at 5Hz for 2 seconds (scale bar, fractional change in reflectance from reference in absolute values). The location of the peak and 90% of maximum isoline were mapped on the barrel field after aligning the blood vessels present in the reconstructions of the serial tangential sections with those present in the pial surface photograph of the living animal. **B, D:** overlay of peak (x) and 90% maximum isolines locations of 9 intrinsic signals evoked by sequential stimulation of 9 whiskers

in the same WT and reeler mouse, respectively. The spatial relationship between the functional intrinsic signals locations show an rough but adequate match with those of individual structural barrels. Scale bar: 250 μ m. Reproduced from Guy et al., 2014 under the terms of the Creative Commons Attribution Non-commercial License.

A degree of mismatch exists between the functional and the anatomical maps however, in that the peak of the intrinsic signals rarely perfectly matched the barrel centers. This can be explained by at least two facts. On the one hand, the exact location of the center of an intrinsic signal evoked by single whisker stimulation is determined not only by the center of the corresponding barrel, but also by the location of the nearest penetrating arteriole (Blinder et al., 2013), suggesting that a small degree of intrinsic, physiological mismatch between the intrinsic signal and the underlying barrel can easily be observed with this method. On the other hand, the accuracy of our reconstructions and warping algorithm are limited. Any inaccuracies in the alignment of successive serial sections or in the alignment of blood vessels during the warping process are likely to add up and contribute to the observed mismatch. This technical component is likely the primary contributor to the shift observed in our experiments. The mismatch itself, however, bears little consequence on the observation that WT and *reeler* functional maps are highly similar in their spatial arrangement and the ensuing conclusion that somatotopy exists in the *reeler* barrel cortex, and should not be interpreted as illustrating a large and systematic biological mismatch between structural and functional maps (Dubroff et al., 2006).

In summary, the present data offers direct evidence for somatotopy in the *reeler* barrel cortex and, to our knowledge, the first derived from *in vivo* functional imaging approaches.

Single whisker stimulus representation in barrel cortex

Beyond mapping the localization of the functional representation of individual whiskers, intrinsic imaging may help us probe the responsiveness of cortical networks to sensory stimulation by measurement of the amplitude of the evoked intrinsic signal. In particular, how the cortex responds to whisker stimulation of varying frequencies constitutes a property worthy of investigation, since rodents can use a range of frequencies with which to

whisk during exploratory behaviour. We therefore asked how a discrete parameter of individual whisker stimulation such as frequency represented in the barrel cortex. We investigated this question by stimulating whisker C2 for 2 seconds at frequencies of 1, 5, 10 and 25 Hz, a frequency range that overlaps with spontaneous whisking in awake behaving rodents (Carvell and Simons, 1990), and measured the peak amplitude of the response (figure 6 A, B). The amplitude of the response increased with increasing stimulation frequency in both genotypes. Interestingly, the response amplitude in *reeler* were higher than in WT at low frequencies (1 and 5 Hz), before being overtaken at higher frequencies (10 and 25 Hz). This result may potentially indicate that the dynamic range of response amplitude in which stimulus frequency can be encoded is somewhat narrower in *reeler*. Statistical analysis, however, concluded that this effect was not statistically significant (two way ANOVA with repeated measures, genotype and frequency; effect of frequency, $p < 0.001$; no effect of genotype, $p = 0.71$; no genotype*frequency interaction, $p = 0.67$; $n = 11$ WT and 12 *reeler*). We conclude that under similar experimental conditions, the intrinsic signals evoked by single whisker stimulation are comparable across the range of frequencies we tested. Therefore, in spite of the loss of lamination and resulting cortical disorganization, cortical processing of sensory information in the barrel cortex as measured with intrinsic imaging seems indistinguishable between *reeler* and WT.

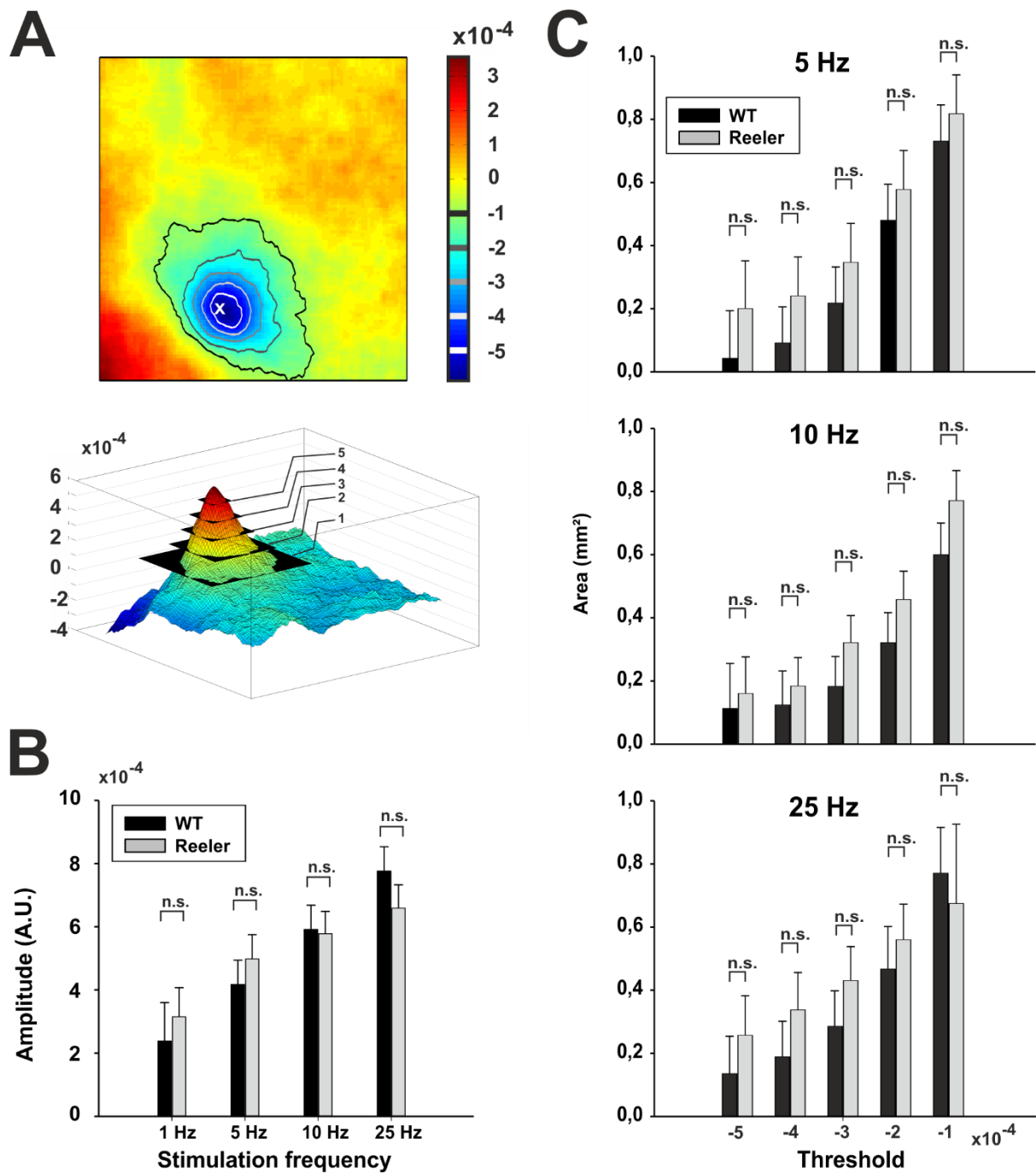


Figure 6. Stimulus representation in somatosensory cortex. **A:** top, representation of whisker C2 overlaid with threshold isolines. The level of subsequent thresholds is indicated on the scale bar, which represents fractional change in reflectance. The asterisk labels the peak amplitude of the evoked response. Bottom, same data as top in absolute value. **B:** peak amplitude of evoked response (in fractional change in reflectance, absolute value) as a function of stimulation frequency (mean \pm sem, n.s.: non-significant, ANOVA, $p=0.71$). **C:** Area encompassed within isolines of thresholds indicated in **A** as a function of stimulation frequency (in mm^2 , mean \pm sem, n.s.: non-significant, ANOVA, $p=0.12$, $p=0.09$ and $p=0.35$ for 5, 10 and 25 Hz, respectively). The 1 Hz stimulation frequency did not evoke responses that consistently reached threshold values and is therefore not represented

here. N= 11 WT and 12 *reeler*. Reproduced from Guy et al., 2014 under the terms of the Creative Commons Attribution Non-commercial License.

Transcolumnar connectivity revealed by intrinsic imaging

In addition to the functional organization of the barrel cortex and its responsiveness to sensory stimulation, intrinsic imaging can reveal differences in functional connectivity, and in particular transcolumnar connectivity. Indeed, tactile information in the rodent whisker to barrel pathway reaches the somatosensory cortex primarily through TC synapses clustering in LIV barrels. From there, information spreads vertically through intracolumnar projections from LIV to the supra- and infragranular layers, but also horizontally through transcolumnar projections originating in LII/III and V (Petersen et al., 2001; Schubert et al., 2007; Staiger et al., 2015), which contributes to the horizontal spread of the evoked intrinsic signal (Wester and Contreras, 2012). The sensory evoked intrinsic signals we recorded in our experiments typically covered an area spanning several barrels (figure 5 A and C; notice the broad “base” of the signal just above background), representing the horizontal span of corticocortical connections to neighbouring columns. In order to compare the span of transcolumnar connectivity, we measured the area contained within fixed activation thresholds (1 to 5×10^{-4}) and compared both genotypes on that basis (figure 6 A, C and table 1; Chen-Bee et al., 1996; Masino and Frostig, 1996). At all frequencies tested (5, 10 and 25 Hz), the area encompassed by the intrinsic signal increased as the threshold was lowered, a result that was entirely expected. The areas measured in *reeler* were larger than in WT, regardless of stimulus frequency or threshold. Statistical analysis (two way ANOVA, genotype and threshold) was carried out separately for each frequency. We consistently found an effect of the threshold on the area ($p < 0.01$ for all frequencies, $n = 11$ WT and 12 *reeler*) but not of the genotype ($p = 0.12$; $p = 0.09$ and $p = 0.35$ for 5, 10 and 25 Hz respectively) and no genotype *threshold interactions ($p = 0.99$; $p = 0.97$ and $p = 0.96$ for 5, 10 and 25 Hz respectively). These results do not support the hypothesis that *reeler* transcolumnar connectivity differs from WT in its horizontal reach.

Genotype		WT			<i>Reeler</i>		
Frequency (Hz)		5	10	25	5	10	25
Threshold (*10 ⁻⁴)	-5	0.04 (0.15)	0.11 (0.14)	0.13 (0.12)	0.20 (0.15)	0.16 (0.11)	0.26 (0.12)
	-4	0.09 (0.11)	0.12 (0.11)	0.19 (0.11)	0.24 (0.12)	0.18 (0.09)	0.34 (0.12)
	-3	0.22 (0.11)	0.18 (0.09)	0.28 (0.11)	0.35 (0.12)	0.32 (0.08)	0.43 (0.11)
	-2	0.48 (0.11)	0.32 (0.09)	0.47 (0.13)	0.58 (0.12)	0.46 (0.09)	0.56 (0.11)
	-1	0.73 (0.11)	0.60 (0.10)	0.77 (0.14)	0.82 (0.12)	0.77 (0.09)	0.67 (0.25)

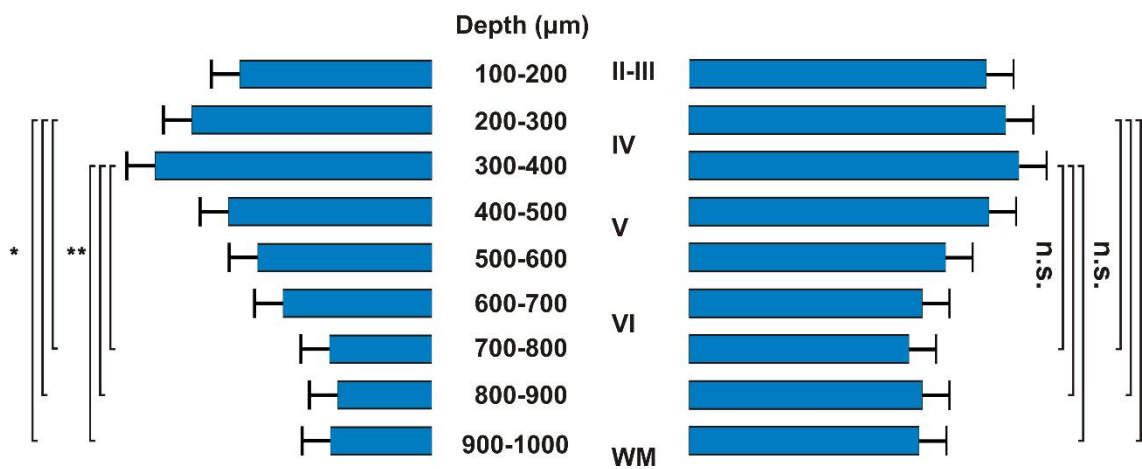
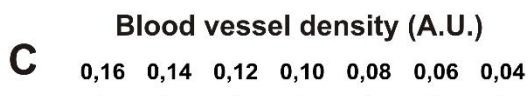
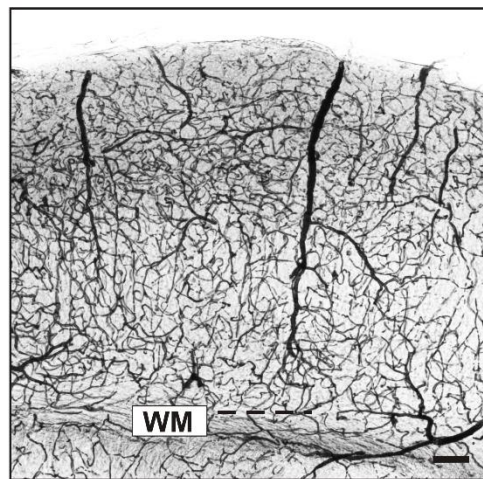
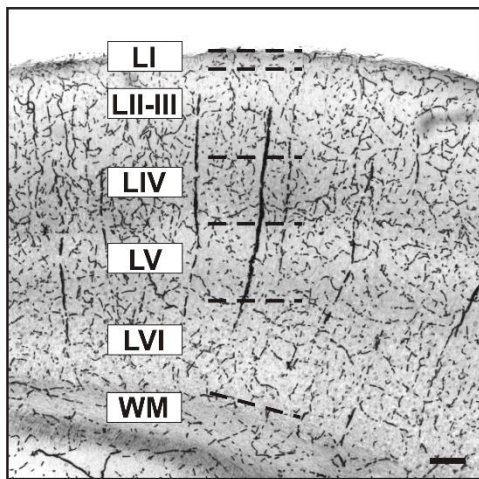
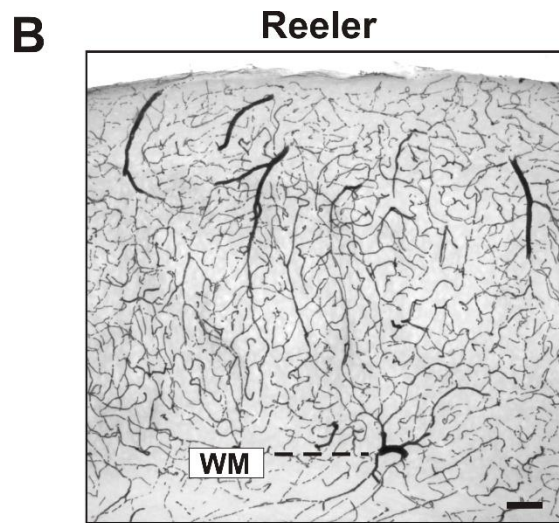
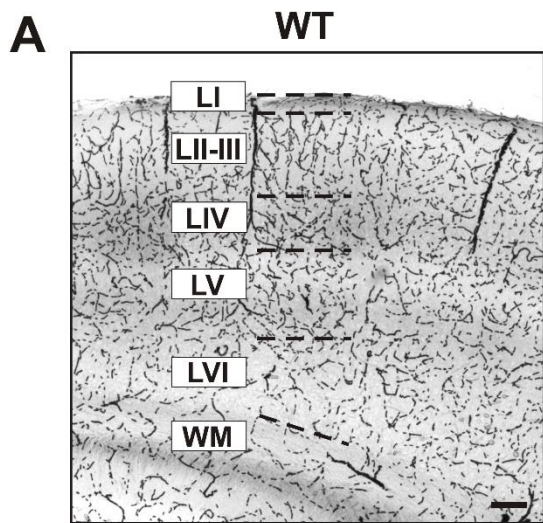
Table 1. Areal quantification of the sensory evoked intrinsic signal. Cortical area covered by intrinsic signal evoked by whisker stimulation at different frequencies in *reeler* and WT. The average areas within absolute activation thresholds are given in mm² with standard error of the mean in parenthesis (n=11 WT, 12 *reeler*). Adapted from Guy et al., 2014 under the terms of the Creative Commons Attribution Non-commercial License.

Cortical vasculature in *reeler* and wild type mice

As a functional imaging technique, optical imaging of intrinsic signals measures multi-component hemodynamic signals including haemoglobin oxygenation level, blood flow and volume (Malonek et al., 1997; Vanzetta et al., 2008). A difficulty in the interpretation of quantitative measures of the intrinsic signal such as amplitude comes from the fact that hemodynamic signals are a surrogate, rather than direct, measure of neuronal activity. Indeed, the transfer function, the quantitative relationship between neural activity and hemodynamic signals is not known explicitly in the present study and might confound the interpretation of our results. While simultaneous recordings of both neural and hemodynamic signals is the most straightforward approach for estimating the transfer function, they are technically challenging and beyond the scope of the present study (Cardoso et al., 2012).

However, functional mapping with intrinsic imaging, as presented here, also depends critically on there being a densely interconnected microvascular network in the cortical area under scrutiny, capable of supplying blood to regions of heightened neuronal activity with a high spatial fidelity – a prerequisite that we had the means to investigate (Drew et al., 2011). We therefore asked whether the loss of reelin and the ensuing disturbance in neocortical development also alter the development and patterning of the cortical vascular bed (Lindhorst et al., 2012). We sought to answer this question by staining coronal sections of WT and *reeler* animals with DAB, which reveals the hydrogen peroxidase rich erythrocytes left in the cortical vessels after fixation by immersion in PFA of unperfused tissue and provides a suitable surrogate staining for blood vessels in sections of adult mouse cortex (figure 7 A, B). We measured the density of blood vessels contained in the cortex in 100 μm bins, starting 100 μm below the pia because of the higher background staining immediately below the pia. Results are shown in figure 7 C. The distribution of blood vessels in WT broadly varied with increasing depth, with the supragranular layers containing a higher density of vessels than the infragranular layers. Vascular density peaked at a depth of 300 to 400 μm , which extended across the LII/III to LIV border into LIV in our sections. The vascular density was significantly higher between 200 and 400 μm than from 700 to 1000 μm (ANOVA, $p < 0.05$ in all tests). The vascular density in *reeler* mice followed a similar distribution along the depth of the cortex, peaked between 300 and 400 μm from the pia, but there was no significant difference in the density of blood vessel at different depths. Hence, the radial density of blood vessels across the cortex in *reeler* cortex varies within a narrower spectrum but follows the same pattern than in WT. Thus, the results obtained with intrinsic imaging are unlikely to be skewed by differences in brain perfusion related to distinct anatomical organizations of the cortical vasculature in *reeler* and WT.

Figure 7. Vascular network in the barrel cortex. *A, B:* coronal sections through the somatosensory cortex of two representative WT and *reeler* mice, respectively ($n = 6$ in each group). DAB staining was used to stain erythrocytes in an unperfused brain, providing an indirect but efficient way of revealing the vascular network of the somatosensory cortex. wm: white matter. Scale bar: 100 μm . *C:* Relative density of blood vessels as a function of depth in WT (left) and *reeler* (right) animals. Density was calculated in 100 μm bins from the pia to the white matter. The first 100 μm below the pia were excluded because a heightened background was consistently found near the pia. Histochemistry by Patricia Sprysch. Reproduced from Guy et al., 2014 under the terms of the Creative Commons Attribution Non-commercial License.



Lessons drawn from intrinsic signal imaging

In summary, our functional imaging experiments have unraveled some elementary properties of the *reeler* neocortex. First, we confirm that sensory input reaches the highly disorganized barrel cortex in the *reeler* mouse, and provide further evidence of its somatotopic organization, the first such observation from an *in vivo* preparation. This result demonstrates that a rather precise columnar organization exists in *reeler*, in agreement with previous reports (Caviness et al., 1976; Wagener et al., 2010; Boyle et al., 2011). Second, we found that individual barrel related columns respond with equal strength to a controlled stimulation across a range of behaviorally relevant frequencies, indicating that cortical excitability is not blunted by the loss of cortical layers and the potentially ensuing loss of sequential information processing along the canonical microcircuit, a result that is in agreement with an independent study in the *reeler* visual cortex (Pielecka-Fortuna et al., 2014). Finally, these results provide some indication that the cortico-cortical connectivity of the *reeler* mouse remains comparable to that of WT, as functional activation of one barrel related column spread equally well, and as far as in a normal cortex. It thus appears that a normal functional organization persists in the *reeler* cortex, a finding that was both surprising and mildly disappointing to the author who expected a more obvious physiological phenotype to match the anatomical phenotype.

It is crucial however, to keep in mind that the method chosen, intrinsic signal imaging, is an indirect measure of network activity. As such, it offers only limited insight into the details of cortical connectivity in *reeler*, and little to none with regard to the presence and properties of specific connections between defined cell types as they have been documented in WT. Because of this, while it is an appropriate method when it comes to investigating columnar organization, intrinsic imaging by itself is insufficient to determine whether the canonical microcircuit remains in *reeler*. Instead, one must rely on methods that provide cellular and synaptic resolution. In our search for the canonical circuit of the *reeler* mouse, we decided to turn to *in vitro* electrophysiology on TC brain slices (Porter et al., 2001) to probe the input of the thalamus to a defined excitatory neuron type in the cortex, the SpS, a well described connection that constitutes the input stage of the canonical microcircuit (Lübke and Feldmeyer, 2007; Feldmeyer et al., 2013).

Thalamic axon projection domains in *reeler* and wild type mice

In order to visualize SpS neurons in TC slices through the somatosensory cortex and target them during *in vitro* electrophysiology experiments, we capitalized on the LIV^{tdTomato} mouse line (Guy et al., 2014). As described above, in these animals, tdTomato is expressed in a Cre dependent manner (Madisen et al., 2010) and restricted to excitatory neurons (Xue et al., 2014). Figure 8 shows photographs of representative TC slices, as recovered from *in vitro* electrophysiology experiments. The distribution of tdTomato positive revealed the typical pattern of barrels and barrel equivalents in the somatosensory cortex of WT (figure 8 A' and B'). Quantification of the fluorescence intensity in the WT cortex revealed that tdTomato expression peaked at a depth of about 300 to 500 μm from the pial surface in WT (figure 8 B' and C), consistent with the finding that tdTomato is enriched in LIV neurons. Importantly, however, sparse tdTomato expression could also be found in LV (figure 8 B'). In *reeler* animals (figure 8, D' and E'), the tdTomato fluorescence intensity profile in the *reeler* cortex did not produce a clear peak, but rather seemed to plateau between ~ 400 μm from the pial surface and the white matter (figure 8 E' and F), consistent with the smearing of barrel equivalents characteristic of this mutant. Because SpS neurons are found exclusively in LIV in the WT mouse, and presumably in clusters of LIV equivalent neurons in *reeler*, Cre driven fluorescence is helpful in identifying such cells prior to recordings.

In order to visualize and stimulate TC fibers arising from the VPM specifically, we performed stereotaxic injections of AAV5-ChR2-eYFP to the VPM of WT and *reeler* mice. Three weeks after injection, neurons in the VPM strongly expressed the ChR2-eYFP fusion protein (figure 8, A'' and D''). In WT mice, eYFP expressing fibers were found throughout the depth of the cortex, but were most prominent in LIV and LVb (Fig 8 B''). The fluorescence intensity profile of eYFP in cortex displayed a bimodal distribution, with the strongest peak colocalizing with the peak of tdTomato expression in LIV, and a weaker peak at the LVb/LVla border (figure 8 B''' and C). This pattern of VPM projections to the cortex is well described and in perfect agreement with previous literature in rats (Wimmer et al., 2010; Oberlaender et al., 2012). In *reeler* animals, the distribution of eYFP was similar to that of tdTomato and characterized by the absence of an obvious peak in the fluorescence intensity profile (figure 8 E'' and F) as

well as a strong colocalization with tdTomato (figure 8 E’’’). These results suggest that clusters of tdTomato cells in transgenic *reeler* mice receive most of the VPM input to the cortex, as do LIV barrels in the WT, in good agreement with previous studies (Wagener et al., 2010).

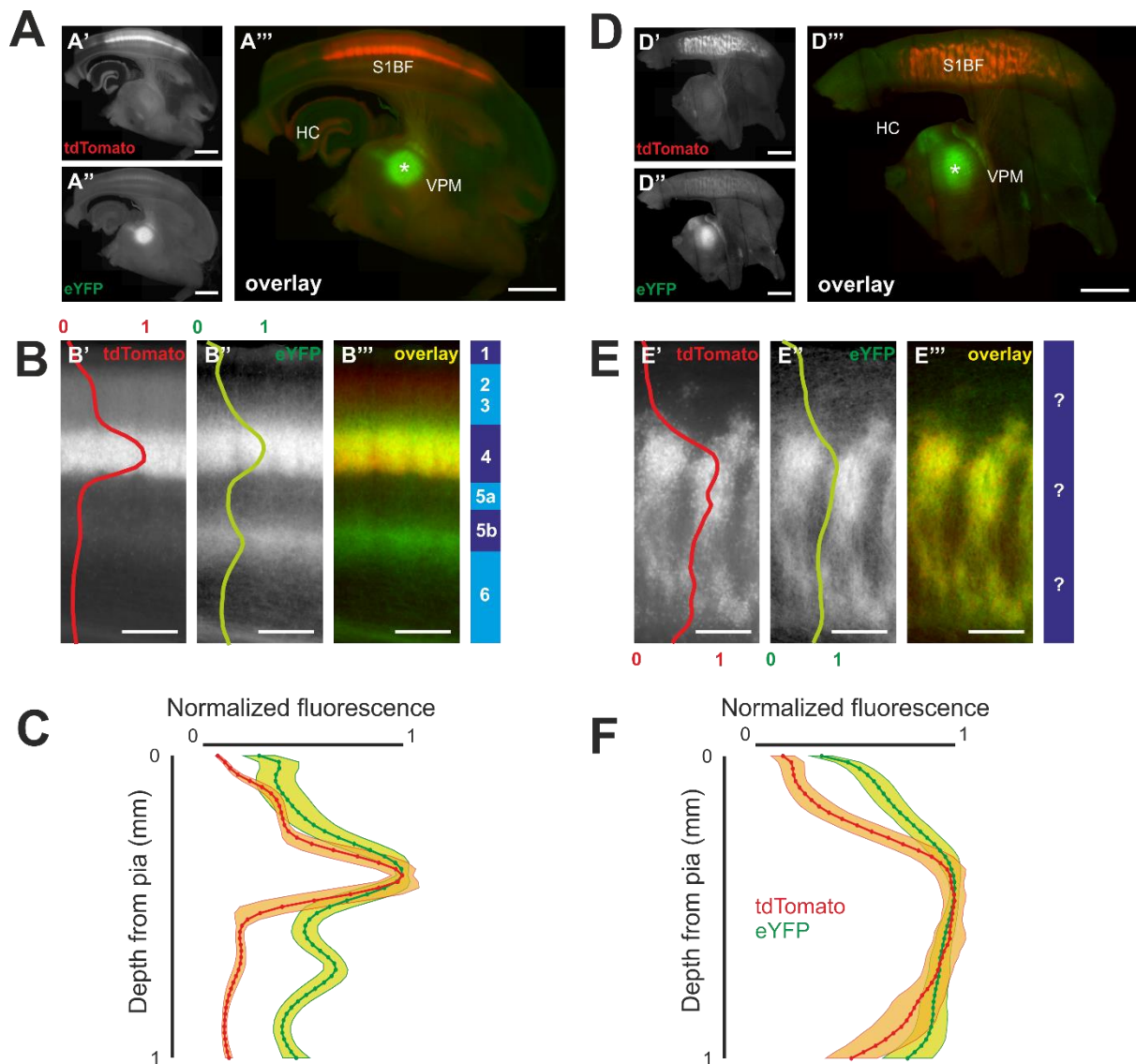


Figure 8. Distribution of tdTomato and eYFP expression in somatosensory cortex. A and D: representative examples of TC slices of WT and *reeler* animals, respectively. tdTomato positive neurons are numerous in the cortex (A' and D', A''' and D'''), while eYFP expression concentrates around the injection site in the VPM (asterisk, A'' and D'', A''' and D'''). Scalebar: 1mm. **B and E:** high magnification images of the somatosensory cortex of a WT and a *reeler* animal respectively, illustrating the clustering of tdTomato expressing neurons into barrels and barrel equivalents (B' and E'). eYFP expressing fibers are clearly visible in both genotypes (B'' and E'') and overlap with the

clusters of tdTomato expressing neurons (B''' and E'''). The superimposed curves represent the normalized fluorescence as a function of depth from the pia of the corresponding image; fluorescence intensity was averaged in 49 bins spanning the cortical thickness. Scale is visible at the top or bottom of each image. Layer borders are represented to the right; layers are by definition inexistent in the reeler cortex. Scalebar: 200 μ m. **C** and **F**: normalized fluorescence intensity versus depth from pia in WT and reeler, respectively. Each curve represents the average \pm SD of 16 brain slices.

Cellular identity of tdTomato positive neurons

Expression of tdTomato in acute TC slices enabled us to target whole cell patch clamp recordings at LIV and LIV equivalent neurons in WT and *reeler*, respectively. More specifically, we targeted LIV SpS neurons, as these cells receive direct input from the VPM (Porter et al., 2001; Inoue and Imoto, 2006; Bruno and Sakmann, 2006). Cells were selected for recordings on the basis of fluorescence, soma shape, presence of a local cluster of similarly shaped somata, and localization within a barrel or cluster of tdTomato positive neurons. Because SpS neurons are only one among several types of excitatory neurons populating LIV barrels (Feldmeyer et al., 1999; Schubert et al., 2003), and because sparse tdTomato expression was also observed in LV neurons, it was necessary to confirm the identity of the neurons we recorded. To that effect, we routinely added biocytin to our intracellular solution in order to recover the morphology of the neurons we recorded. 22 of the 91 neurons included in the present study could be recovered after termination of the recordings, a recovery rate just below 25%.

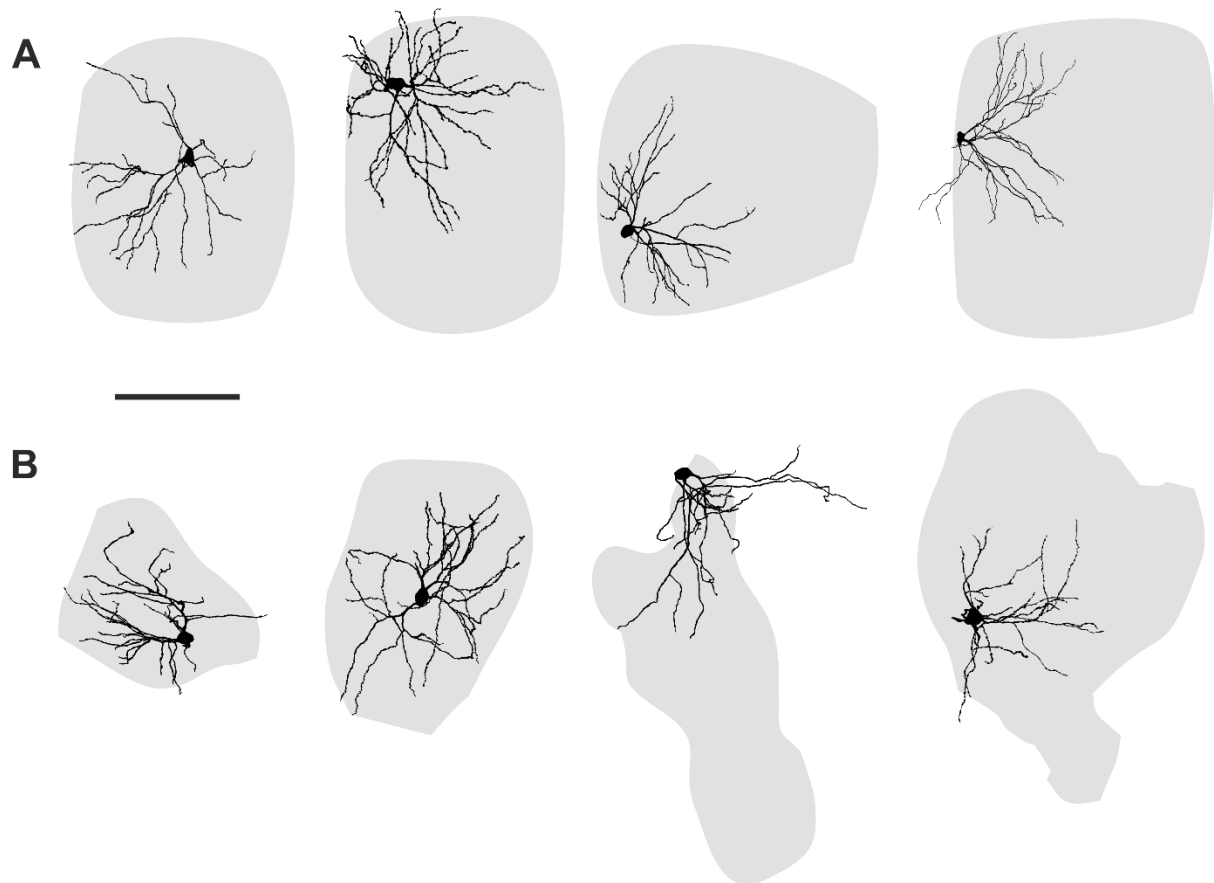


Figure 9. Morphology of biocytin-filled neurons. **A:** representative examples of the morphology of recovered neurons in WT. Cells were reconstructed from TC slices of 4 animals and display the morphological characteristics typical of their class, most notably a dendritic arborization largely restricted to their home barrel (grey shade) and the lack of an apical dendrite. **B:** same as in **A**, in *reeler* animals. Scalebar: 100 μm . Reconstructions were carried out by Alexandra Sachkova.

Representative examples of cellular morphologies are shown in figure 9 and figure 10, A and C. The cells recovered from both genotypes were found to possess morphological properties characteristic of SpS neurons, including the lack of an apical dendrite, 4-6 dendrites confined within the home barrel or cluster, and numerous spines (Feldmeyer et al., 1999; Staiger et al., 2004). Quantitative analysis of 6 neurons in *reeler* and 7 in WT was carried out in order to compare a number of morphological variables, namely the number of primary dendrites, the total length and span of the reconstructed dendrites, and the number of spines and

branching points. The mean values for of these parameters were in agreement with previous literature (Staiger et al., 2004; Sun et al., 2014) and surprisingly similar when comparing genotypes, with no statistically significant difference (table 2). These results indicate that the absence of reelin does not affect the global morphological properties of SpS neurons apart from constraining their dendritic arborisation into a geometry that befits their home barrel.

Although just under a quarter of the neurons we included in the present study could be recovered, all displayed the same morphological characteristics, which indicates that our experimental approach allowed reliable detection of SpS cells. Only one neuron was ever recovered that displayed the semblance of an apical dendrite, which justified its complete exclusion from the dataset presented here. Taking into account the 22 recovered neurons reported here, the proportion of incorrect cell type lies below a mere 5% (1/23). We are therefore reasonably confident in our assumption that the overwhelming majority of the non-recovered neurons we recorded from were also SpS. In conclusion, our use of the LIV^{tdTomato} mouse line enabled us to reliably target SpS neurons, the morphological properties of which are virtually unchanged in the *reeler* mouse.

	Number of primary dendrites	Dendritic length (µm)	Spine count	Branching points	Dendritic span (µm)
WT	5.14 (0.9)	1872.7 (431.9)	768 (161.7)	26.1 (4.4)	132.1 (31.3)
<i>Reeler</i>	4.83 (3.0)	1874.26 (268.1)	774.5 (279.6)	23.1 (3.4)	150 (27.4)
P value	0.138	0.994	0.956	0.101	0.302

Table 2. Quantitative analysis of SpS neuron morphology. Numbers are given as mean and standard deviation (in brackets) of 7 WT and 6 *reeler* biocytin-filled and reconstructed neurons. P values derived from t-tests.

Intrinsic properties of tdTomato positive neurons

The goal of the line of experiments reported here is to investigate the properties of thalamic input to SpS neurons in *reeler* and WT mice. Responses to synaptic input are determined partly by the intrinsic properties of the recorded neurons such as R_{in} or τ . In addition, such properties are instrumental in further ascertaining the identity of the neurons we recorded, and determining whether the absence of reelin can influence the intrinsic properties of defined neuronal classes is also a goal in itself. We therefore characterized the elementary electrophysiological properties of the neurons we recorded prior to investigating their responses to thalamic input. All neurons exhibited the regular spiking firing pattern typical of LIV excitatory neurons (Zhu and Connors, 1997; Feldmeyer et al., 1999; Schubert et al., 2003), regardless of genotype (figure 10 B and D). Additional properties we analyzed included resting membrane potential (V_{RMP}), sag index, rheobase, and medium afterhyperpolarization (mAHP) amplitude. The values for these properties were found to be in agreement with previous literature regarding passive properties of SpS (Schubert et al., 2003) and are summarized in table 3. No significant differences were found between the genotypes in R_{in} (table 3 and figure 10 E) or τ (table 3). It must be noted, however, that significant differences were found in V_{RMP} which was slightly more negative in *reeler* (figure 3 F, t-test, $p < 0.05$) and in the sag index, which was lower in *reeler*. Although the h current underlying the voltage sag is involved in temporal summation, its weakness in SpS and slow kinetics (Magee, 1998) led us to expect little contribution of I_h to the responses to short pulses of light (10 ms). In addition, minor differences in V_{RMP} could not have contributed to any differences between *reeler* and WT as we performed all subsequent recordings at a holding membrane potential of -70 mV in all cells. We therefore reasoned that eventual differences in responses to synaptic input would result from synaptic mechanisms rather than from differences in intrinsic properties between genotypes.

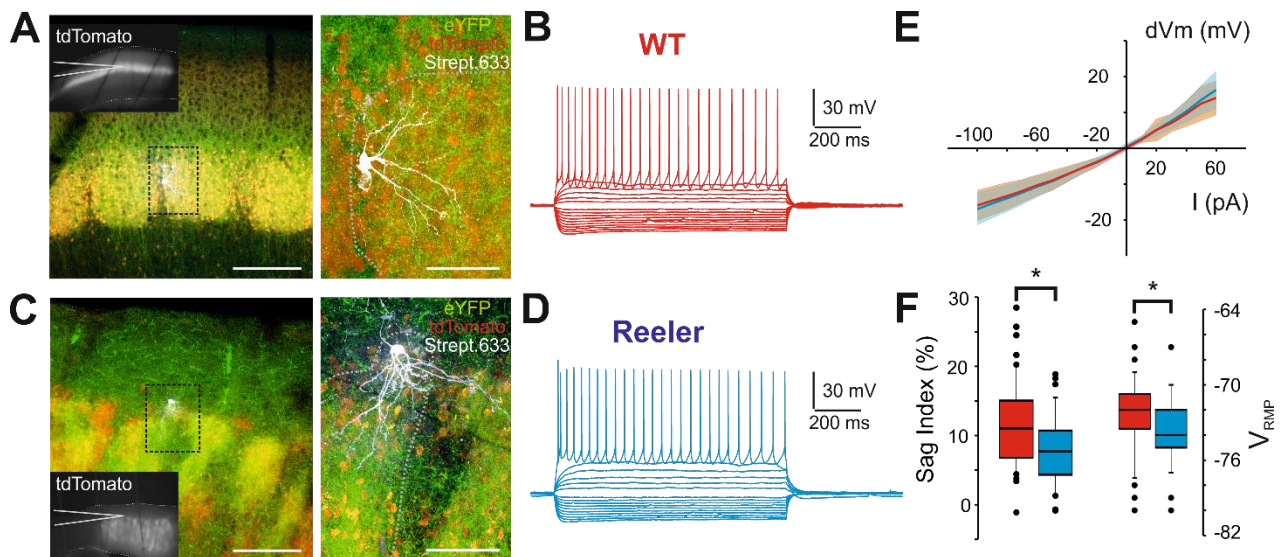


Figure 10. Intrinsic properties of SpS neurons. **A** and **C**: confocal images of biocytin-filled neurons obtained from WT and reeler animals, respectively, obtained with a 10x objective. Left insets: fluorescence images of TC slices acquired during recordings illustrating the approximate position of the recording pipette with respect to clusters of tdTomato expressing neurons. Right: close up on the filled neurons. The grey dotted lines indicate the apparent borders of the home barrel. Scalebar: 200 μm on the left, 50 μm on the right. **B** and **D**: representative electrophysiology of WT and reeler neurons, respectively. Individual traces represent the membrane potential responses to a series of successive current pulses of incrementing amplitude (-100 to +50 pA, 10 pA steps). The firing pattern was obtained by injection of 130 pA in both genotypes. **E**: population I-V curves calculated from data acquired as indicated above and represented as mean \pm SD of 46 WT (red) and 45 reeler (blue) neurons. **F**: Box plots of the sag index (left, measured from responses to -10 pA pulses) and resting membrane potential on breakthrough (right). Both properties were significantly different (sag index: one tailed t-test, $p < 0.005$; membrane potential: one tailed t-test, $p < 0.05$; $n = 46$ WT and 45 reeler). Streptavidin staining was carried out by Patricia Sprysch.

	V _{RMP} (mV)	R _{in} (MΩ)	T (ms)	Sag index (%)	Rheobase (pA)	AHP amp (mV)
WT	-72.4 (3.3)	193.8 (68.6)	15.8 (6.0)	11.4 (6.2)	108.5 (44.1)	15.8 (3.0)
<i>Reeler</i>	-73.6 (2.5)	203.9 (84.7)	14.0 (6.2)	8.1 (4.8)	97.8 (41.3)	16.7 (3.0)
P value	0.032*	0.827	0.065	0.004 **	0.275	0.183

Table 3. Values for intrinsic properties of SpS neurons. Numbers are given as mean and standard deviation (in brackets) of 46 WT and 45 *reeler* neurons. * and **: significant difference at the $\alpha=0.05$ and 0.005 thresholds, respectively. P values derived from t-tests.

Optogenetic control of thalamic relay neurons

The experimental approach chosen here to probe VPM input to SpS neurons relies on direct optogenetic activation of ChR2 expressing fibers. The comparability of the results obtained from such an approach rest on the assumptions that expression levels and diffusion of ChR2 do not differ significantly between genotypes, and that the properties of the presynaptic element, the thalamic relay neuron, are also similar. We therefore acquired intracellular recordings of thalamic relay neurons (TN) in both genotypes to verify the feasibility and comparability of direct light activation of neurons in both strains. TN displayed the bistable firing pattern typical of their class, responding to a depolarizing current injection either with a single burst or a train of APs depending on the membrane potential at which they were held with DC current injection (figure 11 A and B, [McCormick and Bal, 1997](#)). Optical stimulation of the recorded neurons resulted in fast depolarization that increased in amplitude as laser intensity was gradually raised. Using sufficiently high laser intensity, it was possible to reliably elicit spiking in TNs, the pattern of which, burst or single spike, was also determined by membrane potential (figure 11 C and D). The behaviour of TN was thus unaffected by genotype.

The present results are of course insufficient to definitively rule out differences in expression or distribution of ChR2 which may in turn contribute to differences observed in

the responses of SpS neurons to TC fiber stimulation. For instance, the modest number of cells recorded in the thalamus does not allow for a statistically solid comparison of measure of ChR2 expression, such as the minimum laser intensity required to elicit firing of an AP, between *reeler* and WT. In addition, properties of TN neurons measured from somatic recordings may be a poor predictor of the behaviour of their presynaptic boutons in the cortex, such that a lack of difference between genotypes observed in the VPM may not hold true in the cortex. However, the high degree of similarity between *reeler* and WT TN observed here gave us at least little reason to doubt the assumption that the abundant eYFP expressing thalamic fibers in the cortex could be activated reliably and without dramatic differences between genotypes. We conclude that differences in the responses of SpS neurons to TC input would likely result from synaptic mechanisms rather than differences in the intrinsic properties of TN neurons, including their levels of ChR2 expression.

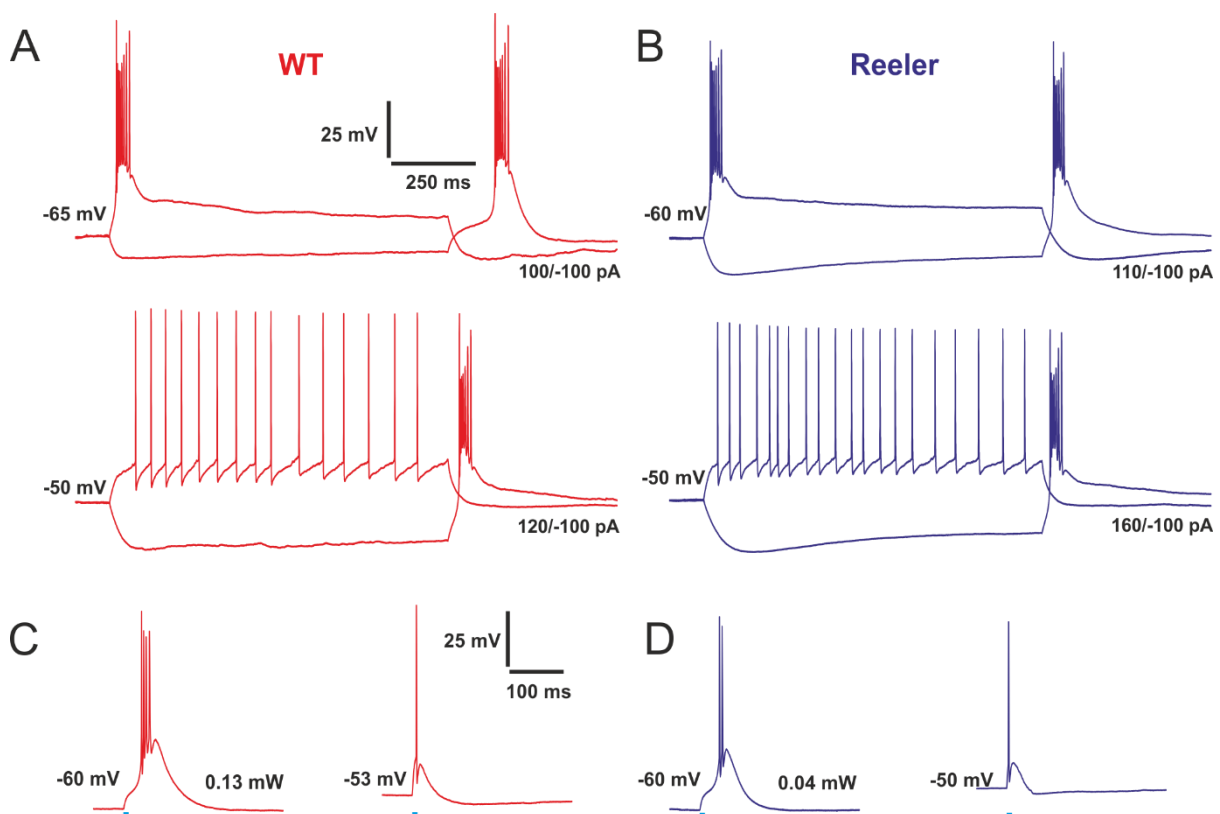


Figure 11. ChR2 evoked responses in thalamic relay neurons. *A and B:* representative firing pattern of thalamic neurons patched in WT in *reeler*, respectively. Top traces shows the bursting firing pattern in response to current injections while the cell is maintained at a relatively hyperpolarized

membrane potential. Bottom traces illustrate the switch to a regular spiking firing pattern observed when maintaining the cell in a relatively depolarized state. Note the rebound burst occurring after all hyperpolarizing pulses regardless of holding membrane potential. **C** and **D**: optogenetic activation of thalamic neurons was sufficient to elicit firing of APs in transfected neurons. Stimulation is indicated by blue squares and lasts for 1ms. A switch in firing pattern (burst to single spike) could be observed upon depolarizing the recorded neurons.

Channelrhodopsin-2 evoked responses in spiny stellate neurons

Confident in our ability to control the presynaptic element, we next compared the properties of thalamic input to SpS neurons in both genotypes. Optical stimulation of thalamic fibers with various laser intensities reliably elicited subthreshold, compound responses in SpS neurons held around -70 mV by DC current injection (figure 12 A and B). These compound responses consisted of multiple, summed EPSPs and often appeared to include sharp repolarizing events reminiscent of GABAergic inhibition (figure 12 A and B, insets, arrows). Feedforward inhibition is a well described phenomenon in LIV of the WT cortex, and is brought about by cortical interneurons that receive direct input from the thalamus and, in turn, project to local excitatory neurons (Swadlow, 1995; Swadlow, 2003; Inoue and Imoto, 2006; Sun et al., 2006; Porter et al., 2001). Because a demonstration that this essential circuit motif is preserved in *reeler* is lacking, we seized the opportunity to document its existence with our experimental approach. We reasoned that the apparent amplitude or strength of the putative inhibitory potentials observed in compound responses could be modulated by holding the recorded neurons at varying membrane potentials with respect to the reversal potential of inhibition. We therefore repeated TC fibers stimulation while holding the cell at -70, -60 and -90 mV and observed that the repolarizing events could indeed be modulated by membrane potential, such that they appeared stronger if the neuron was held around -60 mV (figure 12 D). Conversely, they reversed polarity and became depolarizing at a membrane potential of -90 mV, below the reversal potential for chloride, in agreement with GABA_A receptor-mediated inhibition. In order to verify that compound responses included inhibition, we performed similar recordings in the presence of 1 μM of the GABA_A receptor blocker Gabazine (figure 12 E). Under these conditions, stimulation of thalamic fibers resulted in far stronger responses in SpS neurons, consisting

of large and long lasting depolarization accompanied by firing of numerous action potentials, and occasional Ca^{2+} plateaus, consistent with blockade of GABA_A mediated inhibition. Washing out Gabazine restored the ChR2 evoked responses to their original appearance. These results did not differ between genotypes and demonstrate that *reeler* SpS neurons receive both thalamic input as well as GABAergic inhibition, probably feedforward inhibition provided by local fast-spiking basket cells, a circuit motif well described in the WT cortex (Swadlow, 1995; Swadlow, 2003; Inoue and Imoto, 2006; Sun et al., 2006; Porter et al., 2001). In addition, excitatory inputs probably arose from recurrent excitation as well as direct thalamic input. Indeed, SpS neurons are known to readily engage in reciprocal connection, and it is therefore highly probable that recurrent excitation accounts for at least a fraction of the depolarization observed in response to TC fibers stimulation (Feldmeyer et al., 1999; Cowan and Stricker, 2004; Lefort et al., 2009).

A further goal of our recordings was to determine whether a difference exists in the strength of thalamic input to SpS neurons between the genotypes. In order to compare the strength of the responses to thalamic input, we asked how much an optical stimulation could depolarize WT and *reeler* SpS neurons. We repeatedly stimulated TC fibers with an interstimulus interval of 6 s and laser power of ~ 0.04 mW and calculated the membrane potential variation (dVm) evoked in the recorded SpS by subtracting the average membrane potential measured in a 50 ms window starting 100 ms before stimulus onset from individual traces. Three traces per neuron were then averaged, and dVm was averaged across 17 WT and 13 *reeler* neurons in 4 ms bins, resulting in a peristimulus time histogram of membrane potential variation (figure 12 C). The latency to the response onset was in agreement with monosynaptic input and not significantly different between genotypes (figure 12 H, 2.5 ± 0.7 ms and 2.7 ± 0.8 ms in *reeler*, rank-sum test), and the responses peaked within 4-8 ms after stimulus onset in both genotypes. The peak dVm, however, was significantly higher in *reeler*, with *reeler* SpS remaining significantly more depolarized after stimulation for a sustained period of time (up to ~ 45 ms; bin by bin comparison, t-tests, $p < 0.05$). Because we found no significant difference in either R_{in} or τ between *reeler* and WT neurons (table 3), this difference in the magnitude of evoked responses most likely results

from differences in synaptic input, such as, for instance, a shift in the balance of excitation and inhibition.

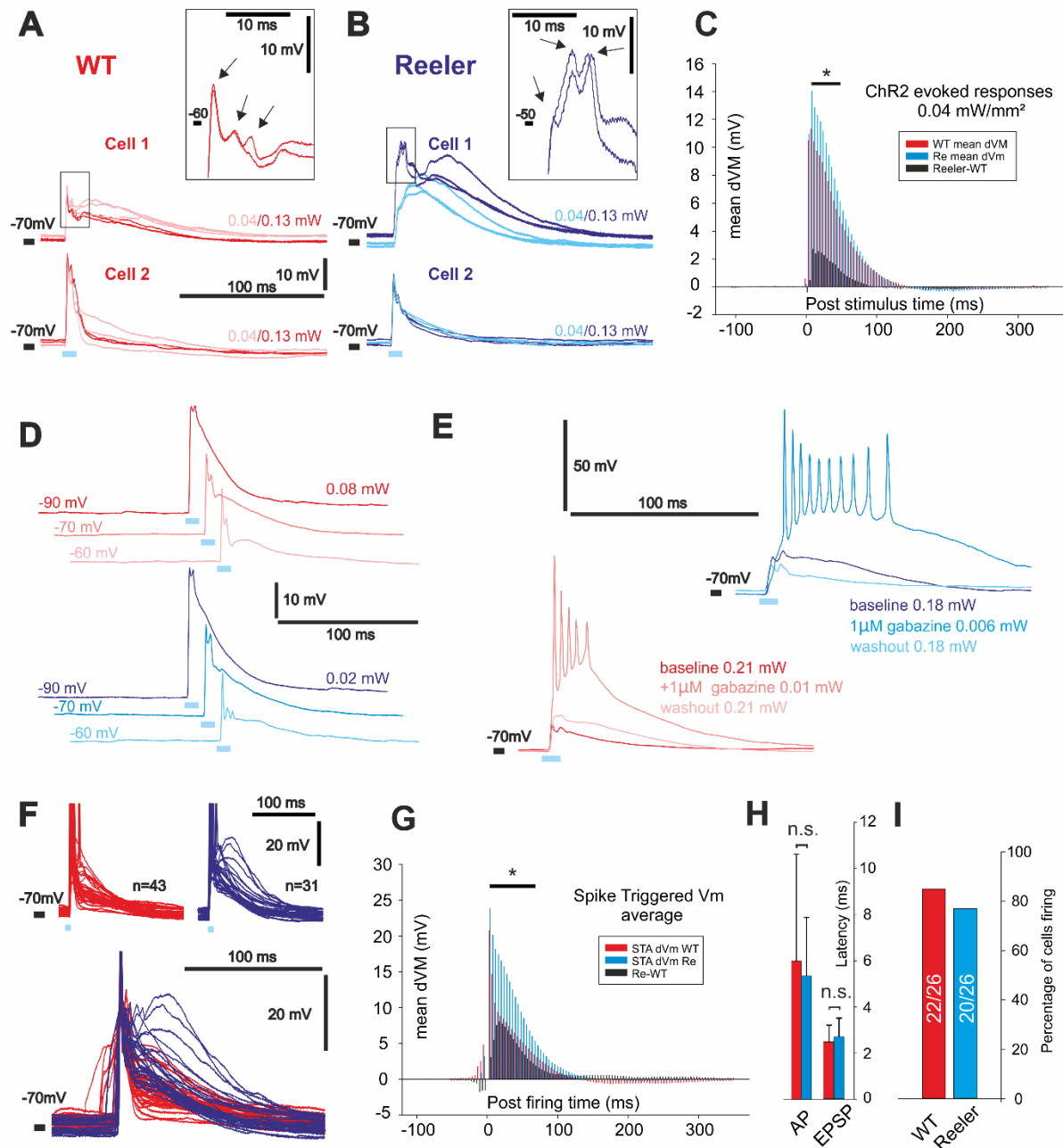


Figure 12. ChR2 evoked responses in SpS neurons. *A and B:* representative examples of subthreshold responses to optical stimulation of thalamic afferent in SpS neurons in WT (red) and reeler (blue), respectively. In all four cells, ChR2 stimulation evoked compound responses that appeared to involve excitation as well as inhibition (inset). Insets illustrate magnified view of individual responses; arrows point to the onset of apparent inhibitory post synaptic potentials (IPSPs). Scalebars in A apply to B. *C:*

average membrane potential variation (dVm) around ChR2 stimulation in 4 ms bins. Baseline was calculated from -100 to -50 ms relative to stimulus onset. Black bars represent the average difference between *reeler* and WT. *Reeler* SpS were significantly more depolarized by the stimulation than WT SpS for a duration of up to 45 ms. **D:** modulation of the strength of inhibition by membrane potential. Putative inhibition appeared stronger when the membrane potential (V_{RMP}) was held at -60 mV than at -70 mV. By contrast, IPSPs reversed polarity and became depolarizing when the membrane potential was held at -90 mV, consistent with the GABA_A reversal potential of about -70 mV. **E:** blockade of GABA_A inhibition with 1 μ M Gabazine caused epileptiform activity in both genotypes. **F:** top: overlaid suprathreshold responses in WT (left) and *reeler* (right). APs were truncated at -20 mV. Bottom: same traces as above, aligned to the AP. **G:** average spike triggered membrane potential variation (STA) in 4 ms bins. Baseline was calculated as in C. *Reeler* SpS remained significantly more depolarized after spiking for up to 70 ms. **H:** average \pm SD latencies of subthreshold and AP firing in response to ChR2 stimulation. **I:** proportion of cells that fired in response to a ChR2 stimulation of 10 ms and of sufficient intensity. Percentages were 85% in WT and 77% in *reeler* and not significantly different (Fisher's exact test, $p=0.73$).

In a subset of neurons, we determined whether TC fibers stimulation was sufficient to elicit AP firing in the recorded SpS neurons by gradually increasing stimulus intensity. 22 out of 26 (85%) WT and 20 out of 26 (77%) *reeler* neurons tested for that property responded with an AP after stimulation intensity had passed a sufficient threshold (figure 12 F). We found no significant difference in either the proportion of cells firing (figure 12 I, Fisher's exact test, $p=0.73$) or the laser intensity required between genotypes (rank-sum test, $p=0.76$, median of 0.05 mW in WT and 0.08 mW in *reeler*). Likewise, the latency to AP firing remained unaffected by genotype (figure 12 H, 5.9 ± 4.6 ms in WT, 5.5 ± 2.6 ms in WT and *reeler*, respectively; rank sum test). Aligning individual traces of WT and *reeler* neurons to the AP indicated that *reeler* neurons repolarized more slowly after firing (figure 12 F). We therefore calculated the spike-triggered average dVm in 17 WT and 13 *reeler* neurons, excluding the bin containing the AP (figure 12 G). We found that *reeler* SpS remained significantly more depolarized after firing for a long period of time (~ 70 ms, bin by bin comparison, t-tests, $p<0.05$), an effect that was qualitatively similar to that observed in subthreshold responses but surpassed it in magnitude and duration. Such an effect may in principle be due to a weakened AP afterhyperpolarization in *reeler*. However, because we found no significant differences in the AHPs between *reeler* and WT (table 3), we again conclude that the slower repolarization of *reeler* SpS neurons after firing an AP evoked by TC fibers stimulation is

likely the result of altered synaptic inputs, and in particular a shift in the balance of excitation and inhibition.

Taken together, these results indicate that the net excitation brought to bear by TC fibers and local network input combined is greater in *reeler* than in WT SpS neurons. Furthermore, the proportion of *reeler* SpS neurons firing in response to TC fibers input being no different than that in WT suggest that TC fibers input is at least as effective at recruiting SpS neurons in both genotypes, which was expected given that our intrinsic signal imaging revealed that cortical networks are equally responsive to whisker stimulation in both genotypes.

Properties of thalamic input to *reeler* spiny stellate neurons

Stimulation of TC fibers typically evoked multicomponent postsynaptic responses in targeted neurons. Because of the complex nature of such responses, the actual strength of the TC fibers input is difficult to estimate, as its relative contribution to the response is masked by network effects such as recurrent excitation and feedforward inhibition. We therefore added 0.5 μ M TTX and 0.1 mM 4-AP to the bath chamber, in order to remove the contribution of network effects from the ChR2 evoked responses while preserving the ability to stimulate TC fibers, respectively (Petreanu et al., 2009; Yang et al., 2013). Indeed, TTX, a blocker of voltage gated sodium channels, prevents firing of actions potentials in the slice, which effectively blocks any network activity. The drawback of such an approach is the resulting inability to elicit AP firing in TC fibers, a prerequisite for activation of the voltage activated calcium channels of the presynapse that enable vesicle release. In order to make it possible for a depolarization mediated by laser activation of ChR2 alone to mediate opening of these channels, it is necessary to prevent the fast repolarization mediated by voltage gated potassium channels through the application of the Kv1 potassium channel blocker 4-AP. Application of both TTX and 4-AP results in the fact that only presynaptic boutons, rather than entire fibers, are stimulated by laser light.

Under these experimental conditions, SpS responded to optical stimulation with monophasic responses of markedly reduced amplitude, consistent with the loss of recurrent excitation (figure 13 A and B), and possibly also as a consequence of the fact that unlike an AP, stimulation of ChR2 will not elevate the membrane potential to positive values given its reversal potential in the vicinity of 0 mV (Lin, 2011; this interpretation remains questionable in the absence of accurate knowledge of the events occurring at the presynapse following ChR2 stimulation, however). In addition, the fact that SpS neurons respond to optogenetic stimulation in a situation where only presynaptic terminals can be stimulated demonstrate that TC input on these neurons is indeed direct, a result that is true for both WT and *reeler* and confirm the predictions of previous studies (Wagener et al., 2010). In order to evaluate and compare the strength of this direct input between genotypes, we repeated our analysis of stimulation evoked dVm with 17 WT and 13 *reeler* neurons and a laser power of ~0.04 mW, obtaining a PSTH of the response to the purely thalamic input (figure 13 C). To our surprise, the peak ChR2 evoked responses were slightly weaker in *reeler* in the absence of network activity, in sharp contrast with our observations on compound responses (bin by bin comparison, t-tests, $p < 0.05$).

The finding that intracellularly recorded responses to TC fibers stimulation differs between genotypes seems to contradict expectations. Indeed, our functional imaging experiments revealed that cortical networks of both genotypes were equally responsive to whisker stimulation, which would lead to the prediction that TC input to these networks does not substantially differ. One of several differences between the two experimental strategies presented here is the nature of the stimulation. In functional imaging experiments, we repeatedly stimulated the whisker at frequencies of 1 to 25 Hz, meaning that short term plasticity may have occurred at the TC synapse on SpS neurons. TC fibers synapses on LIV excitatory neurons are known to undergo short-term depression when repetitively stimulated (Gil et al., 1999; Chung et al., 2002), and we reasoned that differences in short-term depression might compensate for the differences in the responses to TC input between the genotypes. We therefore stimulated TC fibers at frequencies of 1, 5 and 10 Hz, setting the laser power so that the response to the first laser pulse would be of about 5-10 mV (figure 13 D and E). We found that TC input markedly depressed at all frequencies,

irrespective of genotype. In addition, the amplitudes of the evoked EPSPs following the first in a train were not substantially different between genotypes, and in particular they were not higher in *reeler*. Interestingly, the fact that compound responses in *reeler* SpS neurons exceed those in WT while the purely TC input they receive is weaker hints at the existence of compensatory mechanisms which amplify TC input in *reeler*. Such mechanisms, however, do not appear to involve alterations in how TC input adapts to sustained stimulation.

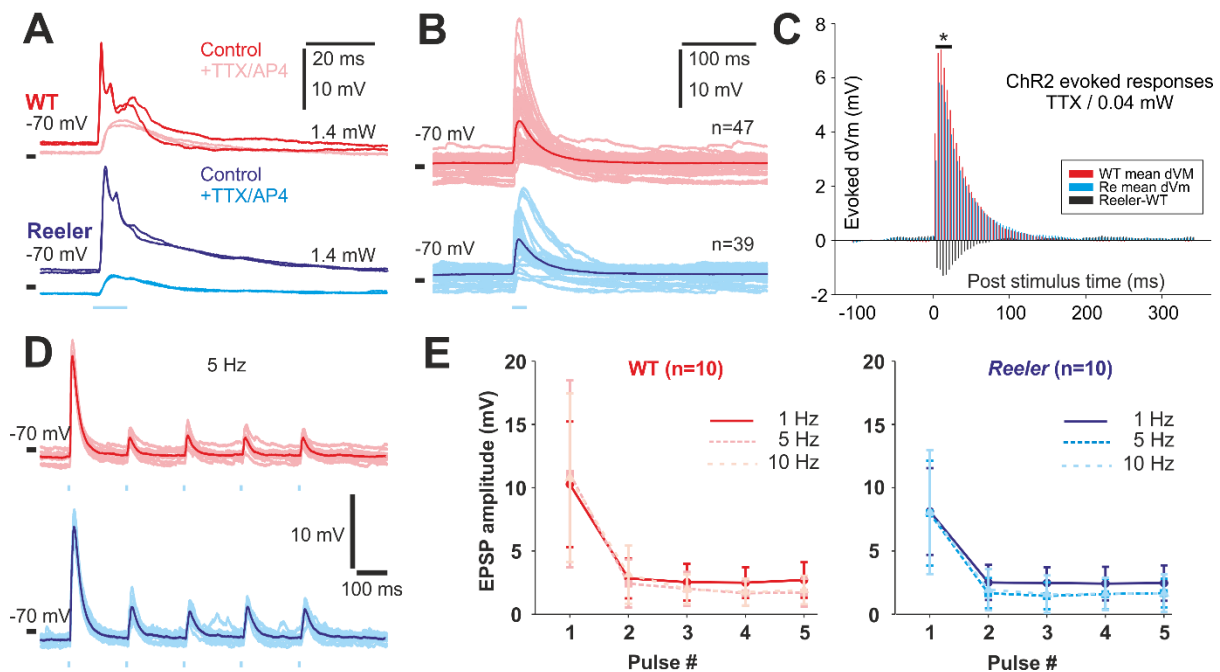


Figure 13. Properties of TC input to SpS neurons. **A:** representative examples of compound and monophasic responses to ChR2 stimulation in the absence and presence of 5 μ M TTX and 100 μ M 4-AP. **B:** overlaid, evoked monophasic responses in WT (red) and reeler (blue). Individual traces are displayed in light hues, averages are dark. **C:** mean membrane potential variation evoked by ChR2 stimulation in the presence of TTX and 4-AP. Black bars represent the average difference between reeler and WT. Baseline was calculated as in Fig 12, C. WT SpS were significantly more depolarized by TC input than their reeler counterparts, in contrast with our findings on compound responses. **D:** representative examples of responses to trains of ChR2 stimulation at 5 Hz in one WT SpS neurons (red) and one reeler SpS (blue). 10 individual traces are displayed in light hues, average traces are dark. **E:** aggregate short-term synaptic plasticity data in both genotype. Massive short term depression was visible at all frequencies in both genotypes, with amplitudes of EPSPs following the first in a train dropping by more than 50%.

Subcellular distribution of thalamocortical input to spiny stellate neurons

TC synapses are distributed over the entire dendritic arbor of LIV excitatory neurons, with a well described propensity for being found at higher densities close to the soma (Schoonover et al., 2014; Jia et al., 2014) and for forming small clusters along dendrites (Benshalom and White, 1986). Such a spatial distribution of synapses may enhance the reliability of sensory transmission, as inputs close to the soma are less affected by dendritic filtering, while synchronous, clustered input are more likely to recruit active dendritic properties (Larkum et al., 2008). We reasoned that the scattering of LIV equivalent neuronal clusters and their afferent thalamic fibers characteristic of the *reeler* phenotype might alter the distribution of TC synapses on SpS cells. We therefore compared the spatial distribution of TC input in SpS neurons in WT and *reeler* by means of subcellular channelrhodopsin-2 assisted circuit mapping (sCRACM, Petreanu et al., 2009; Yang et al., 2013). Briefly, neurons were selected for recording according to the criteria described above, as well as for being located at the edge of their home barrel or barrel equivalent. After bath application of TTX and 4-AP, we restricted the size of the illuminated spot to 25*25 μm and scanned a 225*300 μm area roughly centered on the recorded neuron and covering as much of the barrel or barrel equivalent as possible. Because only presynaptic boutons can be stimulated in such conditions, this method enabled us to map the localization of TC synapses on the dendritic arbors of recorded and reconstructed neurons.

A difficulty of this approach resides in the proper choice of a laser intensity with which to stimulate presynaptic boutons. Indeed, in spite of the blockade of voltage gate sodium channels in the axon, it is difficult to formally exclude the possibility of a purely electrotonic propagation of a ChR2 induced depolarization from one presynaptic bouton to another, nearby bouton through a shared axonal stem. While this effect is of little consequence in situations where stimulation of a large domain of the slice is desired, it can negatively impact the desired spatial resolution of 25 μm in the context of sCRACM experiments, as the stimulation of one field could propagate into another. In order to minimize this effect, we took advantage of the position of the recorded neuron. Indeed, owing to the position of the recorded neuron on the edge to its home barrel, the scanned area encompassed tissue lying both inside and outside of barrel borders. Because the dendrites of SpS neurons are

restricted to their home barrel, this configuration enabled us to set the laser power to the maximal value that evoked no response when stimulating outside of the barrel (i.e. in the infra or supragranular layer in WT) while preserving the responses to a stimulation centered on the soma, thereby providing a calibration procedure adaptable to individual neurons that at least minimized the potential contribution of electrotonically propagated depolarizations to our sCRACM maps.

Representative results of sCRACM experiments are illustrated in figure 6. Reconstructing recovered neurons enabled us to align the sCRACM map with the morphology of the recorded SpS. In WT, the spatial distribution of inputs was characterized by a central cluster of strongly responsive fields, encompassed in a gradually weaker surround (figure 14 A and B). Interestingly, the position of the peak response was consistently found on segments of proximal dendrites rather than on the soma, and always overlapped with the center of the barrel. This is presumably a reflection of the facts that (i) we recorded neurons whose soma was located on the edge, rather than at the center, of the barrel, which presumably constraints SpS dendrites to extend towards the barrel center rather than radiating from it; (ii) proximal dendrites tend to be richer in TC synapses than distal dendrites ([Schoonover et al., 2014](#); [Jia et al., 2014](#)), and (iii) those proximal dendrites receiving strongest inputs in our experiments were also extending through the area of the barrel where the density of TC fibers is expected to be highest ([Wimmer et al., 2010](#); [Oberlaender et al., 2012](#)). Thus the spatial distribution of inputs shown in figure 14 A and B is in good agreement with reported anatomy. In *reeler* animals, we found a qualitatively similar pattern of input distribution (figure 14 C and D), with domains of strong input more centrally located within the barrel or barrel-equivalent than weaker fields. A slight difference was apparent, however, in the fact that the clustering of strongly responsive fields appeared less tight or orderly in *reeler*, where comparatively high amplitude responses were routinely found further along the dendrite than in WT.

In order to obtain a statistical evaluation of input clustering, we used spatial autocorrelation and more specifically Moran's I ([Moran, 1950](#)). Moran's I is an established global measure of

spatial association based on the calculation of a statistic, I , that assesses the degree of correlation or “sameness” among neighboring features of a spatial distribution. The value of I varies from -1 to 1, where a value of 0 indicates a random spatial distribution, a value close -1 indicates a dispersed pattern (such as a chessboard), and a value tending towards 1 indicative of a clustered pattern where similar features are found next to each other. Applying this analysis to sCRACM data offered two advantages. First, it enabled us to determine whether the clustered pattern we believed to have noticed could be validated statistically. Second, and more importantly, the values of I were used as a quantification of how strong the clustering was in individual datasets and enabled a comparison across groups on the basis of an unbiased statistical measure (lanella et al., 2010). In all datasets tested, the spatial pattern of input amplitude distribution was deemed statistically clustered (figure 14 A-D, $p < 0.001$ in all of 13 WT and 14 *reeler* sCRACM maps). Furthermore, the values of I were lower on average in *reeler* SpS, an effect that was statistically significant (figure 14 G, t-test, $p < 0.05$, $n = 13$ WT and 14 *reeler*), indicating a lower degree of clustering of similarly responsive fields.

Finally, we compared the amplitude of TC fibers input to SpS neurons obtained from sCRACM experiments. figure 14 E and F illustrates the distribution of EPSP amplitudes recorded across 673 fields in WT and 683 fields in *reeler* from 13 and 14 individual neurons, respectively, in 1 mV bins. The median EPSP amplitude was significantly lower in *reeler* (ANOVA on ranks, $p < 0.001$), in agreement with the data obtained from full-field stimulation under TTX and 4-AP (figure 12 C). Interestingly, the distribution of amplitude in *reeler* was not best characterized by a general shift of the WT distribution towards zero, but rather by a selective decrease in the number of strongly responsive fields (> 5 mV) and a concomitant increase in the fraction of low amplitude fields (< 5 mV), an effect that was also statistically significant (two sample Kolmogorov Smirnov test, $p < 0.05$). A similar analysis on response latencies yielded no significant difference (ANOVA on ranks, $p = 0.2$, data not shown). Taken together, these results indicate that *reeler* SpS neurons receive an overall weaker, direct TC input with a lower degree of spatial organization, a finding which is likely to reflect differences in the spatial organization of TC synapses on these cells.

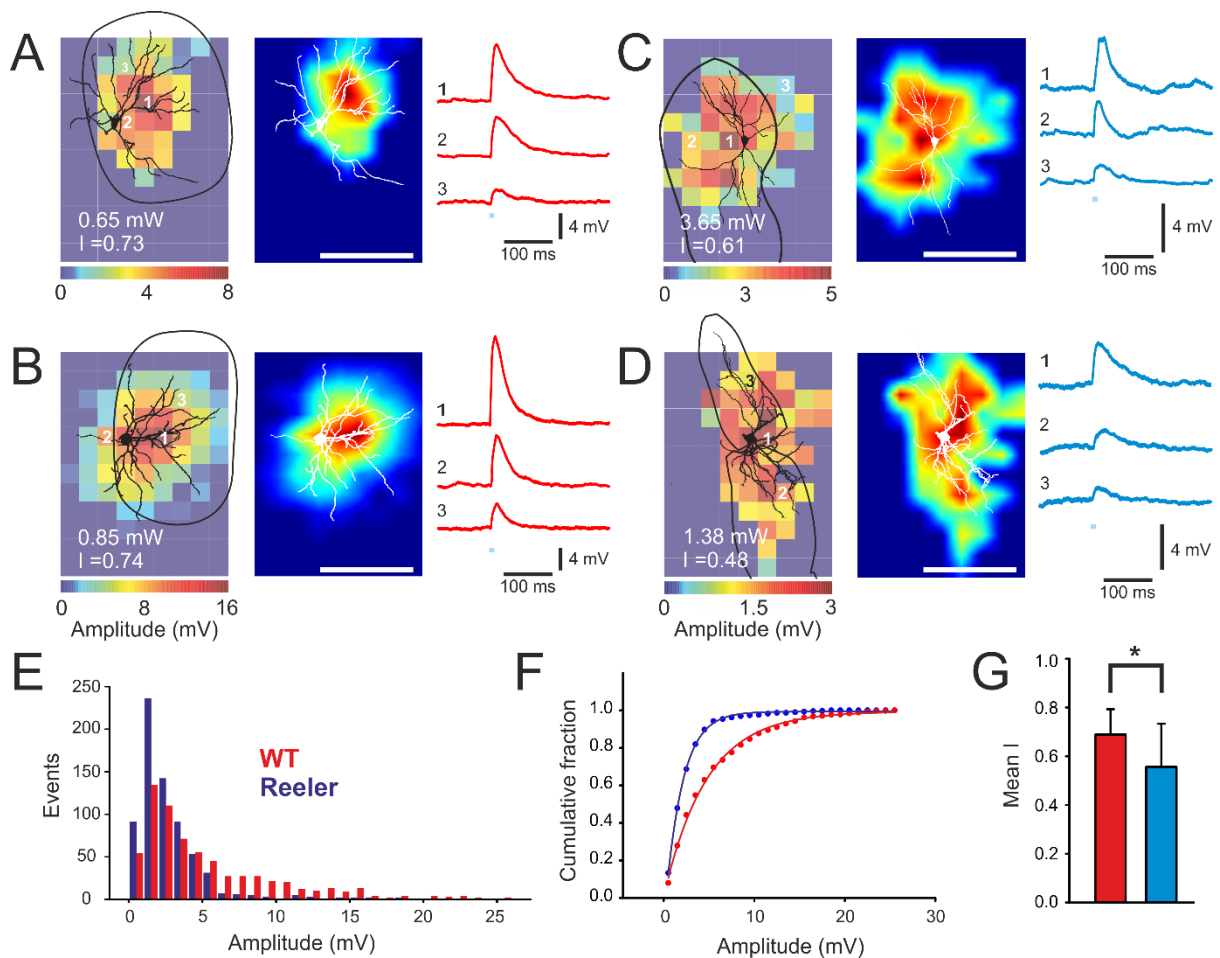


Figure 14. ChR2-assisted mapping of TC input to SpS. **A and B:** two representative datasets obtained from WT SpS. Left: raw amplitude map, overlaid with reconstructions of the recorded neuron and home barrel. The size of individual fields is $25 \times 25 \mu\text{m}$. Middle: same dataset, interpolated to a final resolution of 45×60 . The clustering of strongly responsive fields around a segment of proximal dendrite is clearly visible. Right: example of responses recorded during the sCRACM experiment. Each trace is the average of three repetitions delivered at the same location. The number above each trace corresponds to the location indicated on the raw amplitude map. Blue segments indicate the time of optogenetic stimulation. **B and C:** same as A and B, from reeler animals. **E:** distribution of response amplitudes across our dataset. The amplitudes were significantly lower in reeler ($n=683$ fields, 14 neurons) than in WT ($n=673$, 13 neurons; Kolmogorov-Smirnov test, $p < 0.005$). **F:** cumulative fraction of response amplitude in both genotypes. **G:** mean Moran's I values calculated for 13 WT and 14 reeler mice. The mean I was significantly lower in reeler (one tailed t-test, $p < 0.05$), indicating a lesser degree of spatial clustering of TC input.

TC synapses are predominantly formed on dendritic spines. We sought to determine whether the spatial distribution of dendritic spines on reconstructed neurons was altered in *reeler* in a way that could at least partly account for the results obtained from sCRACM experiments. We therefore conducted a Scholl analysis on 6 *reeler* and 7 WT reconstructed neurons. We quantified the total length of axon and the number of spines in consecutive rings of 25 μm thickness centred on the soma and spanning a total radius of 175 μm . In addition, we calculated the average density of spines in each consecutive ring by dividing the spine count by the total dendritic length measured. The results are illustrated in figure 15.

Figure 15 A shows the distribution of total dendritic length as a function of distance from the soma. In WT SpS neurons, this length increases from a modest value in the perisomatic region to peak between 26 and 50 μm from the center of the soma, and gradually decreases with increasing distance. A similar pattern was observed in *reeler*, with a lower peak and comparatively higher values further away from the soma. A two way ANOVA (distance and genotype) revealed that dendritic length was significantly affected by distance from the soma ($p < 0.001$). No effect of genotype was observed ($p = 0.94$), in line with our previous analysis (see table 2). Interestingly, we observed a genotype * distance interaction ($p < 0.05$), which indicates that the effect of distance differs between genotypes, and indeed, the total length of dendrites was found to peak higher in WT than in *reeler* (Fig 15 A, 26-50 μm , Holm-Sidak post hoc test, $p < 0.05$). The distribution of spines as a function of distance followed a pattern similar to that of dendritic length in both genotypes (Figure 15 B). We found no difference between genotypes in the overall number of spines (two way ANOVA, $p = 0.99$), but the number of spines was significantly affected by distance ($p < 0.001$). We again found an interaction between distance and genotype ($p < 0.026$), and effect which was narrowed down to be due to a significantly lower number of spines within a distance of 50 μm from the soma in *reeler* SpS. The average density of spines (Figure 15 C) was found to be affected by distance as well (two way ANOVA, $p < 0.001$), but we found neither an effect of genotype ($p = 0.63$) nor an interaction ($p = 0.24$). These results demonstrate that the reduction of spine number close to the soma in *reeler* is due to a reduction of average dendritic length in this location, rather than to a specific effect on spine localization along dendrites.

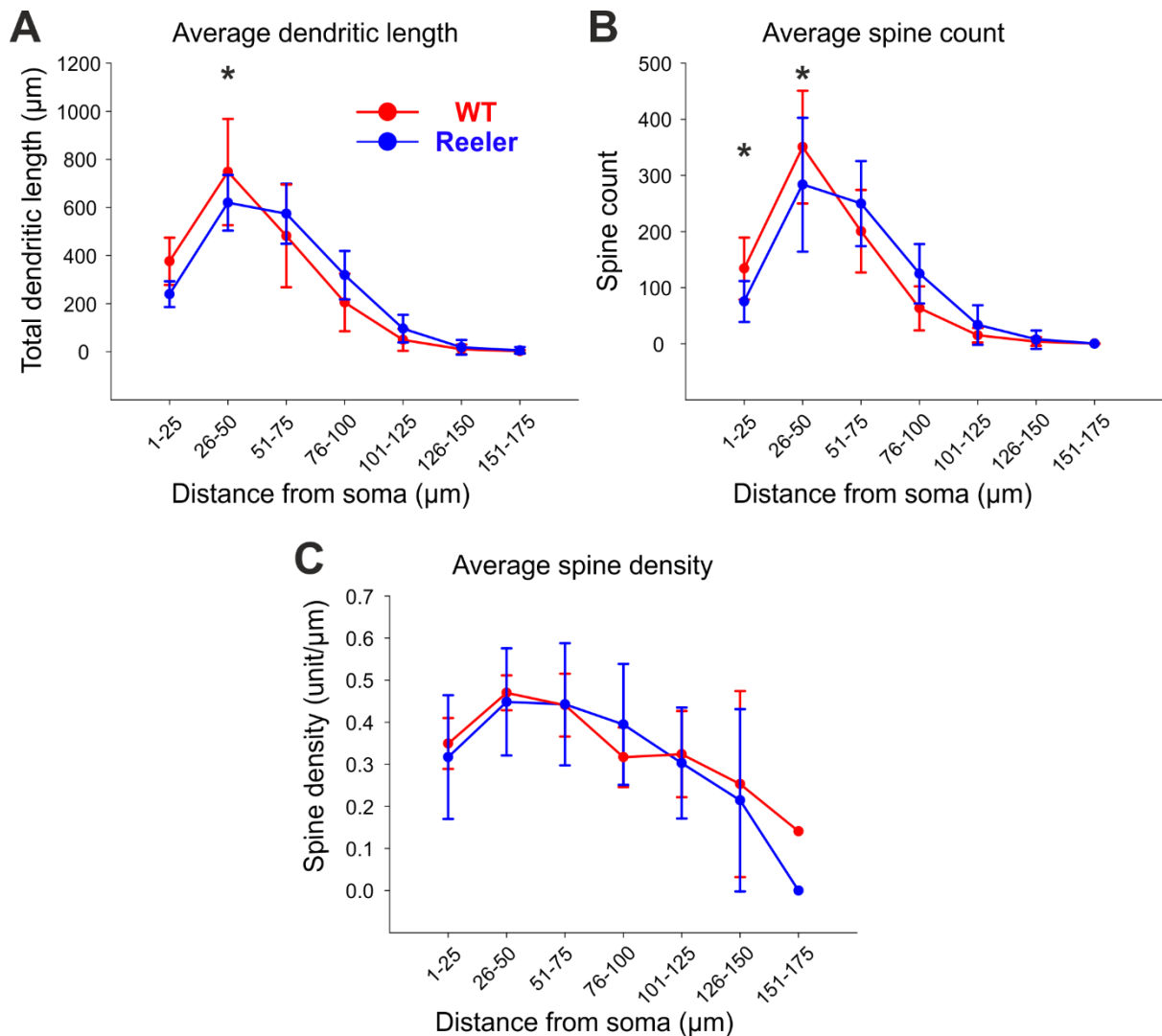


Figure 15. Distribution of spines on the dendrites of reconstructed SpS neurons. **A:** average cumulative length of dendrite in the 7 concentric rings of our Scholl analysis. Every ring has a thickness of 25 μm . Traces represent the average \pm SD of 7 WT (red) and 6 reeler (blue) animals. Average dendritic length was found to be significantly higher in the bin spanning 26 to 50 μm from the soma in WT ($p < 0.05$). **B:** average number of spines as a function of distance from the soma. The number of spines was significantly lower in the first 50 μm in reeler ($p < 0.05$). **C:** dividing the results in **B** by those in **A** reveals the average density of spines as a function of distance from the soma.

Interestingly, the distribution of dendritic spines along the somatodendritic arbor of SpS neurons matches rather well with the sCRACM maps, at least on a qualitative level. The number of spines was found to be highest close to the soma, but not directly on it, in good

agreement with the localization of the most strongly responsive fields in sCRACM maps. In addition, we found that the number of spines proximal to the soma was significantly decreased in *reeler*, an effect that appeared to be compensated for by a concomitant (but not statistically significant) increase in the number of spines found at greater distances away from the soma. This slightly altered pattern of spine distribution may well account, at least partly, for the altered distribution of input strength observed in *reeler* sCRACM experiments. Such a conclusion is subject to caution, however, as the number of spines is a poor indicator of the number of TC synapses actually contacting these spines, as only a relatively small fraction of the total spines are occupied by TC synapses in SpS neurons. The present results therefore support the possibility that subtle alterations in the morphology of *reeler* SpS neurons may contribute to shaping the patterning of TC input; it is almost beyond doubt, however, that effects specific to the TC synapses, such as differences in synaptic weight, also contribute heavily.

Discussion

Functional organization of the *reeler* somatosensory cortex

The most striking characteristic of the *reeler* cortex is its cellular disorganization resulting in the loss of cortical layers. Such a dramatic abnormality would lead many observers expecting major disturbances in the functional organization of the cortex, and in particular in the establishment of functional columnar modules as well as the specific pattern of interlaminar connectivity that forms the canonical columnar microcircuit in WT.

In the present study, we contributed to shedding light on these questions by using a mouse line in which Cre driven fluorescence enables the visualization of clusters of LIV cells in the WT mouse and their equivalent in *reeler*. LIV equivalent cells cluster together and form barrel equivalent structures in *reeler* (Wagener et al., 2010). In tangential sections through the somatosensory cortex, these barrel equivalent structures form the very recognizable pattern of the barrel field, where 5 rows and multiple arcs were unequivocally visible. It is widely considered that individual barrels mark the dimensions of what is referred to as a barrel related column (Lübke and Feldmeyer, 2007; Feldmeyer et al., 2013). The existence of a properly ordered pattern of barrel related columns in *reeler* constitutes the first piece of evidence of a conserved columnar organization in spite of the otherwise massive laminar disorganization. Such results are in perfect agreement with the literature (Caviness and Sidman, 1973; Caviness and Frost, 1976; Caviness and Rakic, 1978; Caviness et al., 1982; Wagener et al., 2010; Boyle et al., 2011).

Beyond providing a map of putative functional columns, barrel equivalents also delineate the domains where the terminal fields of TC axons are expected to be densest. Indeed, layer IV and, to a lesser degree, the LV/VI border are well known to receive the majority of the input from the VPM, although all layers receive some thalamic innervation (Wimmer et al., 2010; Oberlaender et al., 2012). The results of our AAV5 injections, which caused expression

of eYFP in TC fibers, revealed an innervation pattern in perfect agreement with the literature on WT animals, with a strong presence of eYFP in LIV, at the LV/VI border, and a weaker expression in other layers. In *reeler* animals, we found that eYFP expression was highest in clusters of tdTomato positive neurons, indicating a strong innervation of barrel equivalents by thalamic neurons. Furthermore, our electrophysiological recordings revealed that SpS neurons responded to a stimulation of TC fibers, indicating that functional synapses are established in both genotypes. These results confirm and extend previous studies and provide compelling evidence that, similarly to the WT, thalamic input predominantly reaches the cortex by specifically targeting barrels ([Wagener et al., 2010](#)).

A purely descriptive assessment of the cytoarchitecture of the *reeler* barrel field is insufficient to demonstrate another critical aspect of the functional organization of the barrel cortex, which is somatotopy. The barrel field indeed constitutes a somatotopic representation of the whiskers on the snout, where every single whisker is represented by one single barrel ([Woolsey and Van der Loos, 1970](#); [Masino et al. 1993](#)). While solid evidence of somatotopy in *reeler* existed prior to the present study, we hereby provide the first demonstration of somatotopy in the *reeler* barrel cortex from *in vivo* functional imaging using standard methods ([Grinvald et al., 1986](#); [Frostig et al., 1990](#); [Masino et al. 1993](#); [Kleinfeld and Delaney, 1996](#); [Wagener et al., 2010](#)). Stimulation of an individual vibrissa evoked a hemodynamic signal centered on, and peaking at, the location of the corresponding barrel in the barrel field. Upon stimulating a total of nine whiskers in sequence, we observed that the center of their functional representation was shifted with respect to one another, resulting in a pattern that matched the pattern defined by the underlying barrels and barrel equivalents. We conclude that information flow into the cortex retains a columnar and somatotopic organizing principle in the otherwise disorganized *reeler* cortex ([Mountcastle et al., 1957](#); [Mountcastle, 1957 and 1997](#); [Petersen and Sakmann, 2001](#); [Horton and Adams, 2005](#); [Feldmeyer et al., 2013](#)). It follows that the cortical layers are not a prerequisite for the establishment of columnar modules.

Interestingly, the persistence of columnar modules in *reeler* indicates that neurons sharing similar receptive field properties cluster together, as they do in the WT. During cortical development, newly generated neurons deriving from common progenitors migrate radially into the cortex where they form networks of sibling neurons sharing similar receptive field properties, and the *reeler* functional columnar modules revealed here are therefore likely to be composed of neurons sharing a common lineage (Yu et al., 2012; Li et al., 2012). The process of cortical arealization is believed to involve the projection of an arealized protomap already extent at the level of the early proliferative cortical sheet onto the developing cortical plate, through the radial migration of newborn neurons (Rakic, 1988). According to this view, the size and number of (barrel-related) cortical columns are predetermined but can be modulated by thalamic input (Rakic, 1988; Sur and Rubenstein, 2005). In the present study, we found no obvious differences in the number or pattern of barrel related columns between the genotypes, and neither did we find differences in the distribution of thalamic fibers in the cortex, in that it preferentially targeted barrels or barrel equivalents in both genotypes, suggesting that TC pathfinding relies on cell autonomous cues rather than depths dependent cues (Wagener et al., 2010; Wagener et al., 2015). It is therefore conceivable that the loss of reelin, affecting only the radial migration of newborn neurons along radial glia, leaves the arealization of the early proliferative cortical sheet and subsequent formation of columns untouched. Formation of appropriate TC connections ensues. Such a scenario could account for the fact that cortical columns are properly formed in the *reeler* barrel cortex in the absence of laminar organization.

Functional connectivity in *reeler* barrel-related columns

Having established the existence of functional cortical columns in *reeler*, we can turn our attention to the matter of whether or not the canonical circuit is preserved in these mutants. The canonical circuit is composed of the many neurons that populate the cortical column and establish nonrandom, specific connections through which sensory information flows in a sequential manner (Lübke and Feldmeyer, 2007; Feldmeyer et al., 2013). Evidence for the existence of cortical columns alone provides little guarantee that such specific connections are maintained in *reeler*. Previous studies have reported abnormal connectivity outside of the somatosensory cortex. Ectopic and heterologous synapses have been

described in the cerebellum, such as synapses formed by mossy fibers on Purkinje cells in *reeler* cerebellum with no equivalent in WT (Mariani et al., 1977; Wilson et al., 1981; Sotelo, 1990). In the hippocampus, a fraction of fibers from the entorhino-hippocampal pathway are found in ectopic position and innervate inappropriate layers (Borrell et al., 1999). These ectopic fibers are likely to form functional synapses, and a fraction of mossy cells have indeed been found to receive aberrant, direct input from fibers of the perforant path (Kowalski et al., 2010). Furthermore, in the same study, mossy cells which do not receive direct input from the perforant path have been found to respond with a much lower temporal precision to disynaptic activation through stimulation of the perforant path than their WT equivalents. These results indicate that as a population, mossy cells are likely to fire in a much more asynchronous manner in *reeler* with respect to WT, leading to the notion that proper hippocampal network function might be compromised. Whether such misconnections also exist in the somatosensory cortex remains an open question, but their existence has been postulated (Caviness and Rakic, 1978; Caviness and Frost, 1983).

Our functional imaging studies have enabled us to confirm that columnar modules exist in *reeler*, but what have we learned on a more intimate level about the connectivity of the cell types that form these modules in *reeler*? An exhaustive inquiry of this question necessitates the painstaking work of probing every connection described so far in the canonical microcircuit, and is obviously neither within the means of the author, nor the most expedient approach imaginable. While the present work only scratches the surface of intracortical connectivity in *reeler*, some valuable lessons have nevertheless been learned.

First and foremost, our imaging experiments have demonstrated that sensory information from the thalamus reaches the *reeler* barrel cortex in a properly ordered, somatotopic way. Furthermore, our electrophysiological experiments showed that TC synapses are formed directly on SpS neurons, the primary recipients of thalamic input, in both genotypes. The input stage of the *reeler* cortical column is therefore comparable to that of WT and in agreement with the canonical microcircuit (Lübke and Feldmeyer, 2007; Feldmeyer et al., 2013). In addition, the subthreshold responses of SpS neurons to TC activation consisted in long lasting, compound depolarizations including direct, thalamic activation, as well as

numerous EPSPs occurring within several tens of milliseconds after the end of the 10 ms light pulse TC fibers were activated by. The long latency of some of the EPSPs recorded is incompatible with direct input from TC fibers and rather suggests a contribution from recurrent excitation. In WT animals, LIV neurons are known to strongly engage in reciprocal connections, and it is highly plausible that recurrent excitation originating from neighbouring SpS neurons contributed to the compound response we recorded (Zhu and Connors, 1997; Feldmeyer et al., 1999; Egger et al., 1999; Feldmeyer and Sakmann, 2000; Lübke et al., 2000; Schubert et al., 2003; Cowan and Stricker, 2004). In addition, LIV neurons are also targeted by LVI pyramidal cells, which provide yet another putative source of recurrent excitation (Zhang and Deschênes, 1997). Responses of *reeler* neurons were qualitatively similar to that of WT, and we can therefore conclude that intracortical, recurrent excitation can be recruited by TC fibers stimulation alone. While the exact source of the recurrent excitation observed in *reeler* with regard to the neuronal types involved remains elusive, its existence is beyond doubt.

Secondly, our recordings demonstrate that GABAergic inhibition also contributed to the compound responses, indicating inhibitory connections onto SpS neurons from local interneurons. Because we consistently observed the presence of inhibition in subthreshold responses at short latencies (<10 ms), it is highly plausible that feedforward inhibition (FFI) accounted for most of the inhibition observed (Sun et al., 2006). FFI is a well-documented phenomenon in the barrel cortex (Swadlow, 1995, 2002 and 2003). Inhibitory interneurons of LIV not only receive direct thalamic input (Staiger et al., 1996 and 1996), they also respond more vigorously, at lower thresholds, and with shorter latencies (Gibson et al., 1999; Porter et al., 2001; Gabernet et al., 2005; Cruikshank et al., 2007; Hull et al., 2009). Several species of interneurons may contribute to feed forward inhibition, but the more likely candidates share common features such as the expression of Parvalbumin (PV) and a fast-spiking (FS) firing pattern (Porter et al., 2001; Sun et al., 2006). Basket cells, for instance, are driven by TC input and target the soma of neighbouring excitatory neurons, which places them in an ideal position to exert tight inhibitory control over their targets (Sun et al., 2006; Staiger et al., 2009). Although the short latency of inhibition reported here suggests a strong contribution of FFI, we do not exclude the possibility that feedback

inhibition may occur as well, and in fact, we frequently observed sharp repolarizations after the recorded neuron fired an AP, which could not be fully attributed to afterhyperpolarization. Potential sources of feedback inhibition include the basket cells themselves, as well as the barrel-confined inhibitory interneuron, a PV positive, FS interneuron characterized by a dense axonal arborisation restricted to its home barrel and a very high incidence of strong, reciprocal connections with local excitatory neurons (Stalder et al., 2009; Koelbl et al., 2013). Determining which species of interneuron accounts for the inhibition observed in *reeler* is not a byzantine question, since they differ in the strength and kinetics of inhibition they provide (for example, FS cells provide stronger inhibition than regular spiking non-pyramidal neurons, Sun et al., 2006) and in their role in neuronal computation (Wilson et al., 2012). Such cell type specific properties may account for putative alterations in the inhibition received by *reeler* LIV equivalent neurons. While this question is, unlike many interneurons, a spiny one, the fact that LIV equivalent neurons in *reeler* receive thalamus evoked inhibition is beyond dispute.

Our third observation concerns transcolumar connections. The canonical circuit model emphasizes a vertically oriented, translaminar flow of sensory information in the cortical column. But substantial anatomical and functional evidence demonstrate that cortical column communicate with each other as well, through horizontal, transcolumar connections (Schubert et al., 2007; Narayanan et al., 2015). Here, we found that single whisker stimulation evokes a hemodynamic response that spreads further horizontally than the size of the corresponding barrel to encompass a large fraction of the barrel field, in agreement with previous reports (Masino et al., 1993; Masino and Frostig, 1996; Chen-Bee et al., 1996 and 2012; Drew and Feldman, 2009). Our intrinsic signals were acquired from a depth of 300 micrometers below the pia, implying that our signals were dominated by granular and supragranular layer sources in WT animals. Tactile information reaches the somatosensory cortex through TC synapses clustering in LIV barrels. From there, excitation spreads vertically to LII/III and horizontally to neighbouring columns through transcolumar excitatory connections originating from LV and LII/III, resulting in a hourglass-shaped profile of neuronal excitation spread that encompasses a barrel and a large domain of the supra and infragranular layers (Kohn et al., 2000; Petersen et al., 2001 and 2007; Schubert et al.,

2007). This lateral spread of excitation causes single whisker stimulation to evoke hemodynamic signals that cover more than the size of their corresponding barrel to actually encompass a large fraction of the barrel field, and effect that can also be observed with voltage-sensitive dye imaging (Ferezou et al., 2006). Functionally, such connections are thought to broaden the receptive fields of single neurons in neighboring columns (Brecht and Sakmann, 2002; Fox et al., 2003). In *reeler* mice, LII/III and LV fated cells are spread across the depth of the cortex instead of forming distinct layers (Wagener et al., 2010). Because we found no increase (or decrease) in the area covered by the sensory evoked intrinsic signal in *reeler* animals, we conclude that transcolumnar cortico-cortical connections innervate a domain that is similar in size to what is observed in a laminated cortex, and hypothesize that the receptive fields of individual neurons is likely to be equally broad in both genotypes.

In summary, our results indicate that a proper intracortical connectivity in the *reeler* brain is likely to be preserved even in the absence of cortical lamination. We found conclusive evidence for a direct thalamic input on a defined class of LIV equivalent excitatory neuron, as well as convincing indication that a substantial, intracortical excitatory network is recruited by thalamic afferents. We also established that LIV equivalent neurons receive inhibition, with suggestive indication that both feedforward and feedback inhibition are at work in the *reeler* cortex. It thus appears that functional connectivity in the somatosensory cortex is largely unaffected by the loss of reelin, leading to the expectation that cortical function is also largely preserved.

Evoked responses: the *reeler* paradox

Two complementary approaches were used to probe cortical function in response to sensory input in the present study. In a first series of experiments, we used controlled whisker stimulation in anesthetized animals and measured the evoked responses with intrinsic signal imaging. In a second series, we relied on channelrhodopsin-2 to specifically stimulate TC fibers and recorded evoked responses by means of intracellular recordings in a reduced preparation, the TC slice. This dual strategy enabled us to compare a measure of

global network activity, the intrinsic signal, with a measure of evoked activity in a subcomponent of the network, the thalamorecipient LIV SpS neuron. The comparison yielded surprising and unexpected results.

Our intrinsic signal imaging experiments revealed that evoked responses were of similar magnitude in both genotypes across a range of behaviourally relevant stimulus frequencies (Carvell and Simons, 1990). Similar results have been obtained in the visual cortex of *reeler* with intrinsic signal imaging (Pielecka-Fortuna et al., 2014), and a previous study from our laboratory utilizing c-fos expression as a marker of neuronal activity reached yielded the same observations (Wagener et al., 2010). These congruent results naturally suggest that thalamic input was comparable across genotypes in all three studies. Surprisingly, our intracellular recordings indicated that the thalamic input to SpS neurons is slightly, but significantly weaker in *reeler*. These findings are somewhat contradictory and warrant further explanation.

Could the discrepancy be explained by differences inherent to the methods we utilized? As a hemodynamic signal, the intrinsic signal we recorded critically depends on there being a dense microvascular network in the cortex, the development of which might be compromised in *reeler* (Malonek et al., 1997; Vanzetta et al., 2008; Drew et al., 2011; Lindhorst et al., 2012). In order to rule out such a possibility, we quantified the density of the microvascular network using a staining protocol which labels erythrocytes rather than blood vessels. We did not find major differences between the genotypes that may have skewed our functional imaging results, in agreement with the scarce literature on the subject in the *reeler* cortex (Stubbs et al., 2009), and in contrast with literature on the hippocampus (Lindhorst et al., 2012). It may be objected that the method chosen offers at best a crude labelling of blood vessels, insufficiently sensitive for detection of subtle differences; in response, we must emphasize that our results are perfectly in line with those obtained with high-throughput, automated histology coupled with extensive labelling of the cortical microvascular network (Blinder et al., 2013). It appears, therefore, that the loss of

either reelin or cortical layers does not strongly affect the development of a dense cortical blood vessel network.

If the fact that we failed to find a difference between the genotypes in the evoked intrinsic signal, as would be expected if *reeler* received a weaker thalamic input, cannot be explained by differences in the cortical microvasculature, what other possibilities exist? One may argue that another parameter, the neurovascular transfer function, or quantitative relationship between a given amount of evoked neuronal activity and the corresponding hemodynamic signals, is not known explicitly in *reeler* cortex (Cardoso et al., 2012). Without this knowledge, the interpretation of hemodynamic signals with respect to the underlying neuronal processes they represent is delicate. Studies combining functional imaging with electrophysiological recordings have demonstrated that the neurovascular transfer function is not invariant, but can be affected by anaesthesia (Martin et al., 2006) and differs depending on the anatomical structure under investigation (Devonshire et al., 2012). It is therefore conceivable that the neurovascular transfer function is slightly steeper in *reeler*, such that an overall weaker network activity would be translated into a roughly similar hemodynamic signal. The opinion of the author is however that such a coincidence is rather implausible. A more likely methodological source of the discrepancy can be found in the respective resolutions of the methods used. Our electrophysiological recordings provided cellular and sub-millisecond resolution, while hemodynamic signals typically integrates neural activity across far greater spatial and temporal dimensions, with time constants in the range of seconds (Grinvald et al., 1986; Frostig et al., 1990). Neural activity evoked by stimulation of LIV is known to spread through the entire cortical column within a few tens of milliseconds (Petersen and Sakmann, 2001), but the temporal resolution provided by our intrinsic signal imaging protocol was 200 milliseconds. It is therefore likely that our imaging experiments simply lacked the sensitivity to detect a hemodynamic correlate of the otherwise modest difference we found in intracellular recordings.

Finally, one should take into consideration a more interesting and scientifically satisfying possibility. One of the most parsimonious explanations for the lack of difference in the hemodynamic signal between the genotypes is simply that there is not difference in the underlying sensory evoked, network activity. In such a view, favoured by the author, the

observations reported here constitute neither a discrepancy nor a contradiction, but a stimulating paradox: how can cortical networks be equally active in *reeler* if the sensory drive they receive from the thalamus is weaker?

Possible causes of a weakened thalamocortical input in *reeler*

As such, the fact that TC input to SpS is weak is neither surprising nor new, as individual TC synapses have been described as weak (Bruno and Sakmann, 2006). A number of mechanisms that ensure the reliability of sensory transmission in the context of weak synaptic input have been described as well, including convergence and synchronous activation of TC synapses originating from high numbers of VPM neurons on individual LIV excitatory neurons (up to 85 in rats, Bruno and Sakmann, 2006; Wang et al., 2010), enrichment of TC synapses in perisomatic loci (Richardson et al., 2009; Schoonover et al., 2014; Jia et al., 2014), local clustering of synapses along the dendritic arbor, potentially allowing for cooperativity and recruitment of active dendritic properties such as Ca²⁺ and Na⁺ spikes (Larkum et al., 2008), and expression in SpS neurons of voltage insensitive NMDA receptors containing the NR2C subunit (Binshtok et al., 2006). To our knowledge, whether and how the loss of reelin affects these properties is unclear, but accumulating evidence suggest that reelin plays a role in the regulation of synaptic function at both pre and postsynaptic levels. Postsynaptically, reelin modulates the function of NMDA receptors. In cortical and hippocampal neurons, reelin enhances NMDA receptor mediated current and calcium influx through Src family tyrosine kinase (SFKs) and Dab 1 dependent tyrosine phosphorylation of their NR2 subunits (Beffert et al., 2005; Chen et al., 2005; Qiu et al., 2006). The absence of this amplification mechanism in the *reeler* mouse may very well explain the lower responses of SpS neurons to TC input. Reelin has been proposed to regulate presynaptic function as well. In *reeler* hippocampus, the number of presynaptic vesicles is increased while the expression of SNAP25, a protein of the SNARE complex, is decreased (Hellwig et al., 2011). These results point to compromised vesicle fusion and neurotransmitter release, which could easily account for the weaker TC input observed here. Beyond purely synaptic effects, reelin also modulates the outgrowth of dendritic spines. Reelin deficiency results in a reduction of the density and number of dendritic spines in hippocampal pyramidal neurons (Liu et al., 2001; Niu et al., 2008). Because TC synapses

overwhelmingly contact spines (Benshalom and White, 1986), fewer spines may indicate an overall reduction in the number of TC synapses formed onto *reeler* SpS neurons, thereby dampening their responsiveness to thalamic input. Our own results are at odds with data from the hippocampus, however. We found similar numbers of dendritic spines in SpS neurons of the cortex in both genotypes. It is therefore unlikely that such a mechanism would account for the weakened TC input reported here. Together, these data suggest that reelin deficiency can impact synaptic function via mechanisms that are independent of developmental abnormalities.

Compensation mechanisms for a weak thalamocortical input: solving the *reeler* paradox

What mechanisms compensate the weakness of the TC input to SpS neurons in *reeler* and enable normal network activation? One possibility lies in the fact that VPM input does not target only LIV but also LV, and to a lesser degree, all other cortical layers (Wimmer et al., 2010; Meyer et al., 2010; Oberlaender et al., 2012). It is therefore conceivable that in *reeler*, the weaker input to LIV equivalent neurons is compensated for by a concomitant strengthening of TC input to other cell populations. However, such a possibility may not fully account for the fact that the same paradox is observed on the scale of individual *reeler* SpS neurons. Indeed, the compound responses to thalamic stimulation we recorded in *reeler* exceeded that in WT, although the purely thalamic component was weaker. These results indicate that the relative contribution of network effects to the compound response is larger in *reeler*. One excitatory component of the compound response, aside of direct TC input, is recurrent excitation. LIV excitatory neurons readily engage in reciprocally connected networks (Feldmeyer et al., 1999; Egger et al, 1999; Feldmeyer and Sakmann, 2000; Lübke et al., 2000; Cowan and Stricker, 2004), giving birth to the idea that LIV may act as more than just a relay for, but also as an amplifier of, sensory input (Douglas et al., 1995; Suarez et al., 1995; Feldmeyer et al., 1999; Egger et al, 1999; Feldmeyer and Sakmann, 2000; Lübke et al., 2000; Li et al., 2013a and 2013b; Lien and Scanziani, 2013). An appealing idea is therefore that the *reeler* cortex, in order to accommodate a weaker TC sensory input, increases its intracortical amplification. The mechanisms involved may include stronger or more numerous reciprocal connections between nearby LIV equivalent neurons allowing for enhanced recurrent excitation.

An alternative possibility involves differences in TC evoked inhibition in SpS neurons. The present results confirm the existence of FFI in *reeler* SpS in subthreshold, compound responses. Subthreshold responses in *reeler* were stronger than in WT, which can indicate a decrease in inhibitory tone, as suggested by previous authors ([Carboni et al., 2004](#); [Qiu et al., 2006](#)), possibly due to a lower number of synapses formed by fast spiking, PV expressing interneurons in *reeler* ([Xue et al., 2014](#); [Tao et al., 2014](#)). In addition, we found that *reeler* SpS neurons repolarize less sharply after firing an AP than their WT counterparts, which could be caused by a decrease in feedback inhibition. Interestingly, CA1 hippocampal neurons receive reduced spontaneous IPSCs but unchanged EPSCs in reelin haploinsufficient mice, whose reelin expression is reduced by about 50% ([Qiu et al., 2006](#); [Liu et al., 2001](#)). It follows that a decrease in inhibitory tone represents a plausible compensatory mechanism for the weaker TC input in *reeler*. Further experiments are required to precisely disentangle these various possibilities, such as paired recordings of SpS and inhibitory interneurons, which would allow direct comparison of the potency of reciprocal connection as well as of thalamic input between excitatory and inhibitory neurons ([Cruikshank et al., 2007](#)).

Differences in intrinsic properties of SpS neurons are unlikely to account for the weaker TC responses in *reeler*. We found no significant difference between genotypes in input resistance or rheobase, indicating that the lower responsiveness to TC input in *reeler* must result from synaptic, rather than intrinsic, properties. Not all intrinsic properties were equivalent in both genotypes. We observed that *reeler* SpS had a slightly more hyperpolarized resting membrane potential upon breakthrough. In addition, the voltage sag was significantly weaker in *reeler*, indicating possible differences in the hyperpolarization-activated cation current I_h ([Magee, 1998](#)). Such findings are not without precedent. Reelin has been demonstrated to mediate the establishment of a somatodendritic gradient of HCN1 channel density in neocortical pyramidal neurons through its downstream, Dab1 dependent signaling cascade. Disruption of the Reelin/Dab1 signaling pathway results in an impoverishment of the HCN1 content of distal dendrites, leading to a decrease in sag ratio and a hyperpolarized resting membrane potential in that cellular compartment ([Kupferman et al., 2014](#)). Our findings therefore indicate a weakening of I_h in *reeler* SpS neurons. Although I_h has been linked to dendritic integration and temporal summation of inputs in

dendrites of large cortical pyramidal and hippocampal neurons (Magee, 1998; Nolan et al., 2004), much less is known about the role of these channels in smaller neurons such as SpS. At any rate, it is unlikely that differences in I_h contributed much to the differences in synaptically evoked responses reported here. Indeed, the difference in I_h found here could only be detected when using recording and analysis protocols specifically designed to detect it, and even then, it was very modest. So modest, in fact, that we could not see a difference between genotypes in input resistance or time constant, as would be expected if the difference in I_h was large (Magee, 1998). A possible explanation is that the effect of I_h on R_{in} and τ is “diluted” by other, larger sources of variability, in particular cell-to-cell variability in the expression of other conductances contributing to R_{in} and τ . Furthermore, we recorded evoked responses in neurons that were held around a comparable membrane potential of -70 mV, a value at which I_h is only minimally active (Magee, 1998). It must be noted, however, that a small difference in I_h may in principle contribute to the differences in the evoked responses evoked under TTX and 4-AP. Indeed, given its reversal potential of -25 to 40 mV and its very slow deactivation kinetics (Solomon and Nerbonne, 1993; Magee, 1998; Robinson and Siegelbaum, 2003; Biel et al., 2009), I_h can provide a “boost” to synaptically evoked responses. Because I_h is weaker in *reeler*, the smaller boost could account for the relative weakness in TC evoked responses. The same argument does not work for evoked responses, however. A weaker I_h in *reeler* would lead to expect smaller compound responses as well, and we found the opposite to be the case. Therefore, while I_h could at least partly explain the weaker response to TC input in *reeler*, it cannot solely account for the differences in compound responses, and does not solve the *reeler* paradox by itself. Overall, the author holds the view that differences in I_h are unlikely to be large enough to account for the results presented here.

Altered somatodendritic distribution of thalamocortical input in *reeler*

A further difference we observed between *reeler* and WT was in the spatial distribution of TC input on their somatodendritic arbors. sCRACM experiments revealed that TC input was strongest in perisomatic regions, and became weaker further from the soma. In WT, the strongest input was found to be on proximal dendrites close to the center of their home barrel, rather than directly on the field containing the soma, indicating that relative density

of TC fibers, rather than dendritic filtering, was probably the dominant factor shaping the input maps (Petreanu et al., 2009; Wimmer et al., 2010; Oberlaender et al., 2012). Although a qualitatively similar pattern appeared in *reeler*, statistical analysis revealed that the clustering of inputs close to the soma was weaker resulting in a less tight grouping of highly responsive fields around the soma and comparatively higher input from more distant dendritic sites. sCRACM maps provide an approximation of the relative densities of synapses along the somatodendritic arbor (Petreanu et al., 2009). Because the number of TC synapses on WT SpS is higher in proximal rather than distal dendritic compartments (Jia et al., 2014; Schonnoover et al., 2014), a possible interpretation of these results is that they are caused by differences in the dendritic distribution of TC synapses in *reeler*, such that the gradient in synaptic density along dendrites is less steep in *reeler* than in WT or perhaps nonexistent.

We could find some evidence to that effect using a Scholl analysis on the distribution of dendritic spines in our reconstructed neurons. Indeed, the number of spines was slightly but significantly reduced within a 50 μm radius from the soma in *reeler*, which was compensated for by a concomitant increase in spine number at all further distances along the dendritic arbor (this increase did not, however, reach statistical significance), such that the average number of spines remained similar across genotypes. Because the average density of spines (spine count per unit of dendritic length) was not different between the genotypes, these results can be attributed to a slight decrease in the average dendritic path length within a 50 μm radius from the soma in *reeler*, with a compensatory, slight increase at further distances. It is therefore possible that slight alterations in the *reeler* somatodendritic arbor could have contributed to shaping the sCRACM maps. This interpretation must be viewed with caution, however. First, although the majority of TC synapses contact the spines of SpS neurons, the reverse is not true, meaning that dendritic spines are a rather poor predictor of TC synapse localization (Benshalom and White, 1986). Second, our filling, confocal imaging and reconstruction protocols may not have captured the entirety of the spine population, and the number reported here may be underestimated (in spite of being somewhat higher than in published literature, Sun et al., 2014). Finally, the response amplitude measured with sCRACM is determined not only by the number but also the strength of the stimulated synapses, which makes the correlation of anatomical and

functional maps delicate. Nevertheless, these results illustrate that slight morphological alterations in *reeler* may in principle contribute to differentially shaping synaptic inputs.

The sCRACM data revealed yet another difference between the genotypes, namely in the amplitude of the responses, which was lower in *reeler* in agreement with our full-field stimulation experiments. This result may reflect the putatively more scattered distribution of TC synapses suggested above, which would result in a larger fraction of the total amount of TC synapses being located comparatively far from the soma, with the consequence of adding to the average dendritic length that evoked EPSPs travel on their way to the soma and thereby increasing attenuation. An alternative hypothesis leaps to mind, however. The decrease in evoked amplitude observed in sCRACM experiments in *reeler* is best described as a marked reduction in the number of dendritic stimulation points that yielded high amplitude responses, and a concomitant increase in the number of weakly responsive fields. This raises the possibility that tight clustering of TC synapses on SpS dendrites, which has been described in WT ([Benshalom and White, 1986](#); [Lavzin et al., 2012](#)), may not exist in *reeler*. Clustering of TC synapses has been predicted by theoretical work as a putative consequence of LTP learning rules ([Govindarajan et al., 2006](#); [Larkum et al., 2008](#)) and is thought to enable synchronous, cooperative input to recruit active dendritic properties such as Ca²⁺ or Na⁺ spikes. In recent years, this notion has gained experimental support ([Losonczy et al., 2008](#); [Ianella et al., 2010](#); [Makino et al., 2011](#); [Takahashi et al., 2012](#); [Lavzin et al., 2012](#); [Smith et al., 2013](#)), leading to the emergence of a model of memory formation based on the formation of such clusters ([Losonczy et al., 2008](#); [Kastellakis et al., 2015](#)). Interestingly, substantial evidence indicates that hippocampal LTP is regulated by reelin, the absence of which could lead to impaired formation of strong and stable connectivity either as the basis of memory formation or reliable sensory transmission ([Weeber et al., 2002](#); [Beffert et al., 2005 and 2006](#); [Qiu et al., 2006](#); [Trotter et al., 2013](#)). Further experiments are required to ascertain the extent of TC synapse clustering impairment in *reeler* and its consequences on sensory transmission to the cortex.

Functional implications for the *reeler* cortex

Finally, the present study sheds new light on the potential computational consequences of a loss of reelin. *In vivo* extracellular recordings in the anesthetized *reeler* visual cortex have provided evidence of an overall reduction in firing rates in response to visual stimulation (Dräger, 1981). This result can be well explained by the weakening of TC drive described in the present study. In addition, the proportion of cells with sharp orientation tuning is reduced in *reeler* visual cortex (Dräger, 1981), a finding which may be connected to the deficit in visual orientation discrimination observed in these mice (Pielecka-Fortuna et al., 2014). Several synaptic and cellular mechanisms are thought to contribute to the synthesis of receptive fields in sensory cortices, one of which being inhibition (Isaacson and Scanziani, 2011). Inhibition has been involved in modulating receptive fields in several ways depending on the identity of the GABAergic interneurons involved. Dendrite targeting and somatostatin expressing neurons in particular were found to provide subtractive inhibition resulting in a sharpened angular tuning of nearby excitatory neurons of visual cortex (Mao et al., 2011; Wilson et al., 2012). The timing of FFI with respect to excitation also seems to be implicated in receptive field synthesis in the somatosensory cortex, where a shift in the delay of inhibition with respect to excitation underpins direction selectivity (Wilent and Contreras, 2005). Interestingly, Kowalski et al have described a higher heterogeneity in spike timing in *reeler* hippocampal mossy cells in response to electrical stimulation of the perforant path, an effect probably due to aberrant excitatory input in a subset of such cells in *reeler* (Kowalski et al., 2010). Because FFI determines the window of opportunity for temporal summation of EPSPs to cross firing threshold (Swadlow, 2003; Wehr and Zador, 2003; Gabernet et al., 2005), the same form of temporal imprecision in interneurons firing could easily alter the receptive fields of nearby excitatory neurons. Our observation that inhibition may be impaired in *reeler* is therefore of particular interest, as it could explain the abnormalities in receptive field structure observed in this mutant.

Active dendritic properties provide an additional set of mechanisms contributing to the synthesis of receptive fields. Dendritic spiking and NMDA receptor mediated regenerative amplification contribute to the computation of angular tuning in both somatosensory and visual cortices (Lavzin et al., 2012; Smith et al., 2013; but see also Jia et al., 2014).

Recruitment of dendritic computation is facilitated by clustering and synchronous activation of similarly tuned synapses (Larkum et al., 2008). Our own results indicate that the formation of reliable synaptic clusters may be impaired in *reeler*, providing an additional mechanism by which receptive field structure may be altered in this mutant. Determining which of these mechanisms is causal to the *reeler* phenotype with regard to angular tuning abnormalities and orientation discrimination deficits will be central to future research focusing not only on the roles of reelin but also on the function of cortical networks.

Conclusion and perspectives

Although the *reeler* phenotype has been described over half a century ago (Falconer, 1951) and has since provided a fruitful model for the study of cortical development (Herz et al., 2006; Förster et al., 2010; D’Arcangelo, 2014), few investigators have examined the consequences of reelin deficiency on the function of cortical networks. What studies exist relied chiefly on electrophysiological methods, and examined the *reeler* hippocampus (Bliss and Chung, 1974; Ishida et al., 1994; Kowalski et al., 2010), visual cortex (Dräger, 1981; Lemmon and Pearlman, 1981; Simmons and Pearlman, 1983), and somatosensory cortex (Wagener et al., 2010, 2015; Guy et al., 2014), and found at most modest differences. Behavioural studies have failed to report major deficiencies in the basic function of sensory systems (Salinger et al., 2003; Pielecka-Fortuna et al., 2014). The consensus emerging from these studies is that in spite of a few marginal abnormalities, the *reeler* brain retains a connectivity comparable to that of the WT brain and hence, a comparable function. The results reported here are in broad agreement with this notion. Using a combination of functional imaging *in vivo* and electrophysiology *in vitro*, we could elucidate several aspects of the structure and function of the *reeler* somatosensory cortex, and found them to be strikingly normal. We report a functional organization of the *reeler* cortex comparable to that of a WT cortex. Standard patterns of connectivity, such as a concentration of thalamic input on LIV cells and thalamus-evoked FFI, are preserved in *reeler*. Accordingly, the responsiveness of cortical networks seems to be unchanged by reelin deficiency. It would appear that we must align ourselves with the predominant view that aside of the massive cellular disorganization that is its hallmark, nearly all is normal in the *reeler* brain.

However, many of the studies mentioned here reported some abnormalities in the *reeler* brain, such as aberrant connectivity in the hippocampus (Borrel et al., 1999, Kowalski et al., 2010) and the cerebellum (Mariani et al., 1977). Small functional differences such as lower firing rates and a higher incidence of comparatively broad receptive fields were also documented in the visual cortex (Dräger, 1981; Lemmon and Pearlman, 1981). In the present thesis, we also report a potentially important abnormality: the thalamic input to LIV SpS neurons, the main recipients of sensory information in the cortex, is weaker in *reeler*. This rather surprising result is in apparent contradiction with the data obtained from our and others (Pielecka-Fortuna et al., 2014) functional imaging experiment. This paradox prompted us to propose a model of the compensatory changes occurring in the *reeler* circuitry that enable a weaker thalamus to be equally effective at recruiting the cortex. The model is detailed in figure 16 and hypothesizes that the weakness of the thalamic input is rescued either by an increase in the gain of its intracortical amplification by enhanced recurrent excitation, or by a shift in the balance of excitation and inhibition towards more of the former and less of the latter. These hypothetical mechanisms are not mutually exclusive and might act in unison. The model, while possibly erroneous, has the advantage of leading to testable hypotheses, which will guide future work. The strength of recurrent excitation, for example, can be investigated with paired recordings *in vitro*. The balance of excitation and inhibition in evoked activity *in vitro* can be deduced from the corresponding changes in conductance mathematically derived from compound responses (Cruikshank et al., 2007; Monier et al., 2008). Finally, a characterization of the receptive fields on individual neurons in *reeler* cortex can be achieved with 2-photon targeted patch clamp *in vivo*.

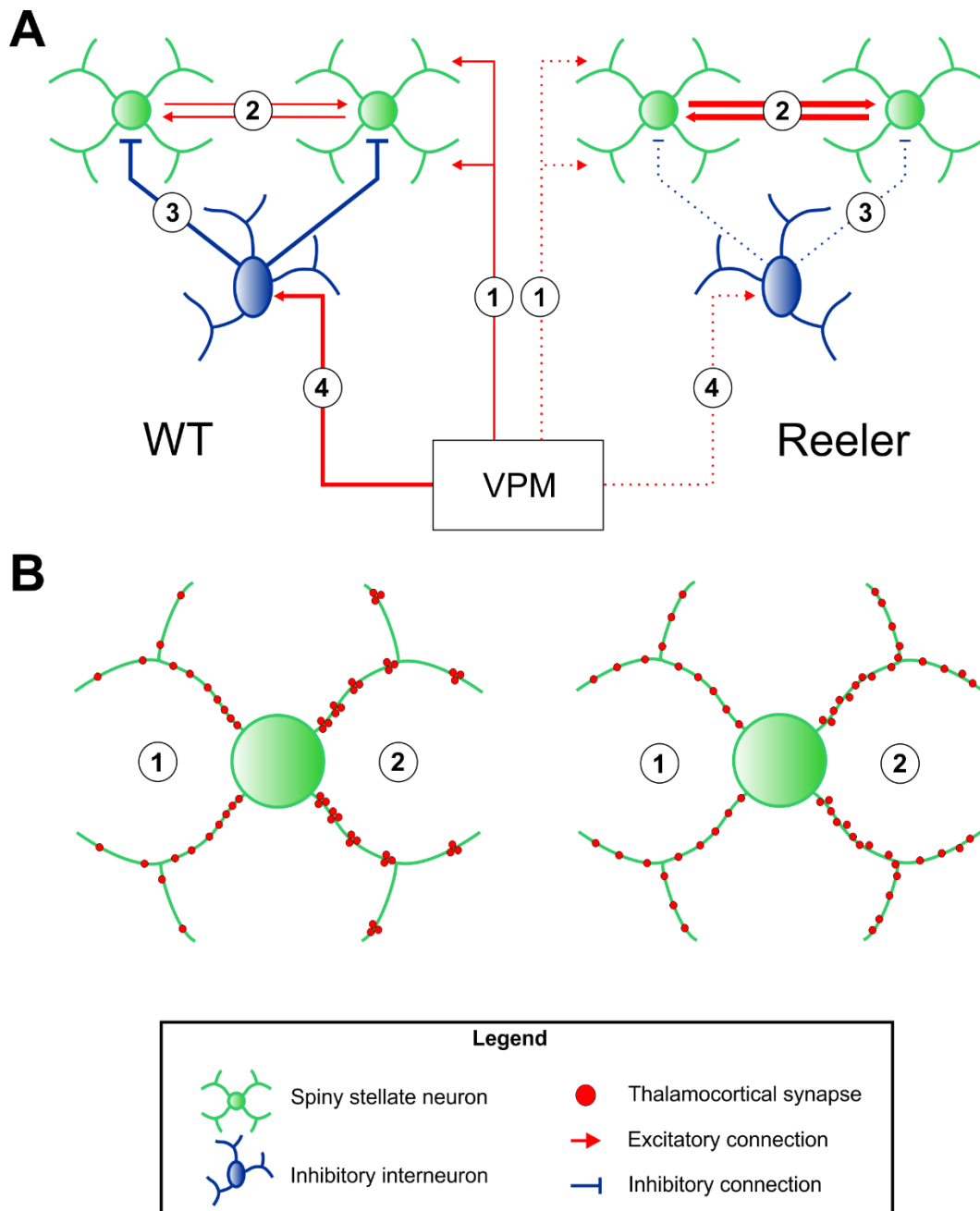


Figure 16. Proposed model of alterations in the circuits of LIV of the reeler somatosensory cortex.
A: circuit diagram of LIV of the normal (WT, left) and mutant (reeler, right) cortex. Red lines indicate excitatory input, blue lines indicate inhibition. A thickening of a line in one diagram with respect to the other represents a connection that is stronger; weaker connections are represented in dashed lines. In both genotypes, SpS neurons receive direct thalamic input (1), but this input is weaker in reeler, as demonstrated in the present study. Two hypothetical, possibly complementary mechanisms compensate for the weakness of the thalamic input, enabling comparable network activation. Recurrent excitation with LIV may be enhanced (2), effectively increasing the gain of intracortical, thalamic input amplification. Alternatively, inhibition may tune itself to a weakened excitation, and become weaker as well (3). This weakening of inhibition could also be brought about by a

concomitant weakening of the TC input to inhibitory interneurons, similarly to TC input to SpS (4). VPM: ventral posteromedial nucleus of the thalamus. **B:** schematic representation of the somatodendritic distribution of TC synapses on SpS neurons the in WT (left) and *reeler* (right) mice. The same number of synapses is represented in both neurons, following two rules of somatodendritic distribution. In WT animals, TC synapses have a weak tendency, exaggerated here, to be found in higher densities closer to the soma; this rule is illustrated on the left side of the neurons (1). In *reeler*, we hypothesize this gradient to be less steep or even non-existent (1). Another rule of TC synapse organization is the formation of small clusters along the dendrite (2). We hypothesize such clusters to be less numerous, to involve fewer synapses, or to be absent altogether from the dendritic arbors of *reeler* SpS (2).

As mentioned above, earlier studies have documented a variety of slight alterations in the *reeler* brain. The importance of these alterations was often belittled by their discoverers, who rather emphasized the more unexpected finding of how broad the similarities were. It is the ambition of the present thesis to contribute to a reappraisal of how relevant these differences may be. The abnormalities documented here indicate that a substantial developmental plasticity enables the *reeler* cortex to compensate its shortcomings, the understanding of which may teach us about plasticity beyond this mutant. Likewise, the subtle weakening and disorganization in TC input we describe may cause equally subtle alterations in the perception these mutants have of their environment; understanding their nature and mechanism will teach us not only about the function of one missing protein, but about the cortex and about perception in all mammals. In other words, although the functional abnormalities in the *reeler* cortex may be mild, it is precisely this quality that makes them interesting and worthy of further research. For whatever the years to come teach us about *reeler*, the years past carried a strangely uplifting message: even a very chaotic brain may think.

Summary

Rodents possess an array of facial whiskers on either side of their snout, which they use to collect tactile information about their surroundings. In layer IV of the somatosensory cortex, individual whiskers are represented by dense clusters of cells called barrels. Together, the barrels form the barrel field, a somatotopic representation of the whiskers on the snout. Layer 4 barrels receive direct sensory input from the thalamus, which is then distributed to all other layers of the cortex along the so-called canonical microcircuit, resulting in widespread cortical activation.

In the *reeler* mouse, the loss of function of the reelin protein causes abnormal development of the cortex leading to the loss of cortical lamination. In this chaotic cortex, neurons that ought to be grouped together in layers are found in ectopic positions, scattered across the cortical depth. Although solid evidence exists that barrel equivalent structures may form in *reeler*, the functional organization and connectivity of its somatosensory cortex remains obscure.

Here, using *in vivo* intrinsic signal optical imaging, we demonstrate that sensory input reaches and activates the barrel cortex of the mutant mouse normally, and that somatotopy persists in spite of laminar disorganization. Furthermore, using *in vitro* whole cell recordings and optogenetics, we demonstrate that thalamic input to layer IV equivalent neurons is direct in *reeler*. Direct thalamic input is weakened, however, while network activity increases with respect to the normal cortex.

These results reveal an unexpected paradox in the *reeler* brain, one that opposes a weakened thalamic input to a normal activation of cortical networks. We propose a model of cortical network changes that solves this paradox, whereby a weakened thalamic input can be rescued by an increase in the gain of its intracortical amplification and an adaptive shift in the excitation-inhibition balance. These results question the hitherto prevailing view that both connectivity and function are left unchanged in the *reeler* mouse, and may contribute to a reappraisal of its relevance as a model of adaptive circuit plasticity.

References

- Ahl AS. The role of vibrissae in behavior: a status review. *Vet Res Commun.* 1986 Jul; 10(4):245-68. Review. PubMed PMID: 3526705.
- Anjum F, Turni H, Mulder PG, van der Burg J, Brecht M. Tactile guidance of prey capture in Etruscan shrews. *Proc Natl Acad Sci U S A.* 2006 Oct 31; 103(44):16544-9. Epub 2006 Oct 23. PubMed PMID: 17060642; PubMed Central PMCID: PMC1621049.
- Armstrong-James M, Fox K. Spatiotemporal convergence and divergence in the rat S1 "barrel" cortex. *J Comp Neurol.* 1987 Sep 8; 263(2):265-81. PubMed PMID: 3667981.
- Badea A, Nicholls PJ, Johnson GA, Wetsel WC. Neuroanatomical phenotypes in the *reeler* mouse. *Neuroimage.* 2007 Feb 15; 34(4):1363-74. Epub 2006 Dec 20. PubMed PMID: 17185001; PubMed Central PMCID: PMC1945208.
- Baillarger J. Recherches sur la structure de la couche cortical des circonvolutions du cerveau. 1840. In: *recherches sur l'anatomie, la physiologie et la pathologie du système nerveux.* Victor Masson, Paris, 1872. Pp VI-VII and 1-46.
- Beffert U, Weeber EJ, Durudas A, Qiu S, Masiulis I, Sweatt JD, Li WP, Adelman G, Frotscher M, Hammer RE, Herz J. Modulation of synaptic plasticity and memory by Reelin involves differential splicing of the lipoprotein receptor Apoer2. *Neuron.* 2005 Aug 18; 47(4):567-79. PubMed PMID: 16102539.
- Beffert U, Durudas A, Weeber EJ, Stolt PC, Giehl KM, Sweatt JD, Hammer RE, Herz J. Functional dissection of Reelin signaling by site-directed disruption of Disabled-1 adaptor binding to apolipoprotein E receptor 2: distinct roles in development and synaptic plasticity. *J Neurosci.* 2006 Feb 15; 26(7):2041-52. PubMed PMID: 16481437.
- Belford GR, Killackey HP. Vibrissae representation in subcortical trigeminal centers of the neonatal rat. *J Comp Neurol.* 1979 Jan 15; 183(2):305-21. PubMed PMID: 762261.
- Benshalom G, White EL. Quantification of TC synapses with SpS neurons in layer IV of mouse somatosensory cortex. *J Comp Neurol.* 1986 Nov 15; 253(3):303-14. PubMed PMID: 3793995.
- Berg RW, Kleinfeld D. Rhythmic whisking by rat: retraction as well as protraction of the vibrissae is under active muscular control. *J Neurophysiol.* 2003 Jan; 89(1):104-17. PubMed PMID: 12522163.
- Biel M, Wahl-Schott C, Michalakis S, Zong X. Hyperpolarization-activated cation channels: from genes to function. *Physiol Rev.* 2009 Jul; 89(3):847-85. doi: 10.1152/physrev.00029.2008. Review. PubMed PMID: 19584315.
- Blinder P, Tsai PS, Kaufhold JP, Knutsen PM, Suhl H, Kleinfeld D. 2013. The cortical angiome: an interconnected vascular network with noncolumnar patterns of blood flow. *Nat Neurosci.* 16(7):889-97.

- Bliss TV, Chung SH. An electrophysiological study of the hippocampus of the '*reeler*' mutant mouse. *Nature*. 1974 Nov 8; 252(5479):153-5. PubMed PMID: 4421774.
- Binshtok AM, Fleidervish IA, Sprengel R, Gutnick MJ. NMDA receptors in layer 4 SpS cells of the mouse barrel cortex contain the NR2C subunit. *J Neurosci*. 2006 Jan 11; 26(2):708-15. PubMed PMID: 16407568.
- Boyle MP, Bernard A, Thompson CL, Ng L, Boe A, Mortrud M, Hawrylycz MJ, Jones AR, Hevner RF, Lein ES. Cell-type-specific consequences of Reelin deficiency in the mouse neocortex, hippocampus, and amygdala. *J Comp Neurol*. 2011 Aug 1; 519(11):2061-89. doi: 10.1002/cne.22655. PubMed PMID: 21491433.
- Borrell V, Del Río JA, Alcántara S, Derer M, Martínez A, D'Arcangelo G, Nakajima K, Mikoshiba K, Derer P, Curran T, Soriano E. 1999. Reelin regulates the development and synaptogenesis of the layer-specific entorhino-hippocampal connections. *J Neurosci*. 19(4):1345-58. PubMed PMID: 9952412.
- Brecht M, Preilowski B, Merzenich MM. Functional architecture of the mystacial vibrissae. *Behav Brain Res*. 1997 Mar; 84(1-2):81-97. PubMed PMID: 9079775.
- Brecht M, Sakmann B. Dynamic representation of whisker deflection by synaptic potentials in SpS and pyramidal cells in the barrels and septa of layer 4 rat somatosensory cortex. *J Physiol*. 2002 Aug 15; 543(Pt 1):49-70. PubMed PMID: 12181281; PubMed Central PMCID: PMC2290465.
- Brecht M. Barrel cortex and whisker-mediated behaviors. *Curr Opin Neurobiol*. 2007 Aug; 17(4):408-16. Epub 2007 Aug 15. Review. PubMed PMID: 17702566.
- Bruno RM, Sakmann B. Cortex is driven by weak but synchronously active TC synapses. *Science*. 2006 Jun 16; 312(5780):1622-7. PubMed PMID: 16778049.
- Carboni G, Tueting P, Tremolizzo L, Sugaya I, Davis J, Costa E, Guidotti A. Enhanced dizocilpine efficacy in heterozygous *reeler* mice relates to GABA turnover downregulation. *Neuropharmacology*. 2004 Jun; 46(8):1070-81. PubMed PMID: 15111013.
- Cardoso MM, Sirotin YB, Lima B, Glushenkova E, Das A. The neuroimaging signal is a linear sum of neurally distinct stimulus- and task-related components. *Nat Neurosci*. 2012 Sep; 15(9):1298-306. doi: 10.1038/nn.3170. Epub 2012 Jul 29. PubMed PMID: 22842146; PubMed Central PMCID: PMC3690535.
- Carvell GE, Simons DJ. 1990. Biometric analyses of vibrissal tactile discrimination in the rat. *J Neurosci*. 10(8):2638-48
- Caviness VS Jr, Sidman RL. Retrohippocampal, hippocampal and related structures of the forebrain in the *reeler* mutant mouse. *J Comp Neurol*. 1973 Jan 15; 147(2):235-54. PubMed PMID: 4682775.
- Caviness VS Jr, Sidman RL. Time of origin or corresponding cell classes in the cerebral cortex of normal and *reeler* mutant mice: an autoradiographic analysis. *J Comp Neurol*. 1973 Mar 15; 148(2):141-51. PubMed PMID: 4700506.

- Caviness VS Jr, Frost DO, Hayes NL. Barrels in somatosensory cortex of normal and *reeler* mutant mice. *Neurosci Lett*. 1976 Sep; 3(1-2):7-14. PubMed PMID: 19604860.
- Caviness VS Jr, Rakic P. 1978. Mechanisms of cortical development: a view from mutations in mice. *Annu Rev Neurosci*.1:297-326. Review.
- Caviness VS Jr. Neocortical histogenesis in normal and *reeler* mice: a developmental study based upon [3H] thymidine autoradiography. *Brain Res*. 1982 Jul; 256(3):293-302. PubMed PMID: 7104762.
- Caviness VS Jr, Frost DO. TC projections in the *reeler* mutant mouse. *J Comp Neurol*. 1983 Sep 10; 219(2):182-202. PubMed PMID: 6194186.
- Chen Y, Beffert U, Ertunc M, Tang TS, Kavalali ET, Bezprozvanny I, Herz J. Reelin modulates NMDA receptor activity in cortical neurons. *J Neurosci*. 2005 Sep 7; 25(36):8209-16. PubMed PMID: 16148228.
- Chen-Bee CH, Kwon MC, Masino SA, Frostig RD. 1996. Areal extent quantification of functional representations using intrinsic signal optical imaging. *J Neurosci Meth*. 68(1):27-37.
- Chen-Bee CH, Polley DB, Brett-Green B, Prakash N, Kwon MC, Frostig RD. 2000. Visualizing and quantifying evoked cortical activity assessed with intrinsic signal imaging. *J Neurosci Methods*. 97(2):157-73.
- Chen-Bee CH, Zhou Y, Jacobs NS, Lim B, Frostig RD. 2012. Whisker array functional representation in rat barrel cortex: transcendence of one-to-one topography and its underlying mechanism. *Front Neural Circuits*. 6:93.
- Chung S, Li X, Nelson SB. Short-term depression at TC synapses contributes to rapid adaptation of cortical sensory responses *in vivo*. *Neuron*. 2002 Apr 25; 34(3):437-46. PubMed PMID: 11988174.
- Clarke E. O'Malley, C.D. The Discovery of the Cortical Layers. In: *The Human Brain and Spinal Cord: A Historical Study Illustrated by Writings from Antiquity to the Twentieth Century*. 1968. Norman Publishing, San Francisco, CA. 1996. Pp 423-437.
- Cowan AI, Stricker C. Functional connectivity in layer IV local excitatory circuits of rat somatosensory cortex. *J Neurophysiol*. 2004 Oct; 92(4):2137-50. Epub 2004 Jun 16. PubMed PMID: 15201316.
- Cragg BG. Absence of barrels and disorganization of thalamic afferent distribution in the sensory cortex of *reeler* mice. *Exp Neurol*. 1975 Dec; 49(3):858-62. PubMed PMID: 1204710.
- Cruikshank SJ, Lewis TJ, Connors BW. Synaptic basis for intense TC activation of feedforward inhibitory cells in neocortex. *Nat Neurosci*. 2007 Apr; 10(4):462-8. Epub 2007 Mar 4. PubMed PMID: 17334362.
- da Costa NM, Martin KA. Whose Cortical Column Would that Be? *Front Neuroanat*. 2010 May 31;4:16. doi: 10.3389/fnana.2010.00016. eCollection 2010. PubMed PMID:20640245; PubMed Central PMCID: PMC2904586.

- D'Arcangelo G, Miao GG, Chen SC, Soares HD, Morgan JI, Curran T. A protein related to extracellular matrix proteins deleted in the mouse mutant *reeler*. *Nature*. 1995 Apr 20; 374(6524):719-23. PubMed PMID: 7715726.
- D'Arcangelo G. The *reeler* mouse: anatomy of a mutant. *Int Rev Neurobiol*. 2005; 71:383-417. Review. PubMed PMID: 16512359.
- D'Arcangelo G, Curran T. Reeler: new tales on an old mutant mouse. *Bioessays*. 1998 Mar; 20(3):235-44. Review. PubMed PMID: 9631651.
- D'Arcangelo, "Reelin in the Years: Controlling Neuronal Migration and Maturation in the Mammalian Brain," *Advances in Neuroscience*, vol. 2014, Article ID 597395, 19 pages, 2014. doi:10.1155/2014/597395.
- Dekimoto H, Terashima T, Katsuyama Y. Dispersion of the neurons expressing layer specific markers in the *reeler* brain. *Dev Growth Differ*. 2010 Feb; 52(2):181-93. doi: 10.1111/j.1440-169X.2009.01153.x. Epub 2010 Jan 7. PubMed PMID: 20067496.
- Devonshire IM, Papadakis NG, Port M, Berwick J, Kennerley AJ, Mayhew JE, Overton PG. 2012. Neurovascular coupling is brain region-dependent. *Neuroimage*. 59(3):1997-2006.
- Diamond ME, von Heimendahl M, Knutsen PM, Kleinfeld D, Ahissar E. 'Where' and 'what' in the whisker sensorimotor system. *Nat Rev Neurosci*. 2008 Aug;9(8):601-12. doi: 10.1038/nrn2411. Review. Erratum in: *Nat Rev Neurosci*. 2008 Sep; 9(9):709. PubMed PMID: 18641667.
- Diamond ME, Arabzadeh E. Whisker sensory system - from receptor to decision. *Prog Neurobiol*. 2013 Apr; 103:28-40. doi: 10.1016/j.pneurobio.2012.05.013. Epub 2012 Jun 6. Review. PubMed PMID: 22683381.
- Douglas RJ, Koch C, Mahowald M, Martin KA, Suarez HH. Recurrent excitation in neocortical circuits. *Science*. 1995 Aug 18; 269(5226):981-5. PubMed PMID: 7638624.
- Dragunow M, Faull R. The use of c-fos as a metabolic marker in neuronal pathway tracing. *J Neurosci Methods*. 1989 Sep; 29(3):261-5. Review. PubMed PMID: 2507830.
- Dräger UC. Observations on the organization of the visual cortex in the *reeler* mouse. *J Comp Neurol*. 1981 Oct 1; 201(4):555-70. PubMed PMID: 7287935.
- Drew PJ, Feldman DE. 2009. Intrinsic signal imaging of deprivation-induced contraction of whisker representations in rat somatosensory cortex. *Cereb Cortex*. 19(2):331-48.
- Drew PJ, Shih AY, Kleinfeld D. Fluctuating and sensory-induced vasodynamics in rodent cortex extend arteriole capacity. *Proc Natl Acad Sci U S A*. 2011 May 17; 108(20):8473-8. doi: 10.1073/pnas.1100428108. Epub 2011 May 2. PubMed PMID: 21536897; PubMed Central PMCID: PMC3100929.
- Dubroff JG, Stevens RT, Hitt J, Hodge CJ Jr, McCasland JS. 2006. Anomalous functional organization of barrel cortex in GAP-43 deficient mice. *Neuroimage*. 29(4):1040-8.
- Ebara S, Kumamoto K, Matsuura T, Mazurkiewicz JE, Rice FL. Similarities and differences in the innervation of mystacial vibrissal follicle-sinus complexes in the rat and cat: a

- confocal microscopic study. *J Comp Neurol.* 2002 Jul 22; 449(2):103-19. PubMed PMID: 12115682.
- Economo C von. Introduction. In: *Cellular Structure of the Human Cerebral Cortex.* 1927. Karger AG, Basel, 2009. Pp 1-31.
- Egger V, Feldmeyer D, Sakmann B. Coincidence detection and changes of synaptic efficacy in SpS neurons in rat barrel cortex. *Nat Neurosci.* 1999 Dec; 2(12):1098-105. PubMed PMID: 10570487
- Falconer DS. Two new mutants, 'trembler' and 'reeler', with neurological actions in the house mouse (*Mus musculus* L.). *J Genet.* 1951 Jan; 50(2):192-201. PubMed PMID: 24539699.
- Feldmeyer D, Egger V, Lubke J, Sakmann B. Reliable synaptic connections between pairs of excitatory layer 4 neurones within a single 'barrel' of developing rat somatosensory cortex. *J Physiol.* 1999 Nov 15; 521 Pt 1:169-90. PubMed PMID: 10562343; PubMed Central PMCID: PMC2269646.
- Feldmeyer D, Sakmann B. Synaptic efficacy and reliability of excitatory connections between the principal neurones of the input (layer 4) and output layer (layer 5) of the neocortex. *J Physiol.* 2000 May 15; 525 Pt 1:31-9. Review. PubMed PMID: 10811722; PubMed Central PMCID: PMC2269927.
- Feldmeyer D, Brecht M, Helmchen F, Petersen CC, Poulet JF, Staiger JF, Luhmann HJ, Schwarz C. Barrel cortex function. *Prog Neurobiol.* 2013 Apr; 103:3-27. doi:10.1016/j.pneurobio.2012.11.002. Epub 2012 Nov 27. Review. PubMed PMID: 23195880.
- Feldmeyer D. Excitatory neuronal connectivity in the barrel cortex. *Front Neuroanat.* 2012 Jul 11;6: 24. doi: 10.3389/fnana.2012.00024. eCollection 2012. PubMed PMID: 22798946; PubMed Central PMCID: PMC3394394.
- Ferezou I, Bolea S, Petersen CC. 2006. Visualizing the cortical representation of whisker touch: voltage-sensitive dye imaging in freely moving mice. *Neuron.* 50(4):617-29.
- Förster E, Bock HH, Herz J, Chai X, Frotscher M, Zhao S. Emerging topics in Reelin function. *Eur J Neurosci.* 2010 May; 31(9):1511-8. doi:10.1111/j.1460-9568.2010.07222.x. Review. PubMed PMID: 20525064; PubMed Central PMCID: PMC2942760.
- Fox K, Wright N, Wallace H, Glazewski S. The origin of cortical surround receptive fields studied in the barrel cortex. *J Neurosci.* 2003 Sep 10; 23(23):8380-91. PubMed PMID: 12968000.
- Fox K. *Barrel Cortex.* Cambridge University Press, Cambridge. 2008.
- Friedberg MH, Lee SM, Ebner FF. Modulation of receptive field properties of thalamic somatosensory neurons by the depth of anesthesia. *J Neurophysiol.* 1999 May; 81(5):2243-52. PubMed PMID: 10322063.
- Frostig RD, Lieke EE, Ts'o DY, Grinvald A. Cortical functional architecture and local coupling between neuronal activity and the microcirculation revealed by *in vivo* high-

- resolution optical imaging of intrinsic signals. *Proc Natl Acad Sci U S A*. 1990 Aug; 87(16):6082-6. PubMed PMID: 2117272; PubMed Central PMCID: PMC54476.
- Frotscher M. Cajal-Retzius cells, Reelin, and the formation of layers. *Curr Opin Neurobiol*. 1998 Oct; 8(5):570-5. Review. PubMed PMID: 9811621.
- Gabernet L, Jadhav SP, Feldman DE, Carandini M, Scanziani M. Somatosensory integration controlled by dynamic TC feed-forward inhibition. *Neuron*. 2005 Oct 20; 48(2):315-27. PubMed PMID: 16242411.
- Garner JP, Dufour B, Gregg LE, Weisker SM, Mench JA. Social and husbandry factors affecting the prevalence and severity of barbering (,whisker trimming') by laboratory mice. *Appl. Anim. Behav. Sci*. 2004. 89:263-282.
- Gennari F. *De Peculiari Structure Cerebri Nonnullisque Ejus Morbis*. Parma, 1784.
- Gibson JR, Beierlein M, Connors BW. Two networks of electrically coupled inhibitory neurons in neocortex. *Nature*. 1999 Nov 4; 402(6757):75-9. PubMed PMID: 10573419.
- Gil Z, Connors BW, Amitai Y. Efficacy of thalamocortical and intracortical synaptic connections: quanta, innervation, and reliability. *Neuron*. 1999 Jun;23(2):385-97. PubMed PMID: 10399943.
- Gilbert CD. Microcircuitry of the visual cortex. *Annu Rev Neurosci*. 1983; 6:217-47. PubMed PMID: 6132585.
- Goffinet AM. 1984. Events governing organization of postmigratory neurons: studies on brain development in normal and *reeler* mice. *Brain Res*. 319:261-296.
- Govindarajan A, Kelleher RJ, Tonegawa S. A clustered plasticity model of long-term memory engrams. *Nat Rev Neurosci*. 2006 Jul;7(7):575-83. Review. PubMed PMID: 16791146.
- Guić-Robles E, Valdivieso C, Guajardo G. Rats can learn a roughness discrimination using only their vibrissal system. *Behav Brain Res*. 1989 Jan 1;31(3):285-9. PubMed PMID: 2914080.
- Guy J, Wagener RJ, Möck M, Staiger JF. Persistence of functional sensory maps in the absence of cortical layers in the somatosensory cortex of *reeler* mice. *Cereb Cortex*. 2015 Sep; 25(9):2517-28. doi: 10.1093/cercor/bhu052. Epub 2014 Apr 23. PubMed PMID: 24759695; PubMed Central PMCID: PMC4537421.
- Grinvald A, Lieke E, Frostig RD, Gilbert CD, Wiesel TN. Functional architecture of cortex revealed by optical imaging of intrinsic signals. *Nature*. 1986 Nov 27-Dec 3;324(6095):361-4. PubMed PMID: 3785405.
- Haidarliu S, Simony E, Golomb D, Ahissar E. Muscle architecture in the mystacial pad of the rat. *Anat Rec (Hoboken)*. 2010 Jul; 293(7):1192-206. doi: 10.1002/ar.21156. PubMed PMID: 20583263.
- Halabisky B, Shen F, Huguenard JR, Prince DA. Electrophysiological classification of somatostatin-positive interneurons in mouse sensorimotor cortex. *J Neurophysiol*. 2006 Aug;96(2):834-45. Epub 2006 May 17. PubMed PMID:16707715.

- Harsan LA, Dávid C, Reisert M, Schnell S, Hennig J, von Elverfeldt D, Staiger JF. Mapping remodeling of TC projections in the living *reeler* mouse brain by diffusion tractography. *Proc Natl Acad Sci U S A*. 2013 May 7; 110(19):E1797-806. doi: 10.1073/pnas.1218330110. Epub 2013 Apr 22. PubMed PMID: 23610438; PubMed Central PMCID: PMC3651497.
- Hartmann MJ. A night in the life of a rat: vibrissal mechanics and tactile exploration. *Ann N Y Acad Sci*. 2011 Apr; 1225:110-8. doi:10.1111/j.1749-6632.2011.06007.x. Review. PubMed PMID: 21534998.
- Heckroth JA, Goldowitz D, Eisenman LM. Purkinje cell reduction in the *reeler* mutant mouse: a quantitative immunohistochemical study. *J Comp Neurol*. 1989 Jan 22; 279(4):546-55. PubMed PMID: 2918086.
- Hellwig S, Hack I, Kowalski J, Brunne B, Jarowjy J, Unger A, Bock HH, Junghans D, Frotscher M. Role for Reelin in neurotransmitter release. *J Neurosci*. 2011 Feb 16; 31(7):2352-60. doi: 10.1523/JNEUROSCI.3984-10.2011. PubMed PMID: 21325502.
- Herz J, Chen Y. Reelin, lipoprotein receptors and synaptic plasticity. *Nat Rev Neurosci*. 2006 Nov;7(11):850-9. Review. PubMed PMID: 17053810.
- Horton JC, Adams DL. The cortical column: a structure without a function. *Philos Trans R Soc Lond B Biol Sci*. 2005 Apr 29; 360(1456):837-62. Review. PubMed PMID: 15937015; PubMed Central PMCID: PMC1569491.
- Hubel DH, Wiesel TN. Receptive fields, binocular interaction and functional architecture in the cat's visual cortex. *J Physiol*. 1962 Jan; 160:106-54. PubMed PMID: 14449617; PubMed Central PMCID: PMC1359523.
- Hubel DH, Wiesel TN. Receptive fields and functional architecture of monkey striate cortex. *J Physiol*. 1968 Mar; 195(1):215-43. PubMed PMID: 4966457; PubMed Central PMCID: PMC1557912.
- Hull C, Isaacson JS, Scanziani M. Postsynaptic mechanisms govern the differential excitation of cortical neurons by thalamic inputs. *J Neurosci*. 2009 Jul 15;29(28):9127-36. doi: 10.1523/JNEUROSCI.5971-08.2009. PubMed PMID:19605650; PubMed Central PMCID: PMC2753516.
- Iannella NL, Launey T, Tanaka S. Spike timing-dependent plasticity as the origin of the formation of clustered synaptic efficacy engrams. *Front Comput Neurosci*. 2010 Jul 14; 4. pii: 21. doi: 10.3389/fncom.2010.00021. eCollection 2010. PubMed PMID: 20725522; PubMed Central PMCID: PMC2914531.
- Inoue T, Imoto K. Feedforward inhibitory connections from multiple thalamic cells to multiple regular-spiking cells in layer 4 of the somatosensory cortex. *J Neurophysiol*. 2006 Oct;96(4):1746-54. Epub 2006 Jul 19. PubMed PMID: 16855112.
- Isaacson JS, Scanziani M. How inhibition shapes cortical activity. *Neuron*. 2011 Oct 20; 72(2):231-43. doi: 10.1016/j.neuron.2011.09.027. Review. PubMed PMID: 22017986; PubMed Central PMCID: PMC3236361.

- Ishida A, Shimazaki K, Terashima T, Kawai N. An electrophysiological and immunohistochemical study of the hippocampus of the *reeler* mutant mouse. *Brain Res.* 1994 Oct 31; 662(1-2):60-8. PubMed PMID: 7859091.
- Jenkinson EW, Glickstein M. Whiskers, barrels, and cortical efferent pathways in gap crossing by rats. *J Neurophysiol.* 2000 Oct; 84(4):1781-9. PubMed PMID: 11024070.
- Jia H, Varga Z, Sakmann B, Konnerth A. Linear integration of spine Ca²⁺ signals in layer 4 cortical neurons *in vivo*. *Proc Natl Acad Sci U S A.* 2014 Jun 24; 111(25):9277-82. doi: 10.1073/pnas.1408525111. Epub 2014 Jun 9. PubMed PMID: 24927564; PubMed Central PMCID: PMC4078833.
- Karagiannis A, Gallopin T, Dávid C, Battaglia D, Geoffroy H, Rossier J, Hillman EM, Staiger JF, Cauli B. Classification of NPY-expressing neocortical interneurons. *J Neurosci.* 2009 Mar 18;29(11):3642-59. doi: 10.1523/JNEUROSCI.0058-09.2009. PubMed PMID: 19295167; PubMed Central PMCID: PMC2750888.
- Kastellakis G, Cai DJ, Mednick SC, Silva AJ, Poirazi P. Synaptic clustering within dendrites: an emerging theory of memory formation. *Prog Neurobiol.* 2015 Mar; 126:19-35. doi:10.1016/j.pneurobio.2014.12.002. Epub 2015 Jan 8. Review. PubMed PMID: 25576663; PubMed Central PMCID: PMC4361279.
- Kinnischtzke AK, Simons DJ, Fanselow EE. Motor cortex broadly engages excitatory and inhibitory neurons in somatosensory barrel cortex. *Cereb Cortex.* 2014 Aug; 24(8):2237-48. doi: 10.1093/cercor/bht085. Epub 2013 Mar 31. PubMed PMID: 23547136; PubMed Central PMCID: PMC4148616.
- Kleinfeld D, Delaney KR. Distributed representation of vibrissa movement in the upper layers of somatosensory cortex revealed with voltage-sensitive dyes. *J Comp Neurol.* 1996 Nov 4; 375(1):89-108. Erratum in: *J Comp Neurol* 1997 Feb 24; 378(4):594. PubMed PMID: 8913895.
- Koelbl C, Helmstaedter M, Lübke J, Feldmeyer D. A barrel-related interneuron in layer 4 of rat somatosensory cortex with a high intrabarrel connectivity. *Cereb Cortex.* 2015 Mar; 25(3):713-25. doi: 10.1093/cercor/bht263. Epub 2013 Sep 26. PubMed PMID: 24076498; PubMed Central PMCID: PMC4318534.
- Kohn A, Metz C, Quibrera M, Tommerdahl MA, Whitsel BL. 2000. Functional neocortical microcircuitry demonstrated with intrinsic signal optical imaging *in vitro*. *Neuroscience.* 95(1):51-62.
- Kowalski J, Geuting M, Paul S, Dieni S, Laurens J, Zhao S, Drakew A, Haas CA, Frotscher M, Vida I. Proper layering is important for precisely timed activation of hippocampal mossy cells. *Cereb Cortex.* 2010 Sep; 20(9):2043-54. doi:10.1093/cercor/bhp267. Epub 2010 Jan 6. PubMed PMID: 20053714.
- Krupa DJ, Matell MS, Brisben AJ, Oliveira LM, Nicolelis MA. Behavioral properties of the trigeminal somatosensory system in rats performing whisker-dependent tactile discriminations. *J Neurosci.* 2001 Aug 1; 21(15):5752-63. PubMed PMID: 11466447.
- Kupferman JV, Basu J, Russo MJ, Guevarra J, Cheung SK, Siegelbaum SA. Reelin signaling specifies the molecular identity of the pyramidal neuron distal dendritic

- compartment. *Cell*. 2014 Sep 11; 158(6):1335-47. doi:10.1016/j.cell.2014.07.035. Epub 2014 Sep 4. PubMed PMID: 25201528; PubMed Central PMCID: PMC4183142.
- Lamprea MR, Cardenas FP, Setem J, Morato S. Thigmotactic responses in an open-field. *Braz J Med Biol Res*. 2008 Feb; 41(2):135-40. PubMed PMID: 18297193.
- Larkum ME, Nevian T. Synaptic clustering by dendritic signalling mechanisms. *Curr Opin Neurobiol*. 2008 Jun; 18(3):321-31. doi: 10.1016/j.conb.2008.08.013. Review. PubMed PMID: 18804167.
- Larriva-Sahd JA. Some predictions of Rafael Lorente de Nó 80 years later. *Front Neuroanat*. 2014 Dec 3; 8:147. doi: 10.3389/fnana.2014.00147. eCollection 2014. Review. PubMed PMID: 25520630; PubMed Central PMCID: PMC4253658.
- Lavzin M, Rapoport S, Polsky A, Garion L, Schiller J. Nonlinear dendritic processing determines angular tuning of barrel cortex neurons *in vivo*. *Nature*. 2012 Oct 18;490(7420):397-401. doi: 10.1038/nature11451. Epub 2012 Sep 2. PubMed PMID: 22940864.
- Lee KJ, Woolsey TA. A proportional relationship between peripheral innervation density and cortical neuron number in the somatosensory system of the mouse. *Brain Res*. 1975 Dec 5;99(2):349-53. PubMed PMID: 1182550.
- Lefort S, Tomm C, Floyd Sarria JC, Petersen CC. The excitatory neuronal network of the C2 barrel column in mouse primary somatosensory cortex. *Neuron*. 2009 Jan 29; 61(2):301-16. doi: 10.1016/j.neuron.2008.12.020. PubMed PMID: 19186171.
- Lemmon V, Pearlman AL. 1981. Does laminar position determine the receptive field properties of cortical neurons? A study of corticotectal cells in area 17 of the normal mouse and the *reeler* mutant. *J Neurosci*. 1(1):83-93.
- Lenschow C, Brecht M. Barrel cortex membrane potential dynamics in social touch. *Neuron*. 2015 Feb 18;85(4):718-25. doi: 10.1016/j.neuron.2014.12.059. Epub 2015 Jan 29. Erratum in: *Neuron*. 2015 Mar 4;85(5):1145. PubMed PMID: 25640075.
- Li Y, Lu H, Cheng PL, Ge S, Xu H, Shi SH, Dan Y. 2012. Clonally related visual cortical neurons show similar stimulus feature selectivity. *Nature*. 486(7401):118-21.
- Li YT, Ibrahim LA, Liu BH, Zhang LI, Tao HW. Linear transformation of thalamocortical input by intracortical excitation. *Nat Neurosci*. 2013a Sep;16(9):1324-30. doi: 10.1038/nn.3494. Epub 2013 Aug 11. PubMed PMID: 23933750; PubMed Central PMCID: PMC3855439.
- Li LY, Li YT, Zhou M, Tao HW, Zhang LI. Intracortical multiplication of thalamocortical signals in mouse auditory cortex. *Nat Neurosci*. 2013b Sep;16(9):1179-81. doi: 10.1038/nn.3493. Epub 2013 Aug 11. PubMed PMID: 23933752; PubMed Central PMCID: PMC3844430.
- Lien AD, Scanziani M. Tuned thalamic excitation is amplified by visual cortical circuits. *Nat Neurosci*. 2013 Sep;16(9):1315-23. doi: 10.1038/nn.3488. Epub 2013 Aug 11. PubMed PMID: 23933748; PubMed Central PMCID: PMC3774518.

- Lin JY. A user's guide to channelrhodopsin variants: features, limitations and future developments. *Exp Physiol.* 2011 Jan;96(1):19-25. doi: 10.1113/expphysiol.2009.051961. Epub 2010 Jul 9. Review. PubMed PMID: 20621963; PubMed Central PMCID: PMC2995811.
- Lindhorst T, Kurz H, Sibbe M, Meseke M, Förster E. Congruence of vascular network remodeling and neuronal dispersion in the hippocampus of reelin-deficient mice. *Histochem Cell Biol.* 2012 May;137(5):629-39. doi:10.1007/s00418-012-0912-9. Epub 2012 Jan 20. PubMed PMID: 22261923.
- Liu WS, Pesold C, Rodriguez MA, Carboni G, Auta J, Lacor P, Larson J, Condie BG, Guidotti A, Costa E. Down-regulation of dendritic spine and glutamic acid decarboxylase 67 expressions in the reelin haploinsufficient heterozygous *reeler* mouse. *Proc Natl Acad Sci U S A.* 2001 Mar 13;98(6):3477-82. PubMed PMID:11248103; PubMed Central PMCID: PMC30678.
- Long SY. Hair-nibbling and whisker-trimming as indicators of social hierarchy in mice. *Anim Behav.* 1972 Feb;20(1):10-2. PubMed PMID: 4677163.
- Lorente de Nó R. Cerebral cortex: architecture, intracortical connections, motor projections. In: *Physiology of the nervous system*, Fulton JF. New York and London, Oxford University Press, 1949.
- Losonczy A, Makara JK, Magee JC. Compartmentalized dendritic plasticity and input feature storage in neurons. *Nature.* 2008 Mar 27;452(7186):436-41. doi:10.1038/nature06725. PubMed PMID: 18368112.
- Luhmann HJ, Huston JP, Hasenöhrl RU. Contralateral increase in thigmotactic scanning following unilateral barrel-cortex lesion in mice. *Behav Brain Res.* 2005 Feb 10;157(1):39-43. PubMed PMID: 15617769.
- Lübke J, Egger V, Sakmann B, Feldmeyer D. Columnar organization of dendrites and axons of single and synaptically coupled excitatory spiny neurons in layer 4 of the rat barrel cortex. *J Neurosci.* 2000 Jul 15;20(14):5300-11. PubMed PMID:10884314.
- Lübke J, Feldmeyer D. Excitatory signal flow and connectivity in a cortical column: focus on barrel cortex. *Brain Struct Funct.* 2007 Jul; 212(1):3-17. Epub 2007 Jun 1. Review. PubMed PMID: 17717695.
- Madisen L, Zwingman TA, Sunkin SM, Oh SW, Zariwala HA, Gu H, Ng LL, Palmiter RD, Hawrylycz MJ, Jones AR, Lein ES, Zeng H. A robust and high-throughput Cre reporting and characterization system for the whole mouse brain. *Nat Neurosci.* 2010 Jan;13(1):133-40. doi: 10.1038/nn.2467. Epub 2009 Dec 20. PubMed PMID:20023653; PubMed Central PMCID: PMC2840225.
- Magee JC. Dendritic hyperpolarization-activated currents modify the integrative properties of hippocampal CA1 pyramidal neurons. *J Neurosci.* 1998 Oct 1;18(19):7613-24. PubMed PMID: 9742133.
- Makino H, Malinow R. Compartmentalized versus global synaptic plasticity on dendrites controlled by experience. *Neuron.* 2011 Dec 22;72(6):1001-11.

doi:10.1016/j.neuron.2011.09.036. PubMed PMID: 22196335; PubMed Central PMCID:PMC3310180.

- Malonek D, Dirnagl U, Lindauer U, Yamada K, Kanno I, Grinvald A. 1997. Vascular imprints of neuronal activity: relationships between the dynamics of cortical blood flow, oxygenation, and volume changes following sensory stimulation. *Proc Natl Acad Sci U S A*. 94(26):14826-31.
- Mariani J, Crepel F, Mikoshiba K, Changeux JP, Sotelo C. Anatomical, physiological and biochemical studies of the cerebellum from Reeler mutant mouse. *Philos Trans R Soc Lond B Biol Sci*. 1977 Nov 2;281(978):1-28. PubMed PMID: 22882.
- Martin C, Martindale J, Berwick J, Mayhew J. 2006. Investigating neural-hemodynamic coupling and the hemodynamic response function in the awake rat. *Neuroimage*. 32(1):33-48.
- Masino SA, Kwon MC, Dory Y, Frostig RD. Characterization of functional organization within rat barrel cortex using intrinsic signal optical imaging through a thinned skull. *Proc Natl Acad Sci U S A*. 1993 Nov 1;90(21):9998-10002. PubMed PMID: 8234348; PubMed Central PMCID: PMC47700.
- Masino SA, Frostig RD. Quantitative long-term imaging of the functional representation of a whisker in rat barrel cortex. *Proc Natl Acad Sci U S A*. 1996 May 14;93(10):4942-7. PubMed PMID: 8643508; PubMed Central PMCID: PMC39384.
- Mayhew JE, Askew S, Zheng Y, Porrill J, Westby GW, Redgrave P, Rector DM, Harper RM. 1996. Cerebral vasomotion: a 0.1-Hz oscillation in reflected light imaging of neural activity. *Neuroimage*. 4(3 Pt 1):183-93.
- McCormick DA, Bal T. Sleep and arousal: TC mechanisms. *Annu Rev Neurosci*. 1997;20:185-215. Review. PubMed PMID: 9056712.
- Mercier BE, Legg CR, Glickstein M. Basal ganglia and cerebellum receive different somatosensory information in rats. *Proc Natl Acad Sci U S A*. 1990 Jun;87(11):4388-92. PubMed PMID: 2349243; PubMed Central PMCID: PMC54115.
- Meyer HS, Wimmer VC, Hemberger M, Bruno RM, de Kock CP, Frick A, Sakmann B, Helmstaedter M. Cell type-specific thalamic innervation in a column of rat vibrissal cortex. *Cereb Cortex*. 2010 Oct; 20(10):2287-303. doi:10.1093/cercor/bhq069. Epub 2010 Jun 9. PubMed PMID: 20534783; PubMed Central PMCID: PMC2936808.
- Meynert T. Der Bau der Gross-Hirnrinde und seine örtlichen Verschiedenheiten, nebst einem pathologisch-anatomischen Corollarium. *Vjschr. Psychiat., Vienna*, 1867-1868, 1:77-93, 198-217 and 1868, 2:88-113.
- Miller KD, Pinto DJ, Simons DJ. Processing in layer 4 of the neocortical circuit: new insights from visual and somatosensory cortex. *Curr Opin Neurobiol*. 2001 Aug; 11(4):488-97. Review. PubMed PMID: 11502397.
- Miller KD. Understanding layer 4 of the cortical circuit: a model based on cat V1. *Cereb Cortex*. 2003 Jan;13(1):73-82. Review. PubMed PMID: 12466218.

- Monier C, Fournier J, Frégnac Y. *In vitro* and *in vivo* measures of evoked excitatory and inhibitory conductance dynamics in sensory cortices. *J Neurosci Methods*. 2008 Apr 30;169(2):323-65. doi: 10.1016/j.jneumeth.2007.11.008. Epub 2007 Nov 22. PubMed PMID: 18215425.
- Moran, P. A. P. (1950). "Notes on Continuous Stochastic Phenomena". *Biometrika* **37** (1): 17–23. doi:10.2307/2332142. JSTOR 2332142.
- Mountcastle VB, Davies PW, Berman AL. Response properties of neurons of cat's somatic sensory cortex to peripheral stimuli. *J Neurophysiol*. 1957 Jul; 20(4):374-407. PubMed PMID: 13439409.
- Mountcastle VB. Modality and topographic properties of single neurons of cat's somatic sensory cortex. *J Neurophysiol*. 1957 Jul; 20(4):408-34. PubMed PMID: 13439410.
- Mountcastle VB. The columnar organization of the neocortex. *Brain*. 1997 Apr;120 (Pt 4):701-22. Review. PubMed PMID: 9153131.
- Narayanan RT, Egger R, Johnson AS, Mansvelder HD, Sakmann B, de Kock CP, Oberlaender M. Beyond Columnar Organization: Cell Type- and Target Layer-Specific Principles of Horizontal Axon Projection Patterns in Rat Vibrissal Cortex. *Cereb Cortex*. 2015 Apr 1. pii: bhv053. [Epub ahead of print] PubMed PMID: 25838038.
- Niu S, Yabut O, D'Arcangelo G. The Reelin signaling pathway promotes dendritic spine development in hippocampal neurons. *J Neurosci*. 2008 Oct 8;28(41):10339-48. doi: 10.1523/JNEUROSCI.1917-08.2008. PubMed PMID: 18842893; PubMed Central PMCID:PMC2572775.
- Nolan MF, Malleret G, Dudman JT, Buhl DL, Santoro B, Gibbs E, Vronskaya S, Buzsáki G, Siegelbaum SA, Kandel ER, Morozov A. A behavioral role for dendritic integration: HCN1 channels constrain spatial memory and plasticity at inputs to distal dendrites of CA1 pyramidal neurons. *Cell*. 2004 Nov 24;119(5):719-32. Erratum in: *Cell*. 2005 Jan 14;120(1):151-2. PubMed PMID: 15550252.
- Oberlaender M, de Kock CP, Bruno RM, Ramirez A, Meyer HS, Dercksen VJ, Helmstaedter M, Sakmann B. Cell type-specific three-dimensional structure of TC circuits in a column of rat vibrissal cortex. *Cereb Cortex*. 2012 Oct;22(10):2375-91. doi: 10.1093/cercor/bhr317. Epub 2011 Nov 16. PubMed PMID:22089425; PubMed Central PMCID: PMC3432239.
- Paxinos, G and Franklin, K B. J. (2001). *The Mouse Brain in Stereotaxic Coordinates*. 2nd Edition. Academic Press, San Diego, USA.
- Petersen CC, Sakmann B. 2001. Functionally independent columns of rat somatosensory barrel cortex revealed with voltage-sensitive dye imaging. *J Neurosci*. 21(21):8435-46
- Petersen CC. The functional organization of the barrel cortex. *Neuron*. 2007 Oct 25;56(2):339-55. Review. PubMed PMID: 17964250.
- Petreaanu L, Mao T, Sternson SM, Svoboda K. The subcellular organization of neocortical excitatory connections. *Nature*. 2009 Feb 26;457(7233):1142-5. doi:10.1038/nature07709. PubMed PMID: 19151697; PubMed Central PMCID: PMC2745650.

- Pielecka-Fortuna J, Wagener RJ, Martens AK, Goetze B, Schmidt KF, Staiger JF, Löwel S. The disorganized visual cortex in reelin-deficient mice is functional and allows for enhanced plasticity. *Brain Struct Funct*. 2014 Aug 15. [Epub ahead of print] PubMed PMID: 25119525.
- Polleux F, Dehay C, Kennedy H. 1998. Neurogenesis and commitment of corticospinal neurons in *reeler*. *J Neurosci*. 18:9910-9923.
- Porter JT, Johnson CK, Agmon A. Diverse types of interneurons generate thalamus-evoked feedforward inhibition in the mouse barrel cortex. *J Neurosci*. 2001 Apr 15;21(8):2699-710.
- Qiu S, Korwek KM, Pratt-Davis AR, Peters M, Bergman MY, Weeber EJ. Cognitive disruption and altered hippocampus synaptic function in Reelin haploinsufficient mice. *Neurobiol Learn Mem*. 2006 May;85(3):228-42. Epub 2005 Dec 20. PubMed PMID: 16376115.
- Qiu S, Zhao LF, Korwek KM, Weeber EJ. Differential reelin-induced enhancement of NMDA and AMPA receptor activity in the adult hippocampus. *J Neurosci*. 2006 Dec 13;26(50):12943-55. PubMed PMID: 17167084
- Ramon Y Cajal, S. (1893). *Nuevo Concepto de la Histologia de los Centros Nerviosos*. Barcelona.
- Rakic P. Specification of cerebral cortical areas. *Science*. 1988 Jul 8;241(4862):170-6. Review. PubMed PMID: 3291116.
- Rice FL, Mance A, Munger BL. A comparative light microscopic analysis of the sensory innervation of the mystacial pad. I. Innervation of vibrissal follicle-sinus complexes. *J Comp Neurol*. 1986 Oct 8;252(2):154-74. PubMed PMID:3782505.
- Rice FL, Fundin BT, Arvidsson J, Aldskogius H, Johansson O. Comprehensive immunofluorescence and lectin binding analysis of vibrissal follicle sinus complex innervation in the mystacial pad of the rat. *J Comp Neurol*. 1997 Aug 25;385(2):149-84. PubMed PMID: 9268122.
- Richardson RJ, Blundon JA, Bayazitov IT, Zakharenko SS. Connectivity patterns revealed by mapping of active inputs on dendrites of thalamorecipient neurons in the auditory cortex. *J Neurosci*. 2009 May 20;29(20):6406-17. doi:10.1523/JNEUROSCI.0258-09.2009. PubMed PMID: 19458212; PubMed Central PMCID:PMC2729683.
- Robinson RB, Siegelbaum SA. Hyperpolarization-activated cation currents: from molecules to physiological function. *Annu Rev Physiol*. 2003;65:453-80. Epub 2002 Nov 19. Review. PubMed PMID: 12471170.
- Mao R, Schummers J, Knoblich U, Lacey CJ, Van Wart A, Cobos I, Kim C, Huguenard JR, Rubenstein JL, Sur M. Influence of a subtype of inhibitory interneuron on stimulus-specific responses in visual cortex. *Cereb Cortex*. 2012 Mar;22(3):493-508. doi: 10.1093/cercor/bhr057. Epub 2011 Jun 10. PubMed PMID:21666125; PubMed Central PMCID: PMC3278313.
- Salinger WL, Ladrow P, Wheeler C. 2003. Behavioral phenotype of the *reeler* mutant mouse: effects of RELN gene dosage and social isolation. *Behav Neurosci*. 117(6):1257-75.

- Sarna JR, Dyck RH, Wishaw IQ. The Dalila effect: C57BL6 mice barber whiskers by plucking. *Behav Brain Res.* 2000 Feb;108(1):39-45. PubMed PMID: 10680755.
- Schoonover CE, Tapia JC, Schilling VC, Wimmer V, Blazeski R, Zhang W, Mason CA, Bruno RM. Comparative strength and dendritic organization of TC and corticocortical synapses onto excitatory layer 4 neurons. *J Neurosci.* 2014 May 14;34(20):6746-58. doi: 10.1523/JNEUROSCI.0305-14.2014. PubMed PMID:24828630; PubMed Central PMCID: PMC4019793.
- Schubert D, Kötter R, Zilles K, Luhmann HJ, Staiger JF. Cell type-specific circuits of cortical layer IV spiny neurons. *J Neurosci.* 2003 Apr 1;23(7):2961-70. PubMed PMID: 12684483.
- Schubert D, Kötter R, Staiger JF. Mapping functional connectivity in barrel-related columns reveals layer- and cell type-specific microcircuits. *Brain Struct Funct.* 2007 Sep;212(2):107-19. Epub 2007 Jun 26. Review. PubMed PMID:17717691.
- Simmons PA, Pearlman AL. 1983. Receptive-field properties of transcallosal visualcortical neurons in the normal and *reeler* mouse. *J Neurophysiol.* 50(4):838-48.
- Simon P, Dupuis R, Costentin J. Thigmotaxis as an index of anxiety in mice. Influence of dopaminergic transmissions. *Behav Brain Res.* 1994 Mar 31;61(1):59-64. PubMed PMID: 7913324.
- Simons DJ, Woolsey TA. Morphology of Golgi-Cox-impregnated barrel neurons in rat Sml cortex. *J Comp Neurol.* 1984 Nov 20;230(1):119-32. PubMed PMID: 6512012.
- Simons DJ, Carvell GE, Hershey AE, Bryant DP. Responses of barrel cortex neurons in awake rats and effects of urethane anesthesia. *Exp Brain Res.* 1992;91(2):259-72. PubMed PMID: 1459228.
- Smith SL, Smith IT, Branco T, Häusser M. Dendritic spikes enhance stimulus selectivity in cortical neurons *in vivo*. *Nature.* 2013 Nov 7;503(7474):115-20. doi: 10.1038/nature12600. Epub 2013 Oct 27. PubMed PMID: 24162850.
- Solomon JS, Nerbonne JM. Two kinetically distinct components of hyperpolarization-activated current in rat superior colliculus-projecting neurons. *J Physiol.* 1993 Sep;469:291-313. PubMed PMID: 7505823; PubMed Central PMCID: PMC1143872.
- Staiger JF, Zilles K, Freund TF. Distribution of GABAergic elements postsynaptic to ventroposteromedial thalamic projections in layer IV of rat barrel cortex. *Eur J Neurosci.* 1996 Nov;8(11):2273-85. PubMed PMID: 8950092.
- Staiger JF, Zilles K, Freund TF. Innervation of VIP-immunoreactive neurons by the ventroposteromedial thalamic nucleus in the barrel cortex of the rat. *J Comp Neurol.* 1996 Apr 1;367(2):194-204. PubMed PMID: 8708004.
- Staiger JF, Masannek C, Bisler S, Schleicher A, Zuschratter W, Zilles K. Excitatory and inhibitory neurons express c-Fos in barrel-related columns after exploration of a novel environment. *Neuroscience.* 2002;109(4):687-99. PubMed PMID: 11927151.
- Staiger JF, Flaggmeyer I, Schubert D, Zilles K, Kötter R, Luhmann HJ. Functional diversity of layer IV spiny neurons in rat somatosensory cortex: quantitative morphology of

- electrophysiologically characterized and biocytin labeled cells. *Cereb Cortex*. 2004 Jun;14(6):690-701. Epub 2004 Mar 28. PubMed PMID: 15054049.
- Staiger JF, Zuschratter W, Luhmann HJ, Schubert D. Local circuits targeting parvalbumin-containing interneurons in layer IV of rat barrel cortex. *Brain Struct Funct*. 2009 Dec;214(1):1-13. doi: 10.1007/s00429-009-0225-5. Epub 2009 Oct 31. PubMed PMID: 19882169; PubMed Central PMCID: PMC2782126.
- Staiger JF, Bojak I, Miceli S, Schubert D. A gradual depth-dependent change in connectivity features of supragranular pyramidal cells in rat barrel cortex. *Brain Struct Funct*. 2015 May;220(3):1317-37. doi: 10.1007/s00429-014-0726-8. Epub 2014 Feb 26. PubMed PMID: 24569853; PubMed Central PMCID: PMC4409644.
- Stanfield BB, Cowan WM. The morphology of the hippocampus and dentate gyrus in normal and *reeler* mice. *J Comp Neurol*. 1979 Jun 1;185(3):393-422. PubMed PMID:438366.
- Steindler DA, Colwell SA. Reeler mutant mouse: maintenance of appropriate and reciprocal connections in the cerebral cortex and thalamus. *Brain Res*. 1976 Aug 27;113(2):386-93. PubMed PMID: 953743.
- Stubbs D, DeProto J, Nie K, Englund C, Mahmud I, Hevner R, Molnár Z. 2009. Neurovascular congruence during cerebral cortical development. *Cereb Cortex*. 19 Suppl 1:i32-41.
- Suarez H, Koch C, Douglas R. Modeling direction selectivity of simple cells in striate visual cortex within the framework of the canonical microcircuit. *J Neurosci*. 1995 Oct;15(10):6700-19. PubMed PMID: 7472430.
- Sun QQ, Huguenard JR, Prince DA. Barrel cortex microcircuits: TC feedforward inhibition in SpS cells is mediated by a small number of fast-spiking interneurons. *J Neurosci*. 2006 Jan 25;26(4):1219-30. PubMed PMID:16436609.
- Sun QQ, Zhang Z, Sun J, Nair AS, Petrus DP, Zhang C. Functional and structural specific roles of activity-driven BDNF within circuits formed by single SpS neurons of the barrel cortex. *Front Cell Neurosci*. 2014 Nov 6;8:372. doi: 10.3389/fncel.2014.00372. eCollection 2014. PubMed PMID: 25414642; PubMed Central PMCID: PMC4222225.
- Sur M, Rubenstein JL. 2005. Patterning and plasticity of the cerebral cortex. *Science*. 310(5746):805-10. Review
- Swadlow HA. Influence of VPm afferents on putative inhibitory interneurons in S1 of the awake rabbit: evidence from cross-correlation, microstimulation, and latencies to peripheral sensory stimulation. *J Neurophysiol*. 1995 Apr;73(4):1584-99. PubMed PMID: 7643169.
- Swadlow HA. TC control of feed-forward inhibition in awake somatosensory 'barrel' cortex. *Philos Trans R Soc Lond B Biol Sci*. 2002 Dec 29;357(1428):1717-27. Review. PubMed PMID: 12626006; PubMed Central PMCID: PMC1693091.
- Swadlow HA. Fast-spike interneurons and feedforward inhibition in awake sensory neocortex. *Cereb Cortex*. 2003 Jan;13(1):25-32. Review. PubMed PMID:12466212.

- Takahashi N, Kitamura K, Matsuo N, Mayford M, Kano M, Matsuki N, Ikegaya Y. Locally synchronized synaptic inputs. *Science*. 2012 Jan 20;335(6066):353-6. doi: 10.1126/science.1210362. PubMed PMID: 22267814.
- Tao HW, Li YT, Zhang LI. Formation of excitation-inhibition balance: inhibition listens and changes its tune. *Trends Neurosci*. 2014 Oct;37(10):528-30. doi: 10.1016/j.tins.2014.09.001. Epub 2014 Sep 20. PubMed PMID: 25248294; PubMed Central PMCID: PMC4189014.
- Tissir F, Goffinet AM. Reelin and brain development. *Nat Rev Neurosci*. 2003 Jun;4(6):496-505. Review. PubMed PMID: 12778121.
- Trotter J, Lee GH, Kazdoba TM, Crowell B, Domogauer J, Mahoney HM, Franco SJ, Müller U, Weeber EJ, D'Arcangelo G. Dab1 is required for synaptic plasticity and associative learning. *J Neurosci*. 2013 Sep 25;33(39):15652-68. doi:10.1523/JNEUROSCI.2010-13.2013. PubMed PMID: 24068831; PubMed Central PMCID:PMC3782631.
- Van Der Loos H. Barreloids in mouse somatosensory thalamus. *Neurosci Lett*. 1976 Mar;2(1):1-6. PubMed PMID: 19604804.
- Vanzetta I, Grinvald A. Coupling between neuronal activity and microcirculation: implications for functional brain imaging. *HFSP J*. 2008 Apr;2(2):79-98. doi: 10.2976/1.2889618. Epub 2008 Mar 18. PubMed PMID: 19404475; PubMed Central PMCID: PMC2645573.
- Vicq d'Azyr F. *Traité d'anatomie et de physiologie avec des planches coloriées représentant au naturel les divers organes de l'Homme et des Animaux*. Francois Didot l'aîné, Paris, 1786. Pp 155- 156.
- Vincent SB. The function of vibrissae in the behaviour of the white rat. *Behavior Monogr*. 1912; 1:1-81.
- Wagener RJ, Dávid C, Zhao S, Haas CA, Staiger JF. The somatosensory cortex of *reeler* mutant mice shows absent layering but intact formation and behavioural activation of columnar somatotopic maps. *J Neurosci*. 2010 Nov 17;30(46):15700-9. doi: 10.1523/JNEUROSCI.3707-10.2010. PubMed PMID: 21084626.
- Wagener RJ, Witte M, Guy J, Mingo Moreno N, Kügler S, Staiger JF. Thalamocortical connections drive intracortical activation of functional columns in the mislaminated *reeler* somatosensory cortex. *Cereb Cortex*. 2015. *In press*.
- Wang HP, Spencer D, Fellous JM, Sejnowski TJ. Synchrony of thalamocortical inputs maximizes cortical reliability. *Science*. 2010 Apr 2;328(5974):106-9. doi:10.1126/science.1183108. PubMed PMID: 20360111; PubMed Central PMCID:PMC2859205.
- Weeber EJ, Beffert U, Jones C, Christian JM, Forster E, Sweatt JD, Herz J. Reelin and ApoE receptors cooperate to enhance hippocampal synaptic plasticity and learning. *J Biol Chem*. 2002 Oct 18;277(42):39944-52. Epub 2002 Aug 7. PubMed PMID: 12167620.
- Wehr M, Zador AM. Balanced inhibition underlies tuning and sharpens spike timing in auditory cortex. *Nature*. 2003 Nov 27;426(6965):442-6. PubMed PMID:14647382.

- Welker C, Woolsey TA. 1974. Structure of layer IV in the somatosensory neocortex of the rat: description and comparison with the mouse. *J Comp Neurol.* 158(4):437-53.
- Welker C. 1976. Receptive fields of barrels in the somatosensory neocortex of the rat. *J Comp Neurol.* 166(2):173-89.
- Welker E, Hoogland PV, Van der Loos H. Organization of feedback and feedforward projections of the barrel cortex: a PHA-L study in the mouse. *Exp Brain Res.* 1988;73(2):411-35. PubMed PMID: 3215316.
- Welt C, Steindler DA. Somatosensory cortical barrels and thalamic barreloids in *reeler* mutant mice. *Neuroscience.* 1977;2(5):755-66. PubMed PMID: 593554.
- Wester JC, Contreras D. Columnar interactions determine horizontal propagation of recurrent network activity in neocortex. *J Neurosci.* 2012 Apr 18;32(16):5454-71. doi: 10.1523/JNEUROSCI.5006-11.2012. PubMed PMID: 22514308; PubMed Central PMCID: PMC3415278.
- Wilent WB, Contreras D. Dynamics of excitation and inhibition underlying stimulus selectivity in rat somatosensory cortex. *Nat Neurosci.* 2005 Oct;8(10):1364-70. Epub 2005 Sep 11. PubMed PMID: 16158064.
- Wilson NR, Runyan CA, Wang FL, Sur M. Division and subtraction by distinct cortical inhibitory networks *in vivo*. *Nature.* 2012 Aug 16;488(7411):343-8. doi:10.1038/nature11347. PubMed PMID: 22878717; PubMed Central PMCID: PMC3653570.
- Wimmer VC, Bruno RM, de Kock CP, Kuner T, Sakmann B. Dimensions of a projection column and architecture of VPM and POM axons in rat vibrissal cortex. *Cereb Cortex.* 2010 Oct;20(10):2265-76. doi: 10.1093/cercor/bhq068. Epub 2010 May 7. PubMed PMID: 20453248; PubMed Central PMCID: PMC2936807.
- Wolfe J, Mende C, Brecht M. Social facial touch in rats. *Behav Neurosci.* 2011 Dec;125(6):900-10. doi: 10.1037/a0026165. PubMed PMID: 22122151.
- Wong-Riley MT, Welt C. 1980. Histochemical changes in cytochrome oxidase of cortical barrels after vibrissal removal in neonatal and adult mice. *Proc Natl Acad Sci U S A.* 77(4):2333-7.
- Woolsey TA, Van der Loos H. The structural organization of layer IV in the somatosensory region (SI) of mouse cerebral cortex. The description of a cortical field composed of discrete cytoarchitectonic units. *Brain Res.* 1970 Jan 20;17(2):205-42. PubMed PMID: 4904874.
- Wright AK, Norrie L, Ingham CA, Hutton EA, Arbuthnott GW. Double anterograde tracing of outputs from adjacent "barrel columns" of rat somatosensory cortex. Neostriatal projection patterns and terminal ultrastructure. *Neuroscience.* 1999 Jan;88(1):119-33. PubMed PMID: 10051194.
- Wright AK, Norrie L, Arbuthnott GW. Corticofugal axons from adjacent 'barrel' columns of rat somatosensory cortex: cortical and thalamic terminal patterns. *J Anat.* 2000 Apr;196 (Pt 3):379-90. PubMed PMID: 10853960; PubMed Central PMCID: PMC1468074.

- Xue M, Atallah BV, Scanziani M. Equalizing excitation-inhibition ratios across visual cortical neurons. *Nature*. 2014 Jul 31;511(7511):596-600. doi:10.1038/nature13321. Epub 2014 Jun 22. PubMed PMID: 25043046; PubMed Central PMCID: PMC4117808.
- Yang W, Carrasquillo Y, Hooks BM, Nerbonne JM, Burkhalter A. Distinct balance of excitation and inhibition in an interareal feedforward and feedback circuit of mouse visual cortex. *J Neurosci*. 2013 Oct 30;33(44):17373-84. doi:10.1523/JNEUROSCI.2515-13.2013. PubMed PMID: 24174670; PubMed Central PMCID:PMC3812505.
- Yu YC, He S, Chen S, Fu Y, Brown KN, Yao XH, Ma J, Gao KP, Sosinsky GE, Huang K, Shi SH. 2012. Preferential electrical coupling regulates neocortical lineage-dependent microcircuit assembly. *Nature*. 486(7401):113-7.
- Zhang ZW, Deschênes M. Intracortical axonal projections of lamina VI cells of the primary somatosensory cortex in the rat: a single-cell labeling study. *J Neurosci*. 1997 Aug 15;17(16):6365-79. PubMed PMID: 9236245.
- Zhao S, Frotscher M. Go or stop? Divergent roles of Reelin in radial neuronal migration. *Neuroscientist*. 2010 Aug;16(4):421-34. doi: 10.1177/1073858410367521. Review. PubMed PMID: 20817919.
- Zhu JJ, Connors BW. Intrinsic firing patterns and whisker-evoked synaptic responses of neurons in the rat barrel cortex. *J Neurophysiol*. 1999 Mar;81(3):1171-83. PubMed PMID: 10085344.

Publications arising from the present thesis

The research presented here is either published or submitted as first author research articles under the following references. For additional publications please look up the curriculum vitae.

Guy J, Wagener RJ, Möck M, Staiger JF. Persistence of functional sensory maps in the absence of cortical layers in the somatosensory cortex of *reeler* mice. *Cereb Cortex*. 2015 Sep;25(9):2517-28. doi: 10.1093/cercor/bhu052. Epub 2014 Apr 23. PubMed PMID: 24759695; PubMed Central PMCID: PMC4537421.

Abstract: In rodents, layer IV of the primary somatosensory cortex contains the barrel field, where individual, large facial whiskers are represented as a dense cluster of cells. In the *reeler* mouse, a model of disturbed cortical development characterized by a loss of cortical lamination, the barrel field exists in a distorted manner. Little is known about the consequences of such a highly disturbed lamination on cortical function in this model. We used *in vivo* intrinsic signal optical imaging together with piezo-controlled whisker stimulation to explore sensory map organization and stimulus representation in the barrel field. We found that the loss of cortical layers in *reeler* mice had surprisingly little incidence on these properties. The overall topological order of whisker representations is highly preserved and the functional activation of individual whisker representations is similar in size and strength to wild type controls. Because intrinsic imaging measures hemodynamic signals, we furthermore investigated the cortical blood vessel pattern of both genotypes, where we also did not detect major differences. In summary, the loss of the reelin protein results in a widespread disturbance of cortical development which compromises neither the establishment nor the function of an ordered, somatotopic map of the facial whiskers.

Guy J, Sachkova A, Möck M, Witte M, Wagener JR, Staiger JF. Thalamic input to clusters of layer 4 fated neurons in the *reeler* somatosensory cortex is monosynaptic but weaker than in WT. *In preparation, soon to be submitted.*

Abstract: Layer 4 of the rodent primary somatosensory cortex contains the barrel field, a somatotopic representation of the whiskers on the snout. Layer 4 barrels receive much of the sensory input to the cortex through a dense innervation by thalamocortical axons (TCAs) arising from the ventroposterior medial nucleus of the thalamus (VPM). In the *reeler* mouse, a profound disruption of cortical development results in the absence of cortical layers and the formation of mispositioned barrel-equivalent clusters of layer 4 fated neurons. Although functional imaging studies suggested that sensory input reaches and activates the cortex, little is known about the cellular and synaptic properties of identified excitatory neurons of the *reeler* cortex. Here, we examined the properties of thalamic input to spiny stellate neurons in the *reeler* barrel cortex by means of *in vitro* whole cell recordings combined with optogenetic activation of TCAs and subcellular channelrhodopsin-2 (ChR2) assisted circuit mapping (sCRACM). Our results indicate that spiny stellate neurons populating clusters of layer 4 fated neurons receive direct input from the lemniscal thalamus, but this input is weaker and its spatial distribution along the somatodendritic arbor appears dispersed with respect to wild type controls. These results question the prevalent notion of unaltered functional connectivity in the *reeler* cortex.

Acknowledgments

Scientific research is no solitary venture, and much gratitude is due to the many people who contributed in one way or another to the successful completion of this thesis and to my upbringing as a scientist.

First and foremost, I would like to express my deep gratitude to Prof. Jochen F. Staiger, my supervisor and head of the Institute for Neuroanatomy at the University Medical Center of Göttingen. Jochen knew how to patiently create an environment in which young scientists may grow, learn and thrive, providing each with a clear scientific direction, the freedom to follow intellectual pursuits, and decisive support when in need. My gratitude cannot be overstated, not least for his patience over the years and the trust he blessed me with.

Many thanks to Dr. Robin J. Wagener, who created the mouse line used in this study, taught me stereotaxic injections, contributed data to a common publication, and provided much advice and help. Dr. Mirko Witte offered precious technical support without which sCRACM would not have been feasible, and for which I am grateful.

Thanks are due to Patricia Sprysch, technical assistant at the Institute for Neuroanatomy, who supported my work for years with professional efficiency. She notably performed the stainings presented in this thesis and took care of genotyping the animals. Anna Dudek deserves gratitude as well for some tests stainings as well as for proofreading my manuscripts.

The reconstructions of biocytin filled neurons so central to the interpretation of sCRACM data were carried out by Alexandra Sachkova, who deserves gratitude for this delicate yet crucial work. Many thanks to my fellow PhD students, Alvar Prönneke and Florian Walker, for their help with confocal microscopy, graphic design, and everything. We had fun together.

I wish to express my gratitude to Prof. Dr. Siegrid Löwel and Prof. Dr. Tim Gollisch, members of my thesis committee, for the critical input and encouragement they supported the project with. I thank Dr. Ivo Vanzetta for skilful introduction to, and technical support with intrinsic signal optical imaging. The Labview script controlling the piezo actuator used in this work was provided by Prof. Dr. Cornelius Schwarz, who thereby earned my gratitude.

I acknowledge the support provided by the Department of Medical Statistics of the University of Göttingen.

Last but not least, I want to emphasize my gratitude to Dr. Martin Möck. Martin did not only teach me *in vitro* electrophysiology and write the Signal scripts used in the analysis of electrophysiological data. His profound expertise, towering intellect, and boundless generosity in supporting colleagues were also deeply inspiring and reassuring over the years.

Finally, I wish to once again thank all my colleagues for their generosity, and particularly Kamila Kiszka, for making the lab such a lovely place to work at.

Thank you.

Julien GUY

Curriculum vitae

Julien Guy

Kiesseestraße 1, 3783 Göttingen

julien.guy@med.uni-goettingen.de

0551 39 7068

Personal information

Born on the 27.08.1983 in Strasbourg, France

French citizenship, marital status: single

Education

2012 – present

Doctorate in Neuroscience

GGNB, sensory and motor neuroscience program

Georg-August University, Göttingen, Germany

2006 – 2008

Joint Master in Neuroscience

Louis Pasteur University, Strasbourg, France;

University of Basel, Switzerland;

Albert Ludwigs University, Freiburg im Breisgau, Germany

Title of the thesis: *pharmacological modelling of age related alterations of the EEG in rats*

2003 – 2006

Licence (Bachelor) in Biology

Louis Pasteur University, Strasbourg, France

2003

Baccalauréat

Lycée épiscopal Saint-Etienne, Strasbourg, France

Professional experience

2010 – present

Wissenschaftlicher Mitarbeiter.

Institute for Neuroanatomy, head: Prof. Dr. med. Jochen F. Staiger

University Medical Center, Göttingen, Germany

2009 – 2010

Akademischer Mitarbeiter im Wissenschaftlicher Dienst.

Freiburg Barrel Group, head: Prof. Dr. med. Jochen F. Staiger

Albert Ludwigs University, Freiburg im Breisgau, Germany

Publications

First author

Guy J, Wagener RJ, Möck M, Staiger JF. Persistence of functional sensory maps in the absence of cortical layers in the somatosensory cortex of *reeler* mice. *Cereb Cortex*. 2015.

Guy J, Sachkova A, Möck M, Witte M, Wagener JR, Staiger JF. Thalamic input to clusters of layer 4 fated neurons in the *reeler* somatosensory cortex is monosynaptic but weaker than in WT. 2015. *Submitted*.

Shared first author

Hassler C, Guy J, Nietzsche M, Plachta DTT, Staiger JF, Stieglitz T. Investigations on the chronic behavior of intracortical polyimide electrodes with a bioresorbable coating. 2015. *Submitted*.

Coauthor

Hassler C, Guy J, Nietzsche M, Staiger JF, Stieglitz T. Chronic intracortical implantation of saccharose-coated flexible shaft electrodes into the cortex of rats. *Conf Proc IEEE Eng Med Biol Soc*. 2011.

Wagener RJ, Witte M, Guy J, Mingo Moreno N, Kügler S, Staiger JF. Thalamocortical connections drive intracortical activation of functional columns in the mislaminated *reeler* somatosensory cortex. *Cereb Cortex*. 2015. *In press*.

Walker F, Möck M, Feyerabend M, Guy J, Wagener RJ, Schubert D, Staiger JF, Witte M. Temporally distinct inhibitory control of Martinotti cells by PV and VIP cells. *In preparation*.

Talks in scientific meetings

Guy J, Staiger JF. Unveiling the functional connectivity of individual barrel cortex neurons using intrinsic signal imaging optical imaging and whole cell recording in wild type and *reeler* mice. Arbeitstagung der Anatomischen Gesellschaft, Würzburg, 2011.

Guy J, Staiger JF. Persistence of a somatotopic sensory map in the absence of cortical layers in the *reeler* mouse. NeuroDOWO, Göttingen, 2013.

Poster

Guy J, Wagener RJ, Witte M, Möck M, Staiger JF. Persistence of thalamocortical input in the absence of cortical layers in the *reeler* mouse. Anatomische Gesellschaft Jahresversammlung, Salzburg, 2014.

Awards

NeuroDowo, Göttingen, 2013. Best speaker.

SFB retreat, Dresden, 2014. Best speaker.

Teaching experience

- | | |
|-------------|--|
| 2013 – 2015 | ENI teaching. Method course at the Institute for Neuroanatomy.
Intrinsic signal optical imaging, perfusion, dissection, histology. |
| 2014 – 2015 | Contributed to the supervision of some technical aspects of the M.Sc. Thesis of Georg Hafner, entitled “The layer- and column-specific afferent connectome of VIP expressing GABAergic interneurons in the mouse barrel cortex: a brain-wide atlas using retrograde rabies virus tracing”. Teaching and supervision of intrinsic signal optical imaging and surgery. |

Additional information

Accreditation to perform animal experiments

FELASA, Category B, since March 2010.

Languages

Native speaker of French. Fluent in English. Intermediate in German (conversational, B1-B2). Notions of Polish (A1).

Programming skills

Solid working knowledge of MATLAB and experience with LabView (I wrote the MATLAB and part of the LabView scripts used in the present study). Notions of R.

